第四军医大学
The Fourth Military Medical University

分类号 R749.3
U D C 616.89
密 级 公开

博士学位论文

精神分裂症幻听的神经影像学基础：基于功能磁共振成像的多模态研究

崔龙彪

培 养 类 别 全日制
学 位 类 型 学术学位
一级学科(专业类) 特种医学
二级学科(专业) 医学心理学
研 究 方 向 变态心理学
指 导 教 师 印弘 教授（主任医师）
培 养 单 位 西京医院放射科

二O一七年五月

独 创 性 声 明

秉承学校严谨的学风与优良的科学道德，本人声明所呈交的论文是我个人在导师指导下进行的研究工作及取得的研究成果。尽我所知，除了文中特别加以标注和致谢的地方外，论文中不包含其他人已经发表或撰写过的研究成果，不包含本人或他人已申请学位或其他用途使用过的成果。与我一同工作的同志对本研究所做的任何贡献均已在论文中作了明确的说明并表示了致谢。

申请学位论文与资料若有不实之处，本人承担一切相关责任。

论文作者签名：_____日期：_____

保 护 知 识 产 权 声 明

本人完全了解第四军医大学有关保护知识产权的规定，即：研究生在校攻读学位期间论文工作的知识产权单位为第四军医大学。本人保证毕业离校后，发表论文等使用本论文工作成果时第一署名单位仍然为第四军医大学。学校可以公布论文的全部或部分内容（含电子版，保密内容除外），可以采用影印，缩印或其他复制手段保存论文；学校有权允许论文被查阅和借阅，并在校园网上提供论文内容的浏览和下载服务。同意学校将论文加入《中国优秀博硕士学位论文全文数据库》和编入《中国知识资源总库》等，并可浏览和下载，同时享受《中国优秀博硕士学位论文全文数据库出版章程》规定的相关权益。

论文作者签名：_____导师签名：_____日期：_____

目　　录

缩略语表

缩略词	英文全称	中文全称
AHRS	Auditory Hallucination Rating Scale	幻听量表
ALFF	amplitude of low-frequency fluctuation	低频振幅
ANOVA	analysis of vaiance	方差分析
APA	American Psychiatric Association	美国精神病学会
AVHs	auditory verbal hallucinations	言语性幻听
BOLD	blood oxygenation level-dependent	基于血氧饱和度的
CBF	cerebral blood flow	脑血流
DALYs	disability-adjusted life years	伤残调整寿命年
DLPFC	dorsolateral prefrontal cortex	背外侧前额叶
DMN	default mode network	默认模式网络
DRD2	D2 dopamine receptor	多巴胺 D2 受体
DSM-IV-TR/V	Diagnostic and Statistic Manual of Mental Disorders, Fourth Edition, Text Revision/Fifth Edition	精神障碍诊断与统计手册第四版修订版/第五版
DTI	diffusion tensor imaging	扩散张量成像
EC	effective connectivity	有效连接
ECT	electroconvulsive therapy	电抽搐治疗
EPI	echo planar imaging	平面回波成像
FA	fractional anisotropy	各向异性分数

FC	functional connectivity	功能连接
fMRI	functional magnetic resonance imaging	功能磁共振成像
FWHM	full width at half-maximum	半高全宽
HCs	healthy controls	健康对照
ICA	independent component analysis	独立成分分析
ICHR	International Consortium of Hallucination Research	国际幻觉研究联盟
MPRAGE	magnetization prepared rapid acquisition gradient echo	磁化准备快速采集梯度回波
PANSS	Positive and Negtive Syndrome Scale	阳性与阴性症状量表
pASL	pulsed arterial spin labeling	脉冲式动脉自旋标记
ReHo	regional homogeneity	局部一致性
ROC	receiver operating characteristic	受试者工作特征
ROI	region of interest	感兴趣区
RSNs	resting state networks	静息态网络
rTMS	repetitive transcranial magnetic stimulation	重复经颅磁刺激
sDCM	stochastic dynamic causal modeling	随机动态因果建模
spDCM	spectral dynamic causal modeling	频域动态因果建模
SZ	Schizophrenia	精神分裂症
tDCS	transcranial direct current stimulation	经颅直流电刺激
VBM	voxel-based morphometry	基于体素的形态计量法
YLDs	years lived with disability	伤残损失寿命年
YLLs	years of life lost	减寿年数

精神分裂症幻听的神经影像学基础：基于功能磁共振成像的多模态研究

博士研究生：崔龙彪

导　　师：印　弘　教授（主任医师）

辅 导 教 师：席一斌　讲师（主治医师）

第四军医大学西京医院放射科，西安 710032

资助基金项目：国家自然科学基金（81571651）

国家留学基金管理委员会 2016 年建设国家高水平大学公派研究生项目（201603170143）

第四军医大学博士学位论文课题资助（2014D07）

原国家重点基础研究发展计划（2011CB707805）

中文摘要

【背景】

明确精神分裂症（schizophrenia，SZ）神经生物学基础的最大障碍在于本病中明显的临床异质性，将 SZ 划分为症状特异性亚组有可能在一定程度上降低这一疾病的异质性。幻听是 SZ 的主要症状之一，也是精神分裂症诊断标准中的一项重要内容，阐明其神经机制对于治疗这一严重的精神疾病具有重要的临床意义。

（1）SZ 言语性幻听涉及多个脑区的异常，但是脑血流（cerebral blood flow，CBF）及其连接模式仍不清楚。

（2）SZ 存在结构网络的 rich club 组织受损，作为主要症状的言语性幻听的结构网络的 rich club 组织特性如何改变未见报道。

（3）研究指出静息态网络（resting state networks，RSNs）改变是 SZ 言语性幻听可能的发病基础。然而，根据直接的在体证据，SZ 言语性幻听在相关脑网络中的

特异性模式尚不明确。

（4）脑功能障碍可能是 SZ 言语性幻听背后的病理生理学基础。然而，SZ 言语性幻听的局部与网络功能缺陷尚未明确。

（5）证据表明听觉与语言处理相关脑区之间相互作用紊乱可能参与 SZ 言语性幻听的病理生理学。然而，这些脑网络中的信息流向尚不清楚。

因此，本研究运用静息态功能磁共振成像（functional magnetic resonance imaging，fMRI），通过 CBF 及其复杂网络、rich club 组织、RSNs、局部与网络功能、有效连接（effective connectivity，EC）探讨 SZ 言语性幻听的神经影像学基础，从而揭示其背后的神经机制。

【方法】

采用静息态脉冲式动脉自旋标记（pulsed arterial spin labeling，pASL）、扩散张量成像（diffusion tensor imaging，DTI）、基于血氧饱和度的（blood oxygen level-dependent，BOLD）-fMRI（BOLD-fMRI）与高分辨结构成像，本研究纳入 SZ 言语性幻听患者、非幻听患者，以及健康对照（healthy controls，HCs），其中（1）中包含首发和非首发患者（每组 25 人），（2）中仅为未经治疗的首发患者（幻听组 n = 15、非幻听组 n = 27、HCs 组 n = 48），（3）、（4）、（5）中也仅为首发患者（幻听组 n = 17、非幻听组 n = 15、HCs 组 n = 19）。

（1）测量并比较每组被试的 CBF 值，计算 CBF 连接，并进一步分析 CBF 连接的拓扑特性，包括聚类系数、特征路径长度、局部效能及全局效能。

（2）检测皮层结构连接的 rich club 组织特性以及 rich club 连接、feeder 连接、local 连接密度。

（3）采用独立成分分析（independent component analysis，ICA）提取 RSNs，行双回归进行被试间分析。然后，采用低频振幅（amplitude of low-frequency fluctuation，ALFF）探索 RSNs 内的局部脑功能。最后，行相关性分析与受试者工作特征（receiver operating characteristic，ROC）分析。

（4）比较这些被试之间的 ALFF 与局部一致性（regional homogeneity，ReHo）。将 ALFF 与 ReHo 均有改变的区域用于功能连接（functional connectivity，FC）分析的种子点。然后，行影像参数与症状间的相关性分析和 ROC 分析。

（5）采用随机动态因果建模（stochastic dynamic causal modeling，sDCM）量化不同脑区之间的有向连接，包括左侧背外侧前额皮层（dorsolateral prefrontal cortex，DLPFC；内部言语监控）、听觉皮层（听觉处理）、海马（回忆）、丘脑（信息滤过），以及 Broca 区（言语产生）。

【结果】

（1）SZ 言语性幻听患者 CBF 及其连接特征：言语监控、想象、产生功能障碍

与 SZ 非幻听患者相比，幻听患者显示出双侧额上/中回与中央后回、右侧补充运动区 CBF 降低；与 HCs 相比，非幻听患者表现为左侧额中回 CBF 降低。另外，幻听组具有独特的连接模式，即全局效能的水平介于 HCs 与非幻听患者之间。

（2）首发 SZ 言语性幻听脑结构网络紊乱

SZ 患者的结构网络依然保存着 rich club 现象，且 rich club 组织较 HCs 明显降低，而 SZ 言语性幻听患者 rich club 组织水平与非幻听患者相比并无变化。进一步的分析发现，与非幻听患者相比，SZ 言语性幻听患者 rich club 连接与 feeder 连接密度并未改变，而 local 连接的密度明显降低。

（3）首发 SZ 言语性幻听信息滤过、语言与听觉处理失衡

ICA 显示听觉网络、默认模式网络、执行网络、运动网络、额顶网络症状特异性紊乱的共活动，主要位于听觉皮层、缘上回、岛叶、壳核、DLPFC、角回、楔前叶与丘脑。ALFF 结果表现出与 RSNs 相似的模式。此外，在 SZ 言语性幻听患者中观测到运动网络的共活动程度与幻听的严重性呈正相关。所有 RSNs 的 ROC 曲线下面积均大于 0.75。

（4）首发 SZ 言语性幻听壳核相关的局部与网络功能缺陷

单因素方差分析（analysis of variance，ANOVA）显示双侧壳核的 ALFF 与 ReHo 差异具有统计学差异，由此用作种子点。与非幻听患者相比，SZ 言语性幻听患者显示出左侧壳核 ALFF 降低、右侧 DLPFC 的 ReHo 升高，以及右侧壳核与左侧 DLPFC、Broca 区的 FC 增强。此外，增强的右侧壳核与左侧 Broca 区的连接强度与 SZ 症状的严重性相关。与 HCs 相比，两组患者均表现出额/顶/颞叶皮层-纹状体-小脑网络内的连接减弱。

（5）首发 SZ 言语性幻听丘脑-听觉皮层-海马连接障碍

sDCM 显示 SZ 言语性幻听患者涉及丘脑-听觉皮层-海马环路的症状特异性 EC 异常，即听觉皮层对丘脑传入的敏感性升高，而海马对听觉皮层输入的敏感性降低。此外，在 SZ 言语性幻听患者中观测到从 Broca 区到听觉皮层的连接强度与言语性幻听的严重性呈正相关。

【结论】

（1）该实验证明 SZ 言语性幻听与内部言语监控及语言处理相关的脑区 CBF 异常，CBF 连接的复杂网络分析提示 SZ 言语性幻听的不同功能单元之间连接障碍。这些发现可能从 CBF 及其连接的水平揭示了本病中言语性幻听的神经机制。

（2）从结构网络的 rich club 组织水平上来讲，言语性幻听作为 SZ 的主要症状并未体现出与其他非幻听患者的明显区别，且皮层 rich club 脑区之间以及 rich club 脑区与非 rich club 脑区的连接与 SZ 言语性幻听并无直接的相互影响，非 rich club 脑区之间的网络与 SZ 言语性幻听的关系更为密切。

（3）SZ 言语性幻听中参与听觉处理、言语产生与监控、感觉信息滤过的脑区功能障碍，倾向于错误的感知推断。基于这些 RSNs 之间的失衡，本实验可能为 SZ 言语性幻听的诊断和治疗提供了新策略。

（4）SZ 言语性幻听可能是由壳核与前额叶皮层的局部与网络功能异常，以及它们之间的连接增强引起的。壳核相关的局部与网络功能缺陷可能反映了 SZ 言语性幻听的神经调节失衡。此外，皮层-纹状体-小脑网络内的连接障碍可能也促进了 SZ 发病。

（5）这些发现首次提示 SZ 言语性幻听患者从丘脑到听觉皮层的兴奋性传入增多，导致缺乏外部听觉刺激时出现听觉感知。上述结果可能为 SZ 言语性幻听背后的神经机制提供全新视角。基于我所发现的在体的直接证据，丘脑-听觉皮层-海马连接障碍也有可能用作 SZ 言语性幻听中潜在的诊断性生物标记物和治疗靶点。

上述发现提示，由于 SZ 患者负责言语想象、启动、产生、监控等任务的语言相关脑区活动失衡，导致内部言语紊乱；同时，内部言语滤过障碍使其对听觉皮层的调节代偿性增强，致使听觉中枢异常活跃；另外，上述信息反馈至海马等记忆相关脑区，言语性回忆异常，进一步促进内部言语紊乱。因此，SZ 言语性幻听患者存在大尺度脑网络结构紊乱，涉及听觉、语言、记忆、信息滤过的脑区局部及相互作用

明显异常可能是 SZ 言语性幻听患者的神经影像学基础，最终导致 SZ 患者在缺乏外部刺激时出现幻听。

关键词：精神分裂症，幻听，神经影像学，脑，功能磁共振成像

Neuroimaging underpinnings of auditory hallucinations in schizophrenia: functional magnetic resonance imaging-based multi-modality study

Candidate for doctor: Long-Biao Cui

Supervisor: Hong Yin

Tutor: Yi-Bin Xi

Department of Radiology, Xijing Hospital, Fourth Military Medical University, Xi'an 710032, China

Sponsored Programs: National Natural Science Foundation of China (81571651)

State Scholarship Fund, China Scholarship Council (201603170143)

Fund for the Dissertation Submitted to Fourth Military Medical University for the Academic Degree of Doctor (2014D07)

National Key Basic Research and Development Program (2011CB707805)

Abstract

Background

One of the major obstacle for the identification of neurobiological underpinnings of schizophrenia (SZ) is the overwhelming clinical heterogeneity of this psychiatric disorder. Dividing SZ into symptom-specific subtypes may reduce heterogeneity to some extent. Auditory hallucinations are one of the cardinal symptoms of SZ, as a main diagnostic criterion in SZ. Elucidation of neural mechanisms underlying auditory hallucinations in

SZ is of great clinical significance for treatment of this debilitating mental disease.

(1) Auditory verbal hallucinations (AVHs) in SZ involve the abnormality of many brain regions, but the pattern of cerebral blood flow (CBF) and its connectivity are still not well understood.

(2) Impaired rich club organization exists in the structural network of SZ, leading to disrupted functional brain dynamics. As a core symptom, altered rich club organization in AVHs has been reported.

(3) Altered resting state networks (RSNs) have been proposed to underpin neural mechanisms of AVHs in SZ. However, AVHs-specific patterns within these brain networks remain unclear in SZ based on the direct evidence *in vivo*.

(4) Cerebral dysfunction may represent pathophysiological underpinnings behind AVHs in SZ. However, regional and network functional deficits for AVHs in SZ remain to be identified.

(5) Evidence suggests the disturbed interactions among auditory and language processing-related brain regions may be crucially implicated in the pathophysiology of AVHs in SZ. However, information flow within these brain networks remains unclear.

Consequently, the current study explored the neuroimaging underpinnings of AVHs in SZ by means of CBF and its complex networks, rich club organization, RSNs, regional and network function, and effective connectivity using functional magnetic resonance imaging (fMRI), thereby shedding light on the neural mechanism behind it.

Methods

Using resting-state pulsed arterial spin labeling (pASL), diffusion tensor imaging (DTI), blood oxygen level-dependent-functional magnetic resonance imaging (BOLD-fMRI) and high-resolution structural imaging, SZ patients with and without AVHs, as well as healthy controls (HCs) were included in this study. Both first-episode and non-first-episode SZ patients were enrolled in (1) (n = 25 in each group), but only medication-naïve first-episode patients were included in (2) (n = 15 in AVHs group, n = 27 in Non-AVHs group, and n = 48 in HCs). As well, only first-episode patients were included in (3), (4)

and (5) (n = 17 in AVHs group, n= 15 in Non-AVHs group, and n = 19 in HCs group).

(1) The CBF values were measured and compared between each group, the CBF connectivity was calculated, and CBF topological properties were further analyzed, including clustering index, characteristic path length, local efficiency, and global efficiency.

(2) Measures of rich club organization, connectivity density of rich club, feeder, and local connections were performed in structural connectivity of the cerebral cortex.

(3) Independent component analysis (ICA) was used to investigate RSNs. Dual regression was implemented to obtain between-subject analysis. We then explored regional brain function within RSNs using amplitude of low-frequency fluctuation (ALFF). Finally, we performed correlation and ROC analyses.

(4) The ALFF and regional homogeneity (ReHo) were compared among these subjects. Areas with both ALFF and ReHo alterations were used as seeds in functional connectivity (FC) analysis. Then we performed correlation analysis between image measures and symptoms and receiver operating characteristic (ROC) analysis.

(5) Stochastic dynamic causal modeling (sDCM) was used to quantify directed connections among distinct brain regions, including the left dorsolateral prefrontal cortex (inner speech monitoring), auditory cortex (auditory processing), hippocampus (memory retrieval), thalamus (information filtering), and Broca's area (language producing).

Results

(1) CBF and its connectivity features of AVHs in SZ: dysfunctional speech monitoring, imagery, and production

AVHs patients exhibited decreased CBF in the bilateral superior and middle frontal gyri and postcentral gyri, and right supplementary motor area compared with SZ patients without AVHs. SZ patients without AVHs showed reduced CBF in the left middle frontal gyrus relative to HCs. Moreover, AVHs groups showed distinct connectivity pattern, an intermediate level between HCs and patients without AVHs in the global efficiency.

(2) **Disrupted structural network of the brain in first-episode schizophrenia with**

auditory verbal hallucinations

Rich club phenomenon was found in the structural networks of SZ patients, with a significant reduction of rich club organization. However, there was no significant difference of rich club organiztion between patients with and without AVHs. Furthermore, relative to Non-AVHs, AVHs patients showed no significant difference in rich club and feeder density but a significant reduction in local density.

(3) Disturbed brain activity in resting state networks of first-episode schizophrenia with auditory verbal hallucinations

ICA revealed symptom-specific abnormal disrupted coactivation within the auditory, default mode, executive, motor, and frontoparietal networks, pronouncedly in the auditory cortex, supramarginal gyrus, insula, putamen, dorsolateral prefrontal cortex, angular gyrus, precuneus, and thalamus. ALFF analysis revealed the similar patterns within these RSNs. Furthermore, a positive correlation between the degree of coactivation within the motor network and the severity of AVHs was observed in SZ patients with AVHs. Area under ROC curve was larger than 0.75 for all the RSNs.

(4) Putamen-related regional and network functional deficits in first-episode schizophrenia with auditory verbal hallucinations

One-way analysis of variance showed significant differences of ALFF and ReHo in the bilateral putamen, thereby being used as seeds. SZ patients with AVHs showed decreased ALFF in the left putamen, increased ReHo in the right dorsolateral prefrontal cortex, and increased right putamen-seeded FC with the left dorsolateral prefrontal cortex and Broca's area relative to those without AVHs. Furthermore, the increased strength of the connectivity between the right putamen and left Broca's area correlated with the severity of SZ symptoms. Both patient groups demonstrated hypoconnectivity within frontal/parietal/temporal cortico-striatal-cerebellar networks compared with HCs.

(5) Thalamic-auditory cortical-hippocampal dysconnectivity in first-episode schizophrenia patients with auditory verbal hallucinations

sDCM revealed symptom-specific abnormal effective connectivity involving the thalamic-auditory cortical-hippocampal circuit in SZ patients with AVHs, with an

increased sensitivity of auditory cortex to its thalamic afferents and a decrease in hippocampal sensitivity to auditory inputs. Furthermore, a positive correlation between the strength of the connectivity from Broca's area to the auditory cortex and the severity of AVHs was observed in SZ patients with AVHs.

Conclusion

(1) The current study demonstrates aberrant CBF in the brain regions associated with inner speech monitoring and language processing in SZ patients with AVHs. The complex network measures showed by CBF-derived functional connectivity indicate dysconnectivity between different functional units within the network of AVHs in SZ. These findings might shed light on the neural underpinnings behind AVHs in this disease at the level of CBF and its connectivity.

(2) From the perspective of rich club organization of structural network, as a main symptom, AVHs in SZ does not reflect significant difference with patients without AVHs. Moreover, AVHs have association with connections non-rich club regions themselves, but not among rich club regions or rich club and non-rich club regions.

(3) These findings indicated dysfunctional brain regions involving auditory processing, language producing and monitoring, and sensory information filtering in AVHs in SZ, predisposing to false perceptual inference. This study may provide a novel insight into strategy for diagnosis and therapy of AVHs in SZ based on imbalance among those RSNs.

(4) AVHs in SZ may be caused by abnormal regional function in the putamen and prefrontal cortex, as well as hyperconnectivity between them. The putamen-related regional and network functional deficits may reflect imbalance in neuromodulation of AVHs in SZ. Furthermore, dysconnectivity within cortico-striatal-cerebellar networks might subserve the pathogenesis of SZ.

(5) These findings for the first time indicate augmented excitatory afferents from the thalamus to the auditory cortex in SZ patients with AVHs, resulting in auditory perception without external auditory stimuli. Our results may provide insights into the neural mechanisms underlying AVHs in SZ. Thalamic-auditory cortical-hippocampal

dysconnectivity may also serve as a potential diagnostic biomarker and therapeutic target of AVHs in SZ based on the direct evidence *in vivo* we found.

These findings indicate that language-related memory retrieval helps to provide the source of inner speech, and active speech imagery, initiation, and production without appropriate monitoring yields excessive inner speech, inducing overmuch auditory input due to deficit information filtering. Therefore, SZ patients with AHVs suffer from disrupted structure of the large-scale brain network. Regional dysfunction and abnormal interaction of brain regions involving auditory sense, language, memory and sensory information filtering might underly the neuroimaging underpinngings of AVHs in SZ, predisposing patients with SZ toward having auditory hallucinations in the absence of external auditory stimuli.

Key words: schizophrenia, auditory hallucinations, neuroimaging, brain, functional magnetic resonance imaging

前　言

精神分裂症（schizophrenia，SZ）是一种严重危害人类健康的重大精神疾病，终生患病率为 1%左右[1]，其防治一直是全球性医学难题[2]。幻听是 SZ 的主要症状之一，高达 60-90%的患者伴有幻听症状，并进一步引发严重的抑郁、功能丧失和行为失控。目前对幻听症状的主要治疗手段是抗精神病药物治疗，但其疗效无法令人满意，仍有 25%-30%的难治性 SZ 幻听患者对抗精神病药物治疗无效而迁延不愈[3, 4]，长期遭受幻听折磨，甚至导致自杀和伤人事件[5]。由于发病机制不清，在抗精神病药物治疗前无法对难治性 SZ 幻听患者进行筛查，使得将近 1/3 的患者不得不承担无效的药物治疗带来的不良反应和经济负担，最终导致治疗延误。因此，深入探究 SZ 幻听的神经机制具有重要的临床意义。

早期针对幻听提出的理论包括：听觉皮层过度激活[6]、内部生成言语的归因错误[7, 8]、标记内部生成事件的伴随放电错误[9, 10]、插入式回忆紊乱[11]等。近年来，功能磁共振成像（functional magnetic resonance imaging，fMRI）对人脑结构及功能成像的研究最为广泛[12-15]，为临床研究 SZ 幻听的神经病理学机制提供了越来越多的客观证据。目前，国际幻觉研究联盟（International Consortium of Hallucination Research，ICHR）及多个研究团队关于 SZ 幻听的 fMRI 研究指出，SZ 幻听的神经机制错综复杂，涉及多种脑结构与功能改变，综合运用多模态 fMRI 技术，从多维层面阐释 SZ 幻听的神经机制十分必要。但是，尽管前期的研究已经为 SZ 幻听积累了一定的神经影像学证据，研究策略、被试选择、分析方法等多方面的局限性导致上述 SZ 幻听的影像学证据的意义还十分有限，更不能应用于指导其诊疗的临床实践过程当中。

因此，本课题拟综合运用静息态 fMRI 技术，通过脑血流（cerebral blood flow，CBF）及其复杂网络、rich club 组织与结构-功能耦联、静息态网络（resting state networks，RSNs）、局部与网络功能、有效连接（effective connectivity，EC）等多模态分析系统地探讨 SZ 言语性幻听的神经影像学基础，从而揭示其背后的神经机制，为这一严重的精神疾病的客观诊断与优化治疗提供有力支撑。

文献回顾

提到精神疾病，最先让我想到的就是荷兰后印象派画家 Vincent Willem van Gogh（文森特·威廉·梵高，生于 1853 年 3 月 30 日），他是表现主义的先驱，对二十世纪的艺术产生了深远影响。Korenveld met kraaien（有乌鸦的麦田，图 1）是其创作于 1890 年 7 月的一幅油画，收藏于阿姆斯特丹梵高博物馆，我有幸于留学期间前往该博物馆参观并欣赏了这幅画作。在生命的最后阶段，他深受精神疾病困扰，于 1890 年 7 月 29 日自杀，这幅作品中冷暖色调的鲜明对比、对现实事物的夸大扭曲、粗大的勾勒线条以及质感强烈的笔触等艺术表现形式可能反映了梵高当时的精神状态。或许正是精神疾病造就了一位艺术天才，然而，绝大多数患者更多的则是痛苦不堪。

图 1　有乌鸦的麦田，文森特·梵高，1890，布面油画

Fig. 1 Korenveld met kraaien, Vincent van Gogh, 1890, olieverf op doek

Korenveld met kraaien is één van de beroemdste schilderijen van Van Gogh. Vaak wordt beweerd dat dit het allerlaatste werk van de kunstenaar zou zijn. De dreigende lucht met kraaien en het doodlopende pad zouden vooruit wijzen naar zijn naderende levenseinde. Dit is echter een hardnekkige mythe.（根据博物馆规定以及出于对作者及其作品的尊重，参观时并未拍照，图片及介绍均摘自 https://www.vangoghmuseum.nl/）

具体而言，根据最新的全球疾病负担分析，*Lancet* 与 *N Engl J Med* 报道称，全球疾病负担最为沉重的是精神与行为障碍，其伤残损失寿命年（years lived with disability，YLDs）占总体负担的 22.7%[16, 17]，高于任何其他疾病分类（图 2A 与 B）；*Lancet* 进一步发表文章指出，**精神分裂症（schizophrenia，SZ）是全球疾病负担的首要原因之一**，在精神与物质相关障碍的 YLDs、减寿年数（years of life lost，YLLs）、伤残调整寿命年（disability-adjusted life years，DALYs）中均占据多数（图 2C）[1]。我国的 SZ 疾病形势同样紧迫，根据国家卫生和计划生育委员会最新公布的《*中国卫生和计划生育年鉴*》2016 卷，该病的平均住院日及医疗费用远超出其他疾病[18]，给患者及其家庭和社会带来沉重的负担。作为严重的精神卫生问题，SZ 是重要的公共卫生问题和较为突出的社会问题已经成为我国和国际社会的广泛共识。本病的公共卫生影响极其惊人，至今仍为精神病学领域的研究热点。

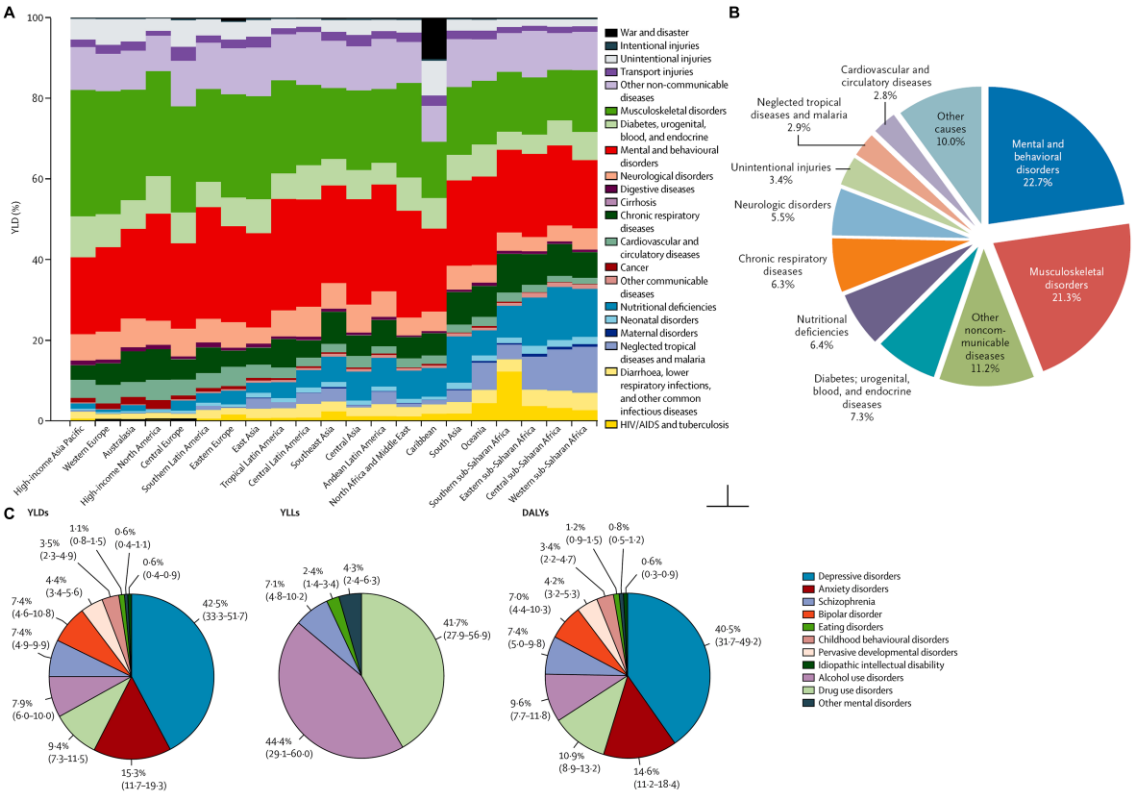

图 2　2010 年全球疾病负担[1, 16, 17]

Fig. 2 Global disease burden, 2010

A: Percentage of YLDs by 21 major cause groupings and region for 2010. B: Shown is the global burden of YLDs due to mental and behavioral disorders, as compared with

disability due to other highest-ranked categories of disorders and conditions. C: Proportion of YLDs, YLLs, and DALYs explained by each mental and substance use disorder group. DALYs, disability-adjusted life years; YLDs, years lived with disability; YLLs, years of life lost.

尽管无法详尽地包括全面反映疾病本质的特征，美国精神病学会最新出版的*《精神障碍诊断与统计手册第五版》*（Diagnostic and Statistical Manual of Mental Disorders, Fifth Edition，DSM-V）仍然延续以往临床医师主观评估的标准诊断 SZ[19]。此外，在 SZ 治疗上，最为常见的失败原因就是口服药物起效慢、依从性差、复发率高；而且，即使给予充分的药物或其他治疗，仍有 20%的 SZ 患者症状几乎仍然无法得到完全缓解，同时，也有高达 1/3 的患者临床反应并不明显[20]。正是由于缺乏能够解释影响治疗或预后的重要个体差异的临床特征，SZ 治疗缺乏个体化策略，治疗效果至今未能取得突破性进展。**SZ 难以实现客观诊断与优化治疗一直是全球性医学难题，而 SZ 发病机制尚不完全清楚是其根本原因。**明确 SZ 的神经机制将极大地促进 SZ 的客观诊断与优化治疗，具有极为重要的临床与社会意义。

1 SZ 幻听的研究意义

如前所述，SZ 是一种严重的病程迁延的精神疾病，全球约有 1%的人口罹患此病[19, 21]。该病以一系列突出的精神功能障碍为特征，具有感知、思维、情感、行为等多方面的障碍和精神活动的不协调以及精神活动与环境的不协调。瑞士医师 Eugen Bleuler 于 1911 年首次提出“schizophrenia”这一疾病术语，尽管人们对于 SZ 的认识已有 100 余年的历史，但明显的临床异质性是探讨本病神经生物学基础的最大障碍[22]，其发病机制至今尚未完全阐明。研究发现，**基于阳性症状对 SZ 进行亚分型有助于降低其临床异质性[23]，有望揭示其发病的神经机制。**

幻觉是普遍公认的 SZ 阳性症状，虽然在很多情况下都可以出现幻觉，但是目前已经把它看做是 SZ 的核心临床特征。其中，幻听最为常见，约有 60-90%的 SZ 患者都伴有幻听[12]。幻听的常见特征包括：具有外源性、对患者的思想或行为进行评论、两个或更多声音之间的对话；幻听的某些特征，无论是内容还是知觉性质，都可能对 SZ 具有相对特异性[21]。另外，幻听仍然是最新出版的 DSM-V 中一项重要的诊断

标准[19]。幻听对 SZ 的疾病负担具有重要影响：病人幻听的体验通常是使人烦躁不安的，明显地干扰其认知功能，并有可能破坏日常活动；有些患者对声音的反应是自杀[24]，而有些则是对命令性幻听表现出暴力行为[25]。了解幻听背后的神经机制对于更好的管理上述不良后果至关重要。因此，**明确 SZ 幻听的神经影像学基础、阐明幻听的神经机制将极大地促进 SZ 的诊断与治疗，具有重要的临床意义。**

另外，幻听也可以为全面探究感觉现象提供证据[26]。有相当数量的健康人在生命的某个或某些时间点经历幻听，也有许多非原发性精神病患者会有短暂的幻听发作，例如帕金森病患者[27, 28]和社区非精神病人群[29]，其中健康人群的幻听发生率为6%[30]。这些类型的幻听与 SZ 幻听之间就可能存在着相同与不同的特征。因此，正如 Hechers 提出的，针对幻听展开详尽的研究也很有可能揭示正常的感觉过程[31]。

2 基于神经影像学的 SZ 幻听研究现状

基于神经影像学的SZ研究已经确定了一些疾病风险的脑结构和功能指标，称为内表型。内表型是可遗传的、可量化的、疾病相关的生物学特征，并被认为介于遗传学和临床表现之间。其中，脑连接障碍就被认为可能是SZ的一种内表型[32]。随着计算机及影像技术的飞速发展，对活体大脑的结构、神经活动及脑功能代谢的研究逐步深入。其中，MRI对人脑结构及功能成像的研究最为广泛，特别是fMRI等技术的发展及应用，为临床研究SZ幻听的内表型与神经机制提供了越来越多的客观证据。

总体而言，高分辨结构成像、基于血氧饱和度的fMRI（blood oxygen level dependent-fMRI，BOLD-fMRI）、扩散张量成像（diffusion tensor imaging，DTI）、动脉自旋标记（arterial spin labeling，ASL）等研究发现，**SZ幻听患者可能的脑结构与功能异常包括灰质体积（颞上回[33, 34]、听觉皮层[35]、丘脑[36]）、白质纤维（半球间听觉通路[37, 38]、丘脑前辐射与内囊前肢[39, 40]、弓状束[41-46]、钩状束[41]、上纵束[47]、前扣带[47, 48]、下枕额束额颞纤维[49]、背侧语言通路[50]）、脑区激活（听觉皮层[34]、颞顶联合区[51]、Broca区[52]、海马[51]）、连接[53]、复杂网络[54]、血流[55-58]等。**

2.1 基于ASL的SZ幻听研究

运用 ASL 技术观察脑组织的血流情况，Homan 的系列研究发现，经颅直流电刺激（transcranial direct current stimulation，tDCS）或经颅磁刺激（transcranial magnetic stimulation，TMS）治疗有效的 SZ 幻听患者听觉皮层 CBF 或局部 CBF（regional CBF，

rCBF）治疗前较治疗后高[55-57]。通过对比 SZ 幻听与非幻听患者，幻听特异性的 CBF 增加位于右侧颞上回与尾状核，降低则位于双侧枕叶皮层与左侧顶叶皮层[58]。尽管 SZ 幻听的 ASL 研究数量有限，上述研究表明，SZ 幻听患者听觉及纹状体区 CBF 升高，或许是其神经活动增强的体现。

2.2 基于 DTI 的 SZ 幻听研究

从方法学的角度上讲，目前，脑连接分析分为结构连接、功能连接（functional connetivity，FC）以及 EC。结构连接也称解剖连接，是指不同脑区的神经元通过神经纤维的连接。主要研究方法有基于 MRI 结构成像和 DTI 等扩散成像的结构连接分析：2007 年，He 等[59]首次提出基于 MRI 结构成像分析结构连接的方法，通过分析脑区间皮层厚度的相关性构建结构连接网络，并且运用复杂网络理论发现了脑结构网络的小世界属性；而基于 DTI 等的结构连接分析主要是建立在白质纤维追踪的基础上，以各个脑区之间的白质纤维束构造结构连接网络。

DTI 能够活体发现 SZ 幻听患者的白质纤维束是否出现异常，是阐明 SZ 幻听可能机制的有效途径。已有研究报道，与对照组相比，SZ 幻听患者半球间听觉通路[37]、双侧弓状束[41-43]、皮质脊髓束[41]、钩状束[41]、胼胝体（下膝部、上膝部以及峡部）[60]、右侧前扣带回吻侧与尾侧的纤维连接[48]的各向异性分数（fractional anisotropy，FA）降低，并且 FA 与幻听严重程度呈负相关[41, 48, 60]。相反，也有研究表明 SZ 幻听患者白质 FA 升高，涉及脑区包括上纵束与前扣带[47]、颞上回皮层下白质[61]、弓状束[44]。具体而言，SZ 幻听患者双侧弓状束 FA 降低的部位是颞叶后部与顶叶之间的连接，以及额叶前下部与顶叶之间的连接，即外侧裂语言通路[42]。同样，另有一项研究也在这一语言通路上发现结构连接与 FC 同时出现异常。在 SZ 幻听患者，连接左侧额下回与颞中回的弓状束表现为 FA 降低，并且 FC 也减低，其结构连接与 FC 之间的关系遭到破坏，而 SZ 幻听患者的各项参数均介于 SZ 非幻听患者与对照组之间，提示中等程度的额颞连接破坏导致了 SZ 幻听症状[43]。一项纳入五个研究的荟萃分析结果显示，SZ 幻听患者左侧弓状束 FA 值降低[62]，更加有力地证明包括外侧裂语言通路的弓状束白质纤维损伤参与 SZ 幻听。在上述研究中，外侧裂语言通路是指 Wernicke 区到 Broca 区、Wernicke 区到 Geschwind 区、Geschwind 区到 Broca 区的连接；钩状束是连接额颞叶最大的白质纤维束，连接额叶的 Broca 区、眶回与颞上回、颞下回、海马旁回等；胼胝体是联系两侧半球的主要横行纤维，半球间听觉通路就

走行其间；上纵束是最长的联络纤维，沿途自额、顶、枕、颞叶接受纤维并发出纤维终止于上述各叶，其中就包括背外侧前额皮层（dorsolateral prefrontal cortex，DLPFC）。FA 变化提示白质纤维的损伤，以上半球间听觉通路、外侧裂语言通路、钩状束、上纵束 FA 的变化，提示负责听觉、语言、记忆等信息处理的连接功能紊乱。我们已经可以发现 SZ 幻听患者可能存在听觉-语言-记忆信息处理网络的白质纤维异常，即结构连接受损。

2.3 基于 BOLD-fMRI 的 SZ 幻听研究

BOLD-fMRI 能够用于观察活体脑内神经元的活动状态，BOLD-fMRI 研究已在 SZ 幻听中积累了较多结果。证据表明，包括听觉网络（听觉皮层与岛叶）、默认模式网络（default mode network，DMN；内侧前额叶、前后扣带皮层、楔前叶、角回与海马）、执行网络（DLPFC 与丘脑）、运动网络（中央前回、补充运动区与壳核）以及额顶网络（Broca 区与 Wernicke 区）在内的 RSNs 中的众多脑区局部异常[57, 63-65]以及相互作用改变[53, 66-75]均在言语性幻听中有所体现。局部功能研究发现，与非幻听患者相比，SZ 幻听患者双侧丘脑、右侧海马及海马旁回的低频振幅（amplitude of low-frequency fluctuation，ALFF）升高，而扣带回与岛叶的 fALFF（fractional ALFF）升高、额极的 fALFF 降低[76]。

BOLD-fMRI 数据更常被用于连接分析，包括 FC 和 EC。FC 是指空间上不相邻脑区的活动在时间上的相关性[77]。因此，任何一种能够度量两个时间序列相关性的方法都可以用来量化 FC。目前主要的研究方法有基于种子点的相关分析、独立成分分析（independent component analysis，ICA）、主成分分析、偏最小二乘回归和聚类分析等。值得一提的是，EC 是指一个脑区的活动对另一个脑区或其自身的活动所施加的因果（间接）影响，不仅强调脑区间活动在时间上的因果关系，还强调信息的流向[77]。运用 BOLD-fMRI 研究 SZ 患者的 FC 时发现，幻听严重程度与左半球的 Broca 区、顶下区与颞中回的激活具有相关性[52]。另外，SZ 幻听患者左侧颞顶联合区、丘脑、海马及纹状体区活动增强[51]，其中颞顶联合区就是听觉-言语感知区。

在方法学上需要指出的是，由于考虑了血流动力学响应过程，随机动态因果建模（stochastic dynamic causal modeling，sDCM）就是一项基于 fMRI 分析脑区间 EC 的技术，目前已经应用于探讨神经精神疾病神经机制的研究当中[78, 79]。本研究将运用 sDCM 分析 SZ 幻听脑区间的 EC，这将有助于其神经机制的深入探究。

另外，RSNs 也是采用 BOLD-fMRI 数据时较为常见的分析，它指的是静息状态下自发活动时相互连接的脑区。Wolf 等[73]对 10 例 SZ 难治性幻听患者与对照组进行比较，选取了 4 个 RSNs 进行分析，结果发现：在言语相关网络中，双侧颞叶活动增强、扣带皮层活动减弱；楔前叶与右侧外侧前额皮层分别在注意及执行控制网络中出现活动异常；其中，幻听严重性与左侧前扣带皮层、颞上回及右外侧前额皮层的活动具有相关性。

2.4 基于其他 fMRI 模态的 SZ 幻听研究

最后，高分辨 MRI、扩散波谱成像（diffusion spectrum imaging，DSI）在 SZ 幻听中也有部分研究。高分辨 MRI T1 像可用于观察活体脑的精细解剖结构，并且常常采用基于体素的形态计量法（voxel-based morphometry，VBM）对数据进行分析。前期研究发现，SZ 幻听患者双侧丘脑[36]及左侧颞上回[33]、颞中回[80]体积降低。基于更大样本量的研究还发现，幻听严重程度与左侧初级听觉皮层、左侧次级听觉皮层、左侧颞上回前部、右侧颞上回（包括初级与次级听觉皮层和颞中、上回）、右侧中央后回、左侧扣带皮层后部延续到楔前叶脑区体积具有相关性[34]。DSI 技术能够反映髓鞘异常改变，DSI 结合 BOLD-fMRI 发现，SZ 幻听患者背侧语言通路结构完整性以及功能偏侧化降低，并且与幻听严重程度呈负相关[50]。另外，Amad 等对海马与 SZ 幻听的关系进行多模态研究，结果表明，海马与丘脑之间的 FC、白质连接（额枕束）、海马体积在仅有幻听和同时伴有幻听与幻视的 SZ 患者中存在差异[67]。由此可见，以上脑区主要涉及听觉皮层、语言区、海马等部位。

2.5 基于 fMRI 的荟萃分析

通过纳入前期研究进行荟萃分析能够更为准确地反映 SZ 幻听的异常所在。在结构方面，正如前文所提及的，一项纳入五个 DTI 研究的荟萃分析发现 SZ 幻听患者左侧弓状束 FA 值降低[62]；在比较 SZ 幻听脑区体积的荟萃分析[81, 82]中，Modinos 等发现，SZ 幻听患者灰质体积降低最为显著的是左侧颞上回及初级听觉皮层，同时，右侧颞上回及初级听觉皮层灰质体积也有降低趋势（**图 3**）。

在比较 SZ 幻听脑区活动的荟萃分析[83-85]中，一项纳入了 10 项 SZ 谱系障碍幻听患者在幻听状态时的 fMRI 或正电子发射体层成像（positron emission tomography，PET）研究的荟萃分析中发现双侧额颞网络（包括 Broca 区、前岛叶、中央前回、额叶岛盖、颞上回、颞中回、顶下小叶、海马和海马旁回）活动增加（**图 4**）[83]。在此

需要指出的是，海马旁回是收集记忆信息的关键区域，负责将信息从海马传递到相关区域，其功能异常可能表现在当幻听状态时对语言区域的触发不足。这些发现提示了 SZ 幻听患者负责言语产生和感知的额-颞-顶网络功能存在异常。

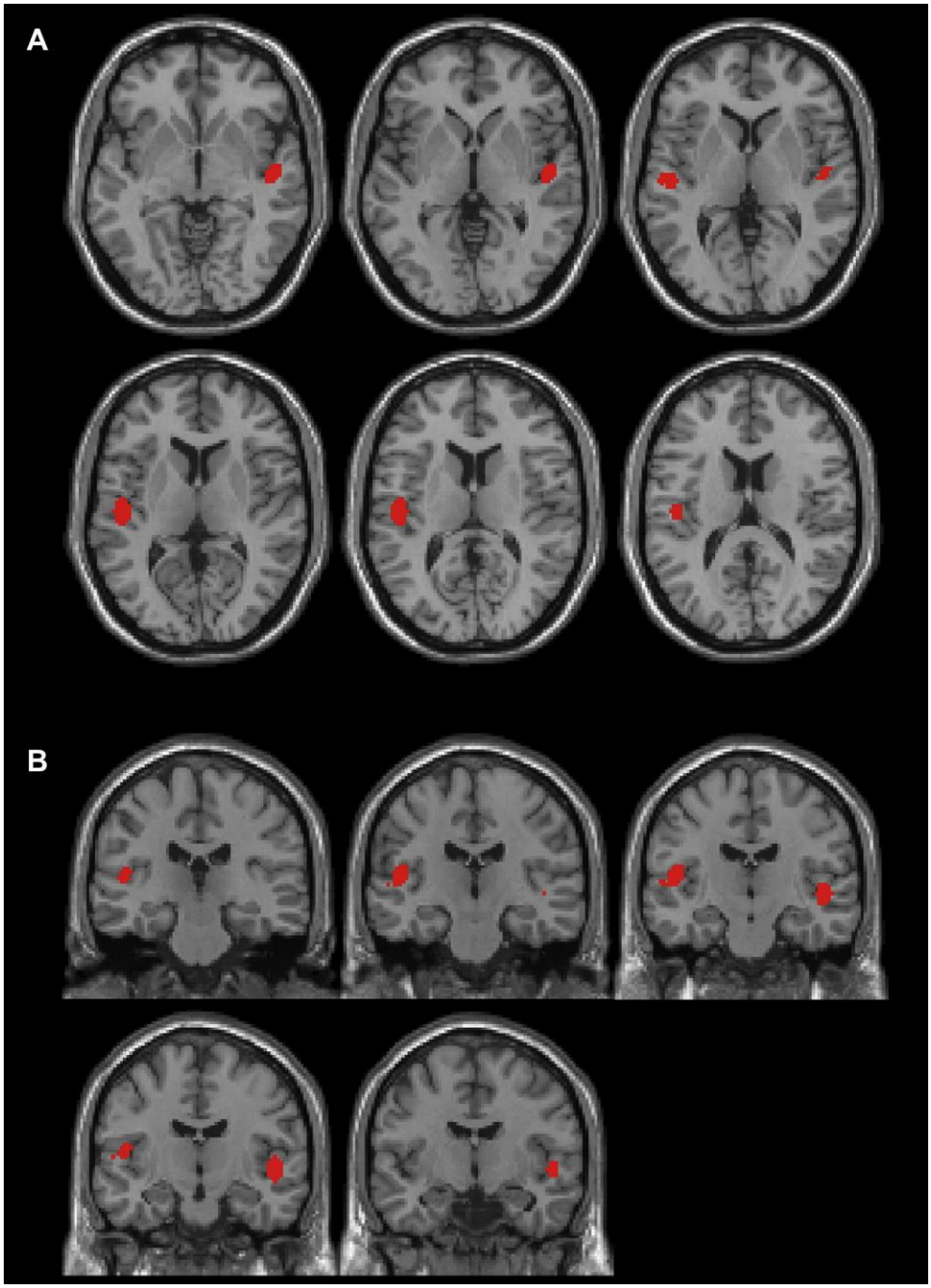

图 3　SZ 言语性幻听患者 VBM 研究的荟萃分析结果[82]

Fig. 3 Results of the meta-analysis of VBM studies in patients with SZ and AVHs

The statisticdepicted here is the proportion of studies reporting at least one significant peakwithina local neighbourhood of size ρ = 10 mm, in axial (A) and coronal (B) views.

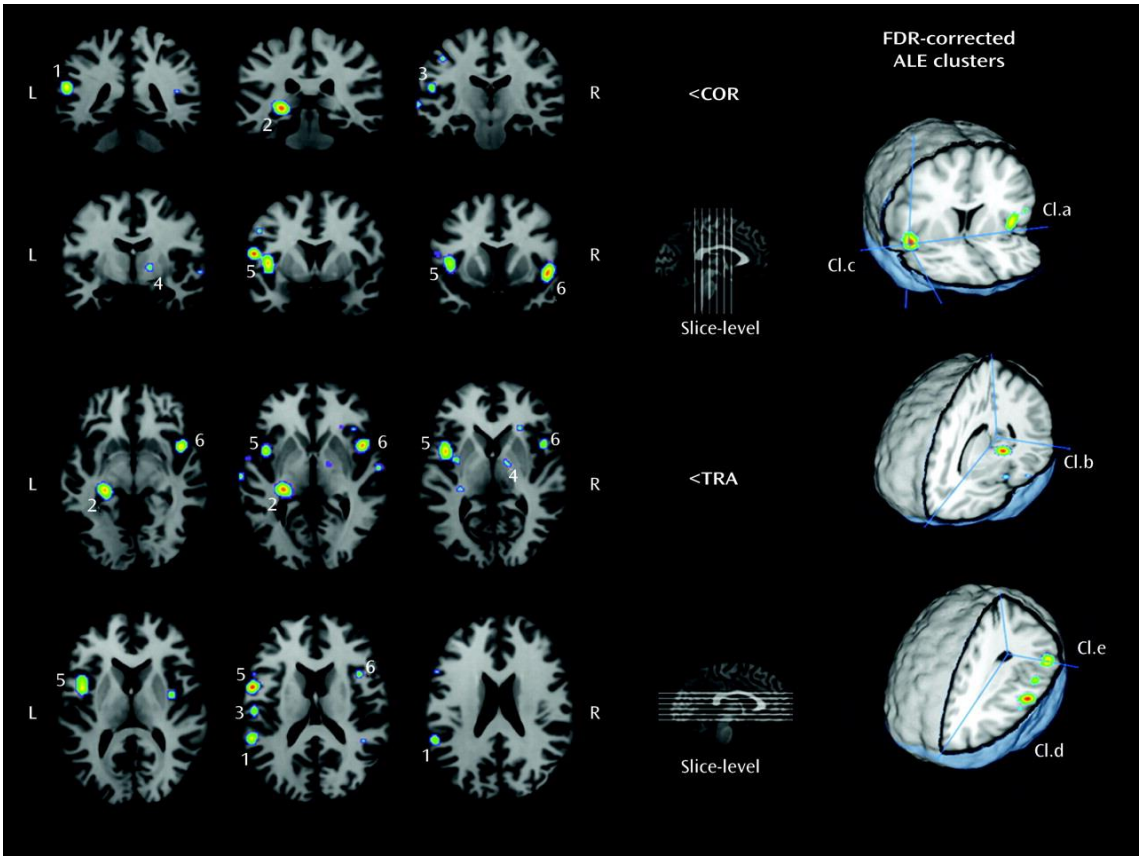

图4　与SZ谱系障碍言语性幻听相关的脑功能活动[83]

Fig. 4 Results of Included Studies Measuring Functional Brain Activity Associated With Auditory Verbal Hallucinations in Subjects With SZ Spectrum Disordersa

The first three columns depict the activation likelihood estimation (ALE) results on coronal (COR) views (upper panel) as well as on transverse (TRA) views (lower panel) of the brain anatomy. The fourth column depicts slice levels shown on sagittal views. The fifth column shows clusters (Cl.a to CI.e) of consistent activity among patients with schizophrenia spectrum disorders experiencing auditory verbal hallucinations, projected over a standardized template. Greater likelihoods were measured within the left inferior parietal lobule, left hippocampus/parahippocampal region, left superior temporal gyrus, Globus pallidum, Broca's convolution, right anterior insula, and frontal operculum. L, Left; R, Right.

另有一篇荟萃分析比较了幻觉的两种形式，即幻听和幻视，所纳入的研究以 SZ

患者为主，结果发现：言语性幻听患者比幻视患者活动升高的脑区包括颞上回、Wernicke 区、Broca 区的右侧同伦脑区；相反，幻视患者比言语性幻听患者活动升高的脑区包括舌回、枕叶皮层及楔叶（图 5）。换言之，前者为语言处理区，后者为视觉处理区。

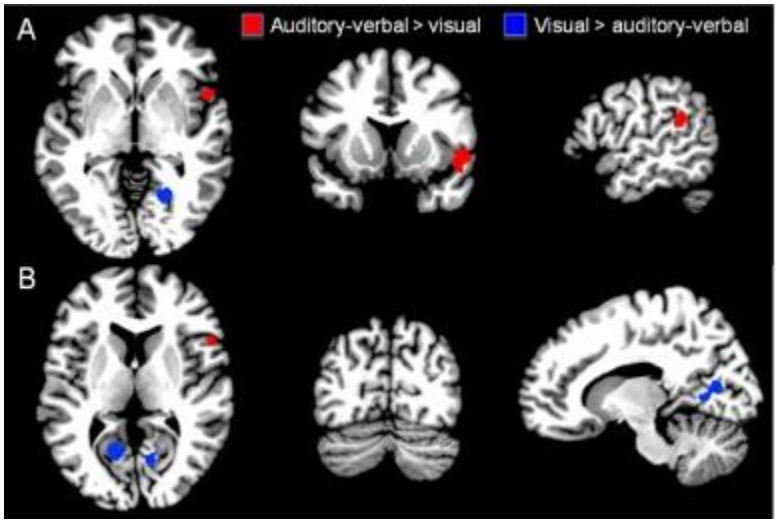

图5　对比言语性幻听与幻视的荟萃分析结果[86]

Fig. 5 Results of the meta-analysis subtraction contrasts between AVHs and VHs

(A) The subtraction contrast of AVHs > VHs elicited significant activity in speech and language processing areas such as superior temporal gyrus, Wernicke area and the right homologue of Broca area; (B) for VHs > AVHs, significant activity was observed in visual processing regions including lingual gyrus, occipital cortex, and cuneus. AVHs, auditory-verbal; VHs, visual hallucinations.

3 SZ 幻听的神经机制假说

迄今为止，SZ 幻听的神经机制尚无定论。最近，Bohlken[87]等综述指出，早期用于解释幻听的理论包括：听觉皮层过度激活（Penfield，1958）[6]、内部生成言语的归因错误（Frith 与 Done，1988; McGuire 等，1995）[7, 8]、标记内部生成事件的伴随放电错误（Feinberg，1978；Allen 等，2006）[9, 10]、插入式回忆紊乱（Copolov 等，2003）[11]。近年来，在原有神经生物学、电生理学、遗传生物学、神经影像学等多种手段的基础上，SZ 幻听神经机制的研究进一步结合 fMRI 技术，并提出如下假说。

3.1 半球间听觉通路异常假说

近期提出的 SZ 幻听的神经机制假说主要关注听觉信息处理障碍，包括半球间听觉通路异常[88]。如图 6 所示，连接双侧听觉皮层（位于颞横回，Brodmann 41、42 区）的半球间听觉通路走行于胼胝体的后 1/3，即峡部与压部。其纤维直径最大（> 3 μm），因此拥有较快的传导速度[89]。该通路的作用是听觉处理与语言理解，如果受损将会扰乱相应听觉区域间的信息流[88]。研究表明，SZ 幻听患者恰恰存在半球间听觉通路异常[60, 90-92]，双侧听觉皮层间的 FC 也降低[93]，这可能是导致 SZ 幻听的重要神经机制。但是，这一假说过于简化，很难全面阐述 SZ 幻听的神经机制。

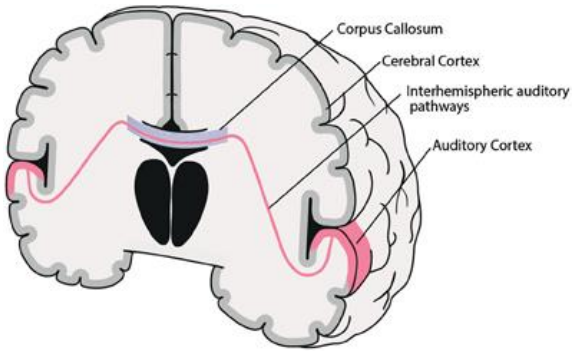

图 6　半球间听觉通路示意图[88]

Fig. 6 Schematic illustration of the interhemispheric auditory pathways

Interhemispheric auditory pathways (red) connecting bilateral auditory cortices run through the posterior third of the corpus callosum (blue).

3.2 丘脑-听觉皮层通路功能亢进假说

关于 SZ 神经递质或受体的假说中，多巴胺活性过度假说最受关注，多巴胺及多巴胺 D_2 受体（D2 dopamine receptor，DRD2）的异常在 SZ 的发病中具有重要意义，拮抗 DRD2 也是目前抗精神病药物的神经生物学基础。中枢多巴胺能神经元通路包括长纤维通路、短纤维通路、超短纤维通路。而 DRD2 则主要分布于黑质-纹状体突触后、皮层-纹状体末梢、垂体、黑质致密部、杏仁核等部位，其中以尾状核、豆状核、伏隔核、嗅球中表达最高（图 7）。如图所示，DRD2 分布区域标记为黄色，多巴胺能神经元长纤维通路包括中脑边缘皮层系统（橙色连线）和黑质纹状体系统（紫色连线）。另外，投射到丘脑的多巴胺能神经元通路突触后膜上的受体也是 DRD2，但其密度仅为纹状体的 1/3[94]。FC 分析显示，SZ 幻听患者伏隔核（纹状体腹侧部，主要为多巴胺能神经元）与中脑边缘皮层系统的脑区连接明显增强[70]。

运用 SZ 动物模型，Chun 等[95]发现丘脑内侧膝状体 DRD2 表达上调，诱发丘脑内侧膝状体向听觉皮层投射中的谷氨酸能神经元谷氨酸释放减少，氟哌啶醇（一代抗精神病药物，DRD2 拮抗剂）与氯氮平（二代抗精神病药物，DRD2 与 5-羟色胺受体拮抗剂）能够逆转上述负性调节；通过小干扰 RNA 敲低 SZ 模型小鼠的内侧膝状体 *Drd2* 基因水平，丘脑-皮层投射对氟哌啶醇与氯氮平的敏感性消除，相反，过表达野生型小鼠的内侧膝状体 *Drd2*，丘脑-皮层投射对氟哌啶醇的敏感性则升高；该研究在 SZ 患者尸检中进一步证实内侧膝状体 DRD2 表达升高。因此，丘脑向听觉皮层投射中的谷氨酸能神经元突触传递紊乱改变了正常的听觉信息流，即丘脑-听觉皮层 DRD2 通路功能亢进可能是导致 SZ 幻听症状的原因。

SZ 连接障碍假说表明 SZ 的症状与不同脑区的神经连接异常有关[79, 96, 97]，特别是丘脑相关网络的功能障碍[98]。丘脑在 SZ 中具有一个显著特征，即强化特定输入而抑制其他输入，表现为将外部言语从内部言语中滤过的受损[99-101]。SZ 中丘脑的这种特性是由于通过外部感觉信息传入的丘脑-皮层 γ 活动调节遭到破坏[99, 102]。而 Pinault 指出，多种神经递质或神经调质（多巴胺、谷氨酸/谷氨酰胺、乙酰胆碱、去甲肾上腺素、5-羟色胺、组胺）对丘脑相关网络的综合作用可能最终导致 SZ 出现幻觉[98]。同样，这一假说仅关注了 SZ 幻听机制中两个重要的脑区，虽然它们很可能是其中的重要环节，但忽略了大脑作为众多脑区及其脑区间连接的这一有机整体，全面系统地概括 SZ 幻听的神经机制尚显不足。

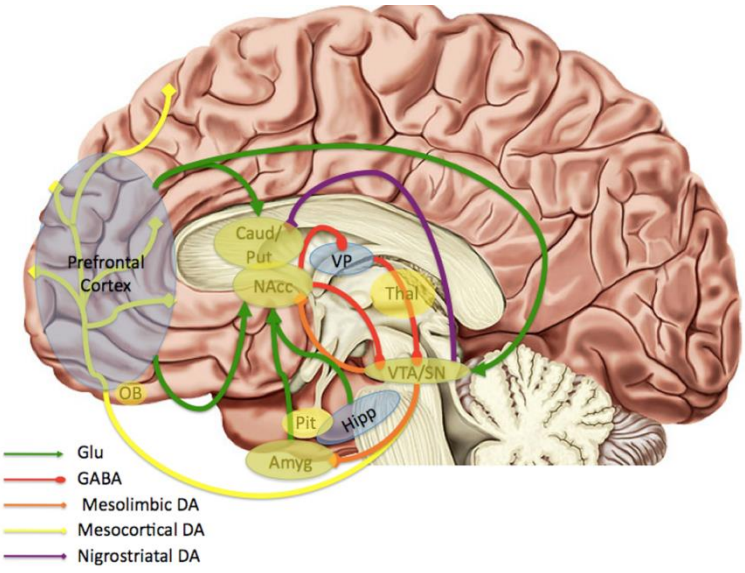

图 7　脑内多巴胺投射通路及 DRD2 的分布示意图[103]

Fig. 7 Schematic illustration of dopamine projection pathways and distribution of DRD2 in the brain

Regions where DRD2 distributes in the brain (yellow). Amyg, amygdala; Caud, Caudate; DA, Dopamine; GABA, GABAergic projections; Glu, glutamatergic projections; Hipp, hippocampus; Nacc, nucleus accumbens; Put, Putamen; SN, substantia nigra; VP, ventral pallidum; VTA, ventral tegmental area.

3.3 脑 RSNs 紊乱假说

较之上述两个理论，从脑网络的角度出发，脑 RSNs 紊乱假说为 SZ 幻听神经机制的探讨提供了更加广阔的视野。SZ 脑网络异常已获得大量证据支持及较为广泛的认可[104, 105]。根据多年的 fMRI 研究结果，ICHR 最新指出包括 SZ 幻听患者 DMN、突显网络与中央执行网络在内的 RSNs 相互作用异常，当语言与感觉网络静息态连接改变时，导致感觉处理的内部状态紊乱（图 8）[106]。

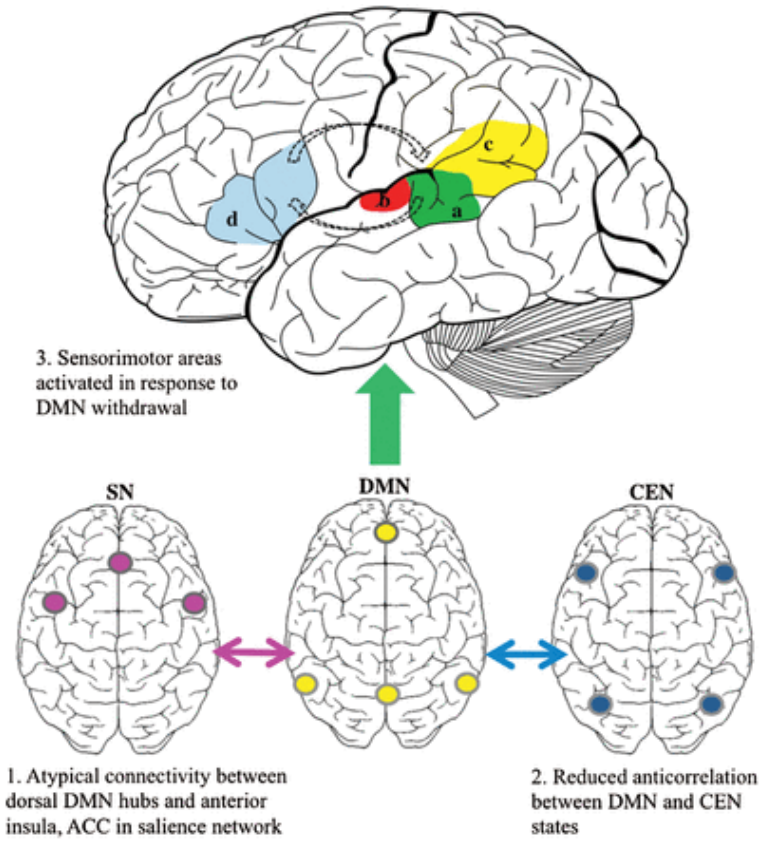

图 8　幻听与脑 RSNs[106]

Fig. 8 Auditory hallucinations and the brain's RSNs

Initial AH studies focused on resting connectivity in auditory and language regions (upper figure), primarily identifying atypical connectivity of left posterior STG (a), PAC (b), and the TPJ area (c). Findings of atypical resting connectivity between left IFG (d) and STG are inconsistent although both areas are often implicated during AH. More recent findings implicate atypical interaction of the DMN, SN, and CEN in those prone to AH (lower figures). CC, anterior cingulate cortex; AH, auditory hallucination; CEN, central executive network; DMN, default mode network; IFG, inferior frontal gyrus; PAC, primary auditory cortex; SN, salience network; STG, superior temporal gyrus; TPJ, temporoparietal junction.

我们前期的研究发现，首发 SZ 幻听患者丘脑体积降低[36]，并且丘脑前辐射 FA 降低[40]，推测由于丘脑体积降低，导致丘脑-皮层投射中的白质纤维损伤，其结果便表现为丘脑对听觉皮层的兴奋性调控代偿性增强；同时，tDCS 或 TMS 治疗有效的 SZ 幻听患者听觉皮层 CBF 或 rCBF 治疗前较治疗后高[55-57]，提示治疗前其神经活动增强，SZ 幻听患者听觉皮层神经活动增强推测可能就是丘脑兴奋性调控的结果。Horga 等[107]发现 SZ 幻听患者杏仁核与听觉皮层和丘脑的连接增强，伴随杏仁核与内侧前额叶皮层的连接减弱。因此，丘脑对听觉皮层的异常调制可能是 SZ 幻听产生的病理机制。

另外，幻觉产生时，在异常或错误推测的预测性编码模型中，编码精度的敏感性控制出现异常[108-110]。无法增强感觉准确性是皮层高级处理中枢的代偿性改变，研究表明，SZ患者就表现出无法调节传递预测性感觉信息的神经元的敏感性[111]。因此，SZ患者丘脑-听觉皮层DRD2通路功能亢进，听觉皮层对丘脑上行传入的反应敏感性增强，进而导致SZ患者在缺乏外部声音刺激时产生听觉，即为幻听。另外，一项最新的心理学研究发现，幻听患者（SZ为主）的认知功能障碍使其无法正常进行自我转换，即不能转换对声音的注意[112]，且事件相关电位研究证明SZ幻听患者的听觉抑制系统受损[113]。综上所述，**与听觉/语言/记忆/信息滤过相关脑区有关的神经通路异常可能是SZ幻听的重要神经机制，可能揭示了SZ幻听的病理生理基础。**

4 当前 SZ 幻听相关神经影像学研究的局限性及解决途径

SZ 幻听神经机制错综复杂，涉及多种脑结构与功能改变，综合运用高分辨 MRI、BOLD-fMRI、ASL、DTI 等神经影像学技术，从涉及脑结构与功能的多个角度阐释 SZ 幻听的神经机制十分必要。但是，尽管前期的研究已经为 SZ 幻听积累了一些神经影像学证据，**研究策略、被试选择、分析方法等多方面的局限性导致上述影像学证据的意义还十分有限**，并不能很好地应用于指导其诊疗的临床实践过程当中。

首先，以往的研究多采用 SZ 幻听患者与对照组直接比较的研究策略，而二者之间的差异不仅包括幻听所反映出来的脑结构和功能异常，同时也包括 SZ 这一疾病本身的脑改变。因此，该研究策略产生的结果是一种混合的效应，而非幻听单一因素所产生的影响。另外一种研究策略是比较 SZ 患者与对照组之后再将其中的幻听相关变量单独提取出来进一步研究，往往也只是做影像参数与幻听量表积分的相关性分析，研究目的也非直接针对幻听。如果想要针对幻听特异性表现展开研究则应将 SZ 患者划分为幻听和非幻听两组并进行比较，此时得到的结果才对幻听更具有特异性，即在去除 SZ 中其他相同的特质，仅体现幻听的异常。这也正是本课题中所采用的研究策略。

其次，在前期的研究中，被试往往是接受过抗精神病药物、重复 TMS（repetitive TMS，rTMS）、tDCS、电抽搐治疗（electroconvulsive therapy，ECT）、心理干预等治疗的非首发 SZ 患者。由于上述治疗措施会对患者的脑结构和功能产生巨大的影响，那么再用这类患者进行研究，所检测到的差异也不能更为确切地反映幻听原本的作用，而是多种混杂因素共同的效应。为了去除这些混杂因素的干扰，需要采用首发未经治疗的 SZ 患者。因此，在本课题的大部分研究中，仅纳入首发患者，从而尽可能降低其他混杂因素带来的干扰。

再次，从方法学上来讲，过去的研究多采用数据驱动（data-driven）的分析方法进行研究，而非假设驱动（hypothesis-driven）。一方面是因为对于 SZ 幻听的理解还不后深入，无法提出较为完善的假设，采用数据驱动的方法更易获得结果，另一方面是由于所采用方法自身的不足，例如 ALFF、ReHo、CBF 等也确实更适宜数据驱动的分析方法。随着对 SZ 幻听的认识不断加深，在后续的研究中可以采用数据驱动与假设驱动相结合的分析方法，即先做数据驱动分析，再根据其结果进一步做假设驱动分析，将数据驱动分析获得的结果作为假设驱动分析的基础。另外，sDCM、GCA 等可进行连接方向分析的相对较新的技术则更适用于假设驱动的分析方法。而

这些改进在本课题的研究中也均有体现。

针对上述提及的SZ幻听相关神经影像学研究的局限性，本课题分别采取了相应措施予以解决，能够在一定程度上化解这些局限性的弊端，以期更为全面、准确地探讨SZ幻听背后的神经基础。另外，针对幻听的功能成像研究被分为两类：一类是状态研究（state-study），另一类是特质研究（trait-study）。前者是指被试正在经历幻听时进行扫描，结果更倾向于幻听状态的体现；后者是幻听患者在扫描时未出现幻听，则是对幻听易感性的研究。据此，本研究属于上述分类中的后者。

5 总结

综上所述，深入探究 SZ 幻听的神经机制具有重要的临床意义，尽管前期 fMRI 研究为 SZ 幻听的神经病理学机制提供了较多证据，但研究策略、被试选择、分析方法等多方面仍存在明显的局限性。因此，**本研究综合运用多模态 fMRI 及数据分析技术，全面探讨 SZ 幻听的神经影像学基础，从而深入阐述其重要的神经机制**。通过对 SZ 幻听的神经影像学基础及神经机制的研究，进一步补充并完善已有的理论，亦可将调控相应脑区或环路的神经活动作为 SZ 治疗的一种具有潜在价值的手段。

正　　文

实验一　精神分裂症言语性幻听言语监控、想象及产生功能障碍：脑血流及其复杂网络研究

Long-Biao Cui, Gang Chen, Zi-Liang Xu, Lin Liu, Hua-Ning Wang, Li Guo, Wen-Ming Liu, Ting-Ting Liu, Shun Qi, Kang Liu, Wei Qin, Jin-Bo Sun, Yi-Bin Xi, Hong Yin

Psychiatry Res Neuroimaging, 2017; 260:53-61.

作为全世界疾病负担的首要原因之一，SZ 是一种严重且复杂的精神疾病，全球患病率约为 1%[1, 19]。言语性幻听是 SZ 的一个特征性症状，容易慢性化并出现耐药[4]。揭示 SZ 言语性幻听背后的神经机制对于治疗这一严重的精神疾病具有重要的临床意义。在过去的十年中，由于现代功能神经影像学方法的进步，基于症状的研究已经为涉及 SZ 言语性幻听的脑区或网络改变提供了初步的认识。作为局部脑功能特征，CBF（脑血流）通常与脑代谢紧密联系，目前 ASL 就可以对它进行定量[114]。

借助 ASL，近期的在体研究已经逐步揭示了一些神经精神疾病的病理生理学基础，包括额颞叶变性、阿尔茨海默病以及 SZ[115-117]。ASL 也已经成功地测量到对 tDCS 或 TMS 临床反应较好的 SZ 言语性幻听患者中左侧听觉皮层与 Broca 区的 CBF 降低[57, 64]。更为重要的是，不同脑区的 rCBF 并非独立，现已发现同伦皮层区域之间的 CBF 同时振动最高，并且 CBF 连接构成的功能网络与解剖连接或 FC 构成网络的网络特性相似[118]。最近，采用 ASL-CBF 数据的组水平 ICA，Kindler 等发现 SZ 患者 DMN 中的 CBF 连接增强[119]。

然而，SZ 言语性幻听的 CBF 及其连接仍不明了。SZ 言语性幻听患者 CBF 改变的脑区是否具有与其他脑区异常的 CBF 连接模式尚不清楚。在本实验中，采用 ASL 从 CBF 及其连接的角度研究静息态下的 SZ 言语性幻听与非幻听患者的脑改变。

1.1 材料

1.1.1 被试

本研究由第四军医大学第一附属医院药物临床试验伦理委员会批准，所有参与者均提供了书面知情同意。被试分别来自我院门诊及当地社区，自 2011 年 5 月至 2013 年 12 月累计 25 名 SZ 言语性幻听患者、25 名 SZ 非幻听患者、25 名健康对照（healthy controls，HCs）纳入本实验，他们的人口学特征匹配。SZ 的纳入标准包括：（1）两位经验丰富的精神科医师根据 DSM 第四版修订版（DSM, Fourth Edition, Text Revision，DSM-IV-TR）对患者进行评估，用全部可用信息做出 SZ 的一致诊断；（2）评价扫描时的阳性与阴性症状量表（Positive And Negative Syndrome Scale，PANSS）积分（≥ 60）[120]；（3）言语性幻听患者是指在过去四周内每天至少有一次言语性幻听，其严重性用幻听量表（Auditory Hallucination Rating Scale，AHRS）[121]评估，未曾或过去两年内未经历幻听的患者为非幻听组；（4）被试为右利手且他们的生物学父母为汉族人。下述排除标准适用于所有组：（1）患有其他轴 I 或 II 精神疾病；（2）接受了 rTMS、tDCS、ECT 或行为学治疗；（3）明显的神经病或系统性疾病；（4）之前 30 天内诊断为物质滥用或之前六个月内诊断为物质依赖；（5）怀孕以及 MRI 检查禁忌症，包括体内安装心脏起搏器或其他金属植入物；（6）MRI 扫描中头动大于 3.0 mm 和/或 3.0 °。言语性幻听与非幻听患者既包含首发未经治疗的 SZ 患者、又包括非首发入组前接受了抗精神病药物治疗的 SZ 患者。通过广告从当地社区招募 HCs，前驱期问卷（Prodromal Questionnaire）[122]用于确认 HCs 中没有任何精神病症状。他们同样由这两名精神科医师评估，患者组的剔除标准同样适用于 HCs。样本的人口学与临床特征描述见**表 1-1**。

1.1.2 仪器设备

实验中使用的主要仪器为 3.0 T 西门子 Magnetom Trio Tim 成像系统与 8 通道相控阵头线圈（德国埃朗根）。

1.2 方法

1.2.1 图像采集

所有影像学数据均在西京医院放射科获取。高分辨 T1 加权 3D 解剖数据运用 3D

磁化准备快速采集梯度回波（3D magnetization prepared rapid acquisition gradient echo，3D MPRAGE）序列采集（TR：2530 ms；TE：3.5 ms；翻转角：7°；视野：256 mm ×256 mm；矩阵：256 ×256；层厚：1 mm；层间距：0 mm；层数：192）。图像分辨率是 1 mm ×1 mm ×1 mm。静息态灌注成像采用脉冲式 ASL（pulsed ASL，pASL）序列采集（TR：2805 ms；TE：13 ms；标记后延迟：1800 ms；翻转角：90°；视野：256 mm ×256 mm；层厚：3 mm；层间距：0.75 mm；层数：31），静息态 ASL 扫描的总采集时间是 4 min 20 s。耳塞与定制的头线圈软垫用于降低成像系统的噪声并减小头动，从而减弱图像扫集时的运动伪影，保证成像质量。数据采集期间嘱被试头部尽量不动、保持清醒、闭眼。扫描开始前和结束后判断被试的清醒状态，被试均确定扫描中他们一直保持清醒。运用 PICORE 灌注模式自动控制图像质量，并在进一步的分析前仔细检查每个被试的图像，从而确保数据质量。

1.2.2 CBF 计算

根据 Wang 等的方法[115, 123, 124]，数据分析在 Arterial Spin Labeling Perfusion MRI Signal Processing Toolbox（ASLtbx; http://cfn.upenn.edu/~wangze/ASLtbx.php）中进行。其中一部分是基于 SPM12（http://www.fil.ion.ucl.ac.uk/spm/）完成的，详细步骤已在上述研究中进行了描述，包括图像重设原点、运动校正、配准到每位被试的结构像然后再到 PET-灌注模板最后用仿射变换到 MNI（Montreal Neurological Institute）空间、高斯核 6 mm 的半高全宽（full width at half-maximum，FWHM）空间平滑、去除非脑组织以及 CBF 量化。

1.2.3 CBF 连接分析

CBF 连接方法的全部描述见于 Melie-Garcia 等的报道[118]。首先，采用将全脑（不包括小脑）分割成 90 个区域的 AAL（automated anatomical labeling）图谱[125]进行脑分割来预处理同组内所有被试的 CBF 图（SZ 言语性幻听患者、SZ 非幻听患者以及 HCs），生成三个“n”（被试数目）行乘以 90（脑区数目）列的矩阵。其次，将每列之间 CBF 值的 Pearson 相关性定义为连接，每组构建一个 90 ×90 的 CBF 连接矩阵。Fisher *z* 检验（http://www.fon.hum.uva.nl/Service/Statistics/Two_Correlations.html）用于比较组间差异。最后，计算网络特性以描述脑 CBF 网络特征。这些 CBF 网络特性（特征路径长度、聚类系数、局部效能与全局效能）的计算稀疏度值从 0.5 到 0.9 的范围内，每步 0.05。

1.2.4 统计学分析

采用两样本 *t*-检验在体素水平比较 CBF 的组间差异。由于被试人口学特征的差异无统计学意义，统计学分析时并未将年龄、性别、受教育年限以及病程作为协变量进行回归。根据 REST（Resting-State fMRI Data Analysis Toolkit）V1.8（http://restfmri.net/forum/REST_V1.8）[126]中的 AlphaSim 校正阈值模块，多重比较校正采用 AlphaSim 法（$P < 0.05$，cluster ≥ 13）。对于每个被试，提取存在组间差异的每个集群的平均 CBF 值用于相关性分析和受试者工作特征（receiver operator characteristic，ROC）分析。相关性分析中，分别计算每组被试的脑功能测量值（CBF 值）与症状严重性（AHRS 与 PANSS 积分）之间的 Pearson 相关系数，多重比较校正的 $P < 0.05$（Bonferroni 校正）时认为差异具有统计学意义。另外，ROC 分析用于评估这些影像学测量值区分 SZ 言语性幻听与非幻听患者的诊断能力。运用 SPSS 软件（version 13.0; SPSS Inc., Chicago, IL, USA）做相关性与 ROC 分析。

1.3 结果

1.3.1 人口学与临床特征

表 1-1 总结了被试的人口学与临床特征。SZ 言语性幻听、非幻听患者与 HCs 在年龄、性别、利手或受教育年限上差异无统计学意义。正如所预料的，SZ 言语性幻听患者的 PANSS 总分与阳性症状积分比非幻听患者更高（$P < 0.05$）。除了 AHRS 积分，SZ 言语性幻听与非幻听患者其他临床特征的差异无统计学意义（$P > 0.05$）。

表 1-1 AVHs 患者（n = 25）、非幻听患者（n = 25）以及 HCs（n = 25）的人口学与临床特征

Table 1-1 Demographic and clinical characteristics of patients with AVHs (*n* = 25), patients without AVHs (*n* = 25), and HCs (*n* = 25)

Characteristics	AVHs patients	Non-AVHs patients	HCs
Age (years)	24 ±7	24 ±5	26 ±5
Sex (male/female)	14/11	13/12	12/13

Education (years)	14 ±2	14 ±2	15 ±2
Handness (right/left)	25/0	25/0	25/0
Duration of illness (months)	14 ±19	18 ±21	—
First episode (yes/no)	17/8	21/4	—
PANSS Total Score	109 ±12*	92 ±22	—
PANSS Positive Score	31 ±6*	21 ±9	—
PANSS Negative Score	27 ±4	23 ±10	—
PANSS General Psychopathology	52 ±8	48 ±9	—
AHRS Score	27 ±5	—	—

The three groups were matched for demographic characteristics. Data are mean ±SD. *$P < 0.05$ versus Non-AVHs patients. PANSS, Positive and Negative Syndrome Scale; AHRS, Auditory Hallucination Rating Scale.

1.3.2 CBF 组间差异

SZ 言语性幻听与非幻听患者之间 CBF 的差异见于表 1-2 和图 1-1。与非幻听患者相比，言语性幻听患者表现为双侧额上/中回与中央后回、右侧补充运动区 CBF 降低。与 HCs 相比，言语性幻听患者表现出双侧额上/中回与中央前回、左侧顶下小叶、额下回与岛叶、右侧中央后回、角回及尾状核 CBF 降低。另外，SZ 非幻听患者比 HCs 降低的 CBF 位于左侧额中回。

表 1-2 CBF 存在差异的脑区

Table 1-2 Brain regions with significant differences in CBF

Regions	**Cluster size**	**Peak *t* value**	**Peak MNI coordinate**		
			X	**Y**	**Z**
AVHs < Non-AVHs					
Right superior frontal gyrus	73	−4.6526	18	62	20
Right superior frontal gyrus	25	−4.4305	24	30	54

Right medial superior frontal gyrus	130	−4.2890	6	56	0
Left medial superior frontal gyrus	16	−4.2936	−10	52	8
Left superior frontal gyrus	14	−4.2184	−26	42	42
Right middle frontal gyrus	22	−4.3143	26	48	34
Left middle frontal gyrus	127	−4.8361	−38	54	14
Left middle frontal gyrus	19	−4.1254	−32	38	36
Right postcentral gyrus	63	−4.4324	24	−34	58
Right postcentral gyrus	48	−4.3835	36	−30	62
Left postcentral gyrus	50	−4.6303	−50	−28	52
Left postcentral gyrus	112	−5.2454	−16	−40	72
Right supplementary motor area	13	−4.5152	16	16	66
Non-AVHs < HCs					
Left middle frontal gyrus	16	−4.2904	−42	54	22

P < 0.05 (correction thresholds by AlphaSim).

1.3.3 CBF 与临床数据的相关性及 ROC 分析

在相关性分析中，存在差异脑区的 CBF 值与 AHRS 及 PANSS 阳性症状积分并无相关性（表 1-3）。ROC 分析显示了 CBF 值区分 SZ 言语性幻听与非幻听患者的能力，降低的 CBF 值的 ROC 曲线下面积列于表 1-4。

1.3.4 CBF 连接模式

本实验计算了三组中 AAL 模板定义的 90 个脑解剖结构之间的 CBF 矩阵（图 1-2）。当呈现三组的连接矩阵时，将 CBF 存在组间差异脑区所在的行标记了出来。图 1-3 呈现了连接系数大于 0.6 或小于−0.6（代表连接系数的 FDR 校正的 *P* 值水平为 0.05）。Melie-Garcia 等的方法只能计算每一组的矩阵[118]，而无法比较组间的连接差异。因此，运用 Fisher *z* 检验比较两组间连接的差异。表 1-5 为言语性幻听与非幻听患者之间 CBF 存在差异脑区的显著连接的 *z* 值。

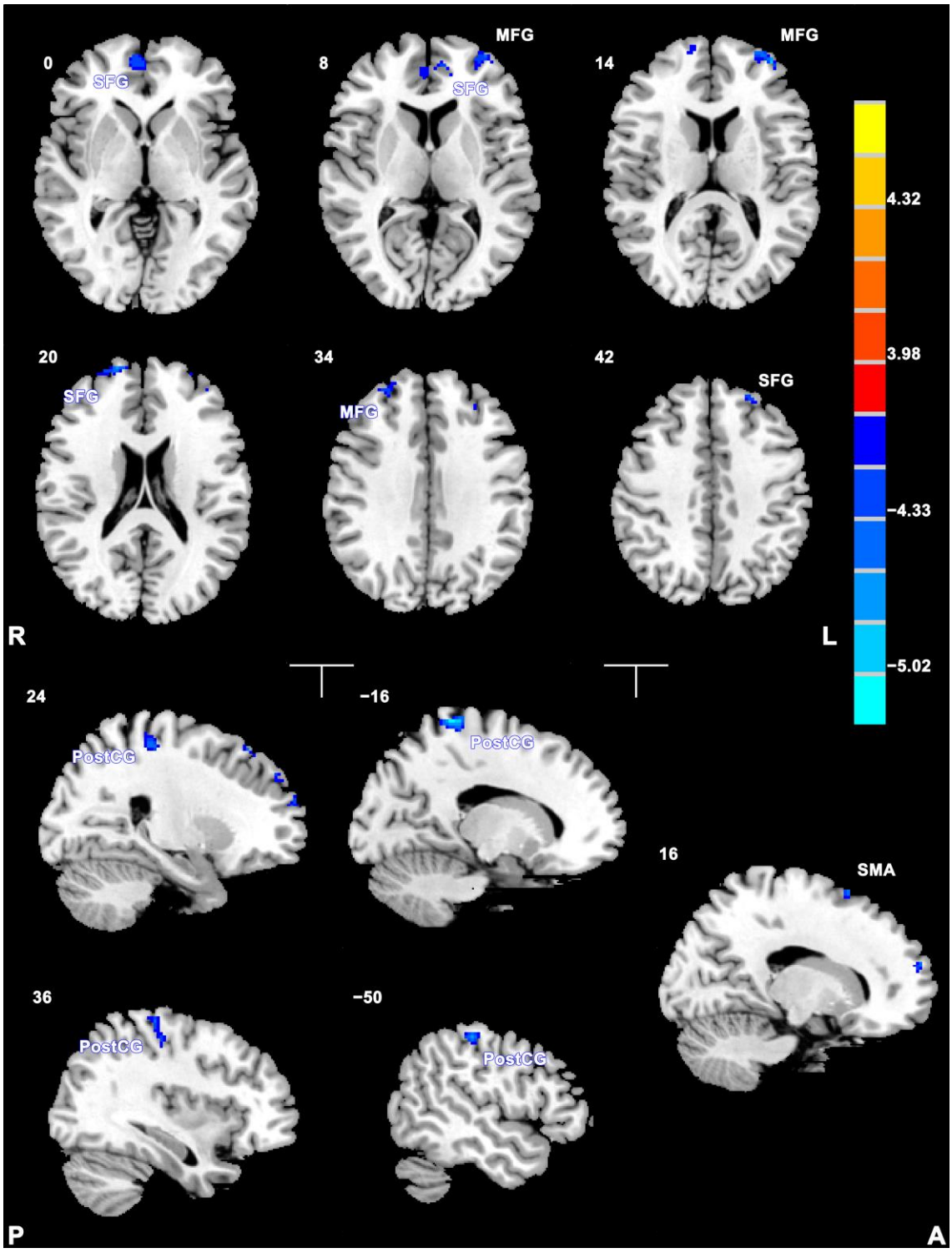

图 1-1 SZ 言语性幻听与非幻听患者之间 CBF 存在差异的脑区

Fig. 1-1 Brain regions with significant CBF differences between SZ patients with and without AVHs

The warm color represents increased CBF, and the cold color denotes decreased CBF. AG, angular gyrus; MFG, middle frontal gyrus; PostCG, postcentral gyrus; SFG, superior

frontal gyrus; SMA, supplementary motor area; SOG, superior occipital gyrus; SPG, superior parietal gyrus.

表 1-3 SZ 言语性幻听患者幻听严重性（AHRS 评分）与 CBF 值之间的相关分析

Table 1-3 Correlation analysis between CBF values and the severity of AHVs (AHRS score) of SZ patients with AVHs

Regions	***r* value**	***P* value**
Right superior frontal gyrus	−0.10	0.63
Right superior frontal gyrus	0.18	0.39
Right medial superior frontal gyrus	−0.22	0.30
Left medial superior frontal gyrus	−0.16	0.43
Left superior frontal gyrus	0.13	0.55
Right middle frontal gyrus	−0.24	0.24
Left middle frontal gyrus	0.04	0.85
Left middle frontal gyrus	0.08	0.71
Right postcentral gyrus	−0.19	0.36
Right postcentral gyrus	−0.21	0.31
Left postcentral gyrus	0.20	0.33
Left postcentral gyrus	0.13	0.52
Right supplementary motor area	−0.18	0.39

表 1-4 ROC 曲线下面积

Table 1-4 Area under ROC curve

Regions	**Area**	**95% CI**
AVHs < Non-AVHs		

Right superior frontal gyrus	0.87	0.77, 0.97
Right superior frontal gyrus	0.81	0.69, 0.93
Right medial superior frontal gyrus	0.87	0.77, 0.97
Left medial superior frontal gyrus	0.84	0.73, 0.95
Left superior frontal gyrus	0.81	0.70, 0.93
Right middle frontal gyrus	0.84	0.74, 0.95
Left middle frontal gyrus	0.88	0.78, 0.97
Left middle frontal gyrus	0.80	0.68, 0.92
Right postcentral gyrus	0.83	0.72, 0.95
Right postcentral gyrus	0.83	0.71, 0.94
Left postcentral gyrus	0.84	0.73, 0.95
Left postcentral gyrus	0.84	0.73, 0.95
Right supplementary motor area	0.82	0.70, 0.94

CI, confidence interval.

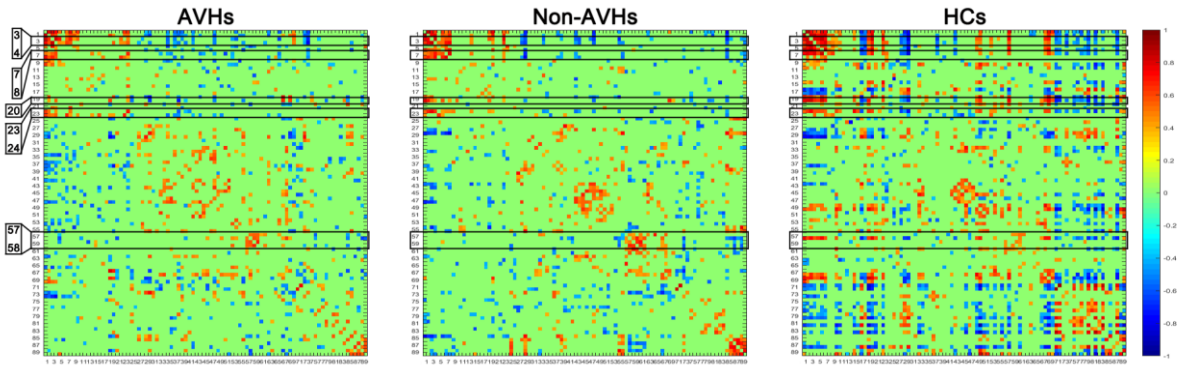

图 1-2 通过计算被试局部 CBF 的 Pearson 相关性获得的 CBF 连接矩阵

Fig. 1-2 The CBF connectivity matrix obtained by calculating Pearson's correlation between regional CBF across subjects

Numbers in AAL atlas on the left side refer to different brain regions with significant CBF differences between SZ patients with and without AVHs. 3, Frontal_Sup_L, left superior frontal gyrus; 4, Frontal_Sup_R, right superior frontal gyrus; 7, Frontal_Mid_L, left

middle frontal gyrus; 8, Frontal_Mid_R, right middle frontal gyrus; 20, Supp_Motor_Area_R, right supplementary motor area; 23, Frontal_Sup_Medial_L, left medial superior fontal gyrus; 24, Frontal_Sup_Medial_R, right medial superior fontal gyrus; 57, Postcentral_L, left postcentral gyrus; 58, Postcentral_R, right postcentral gyrus. The color bar indicates the correlation coefficient value.

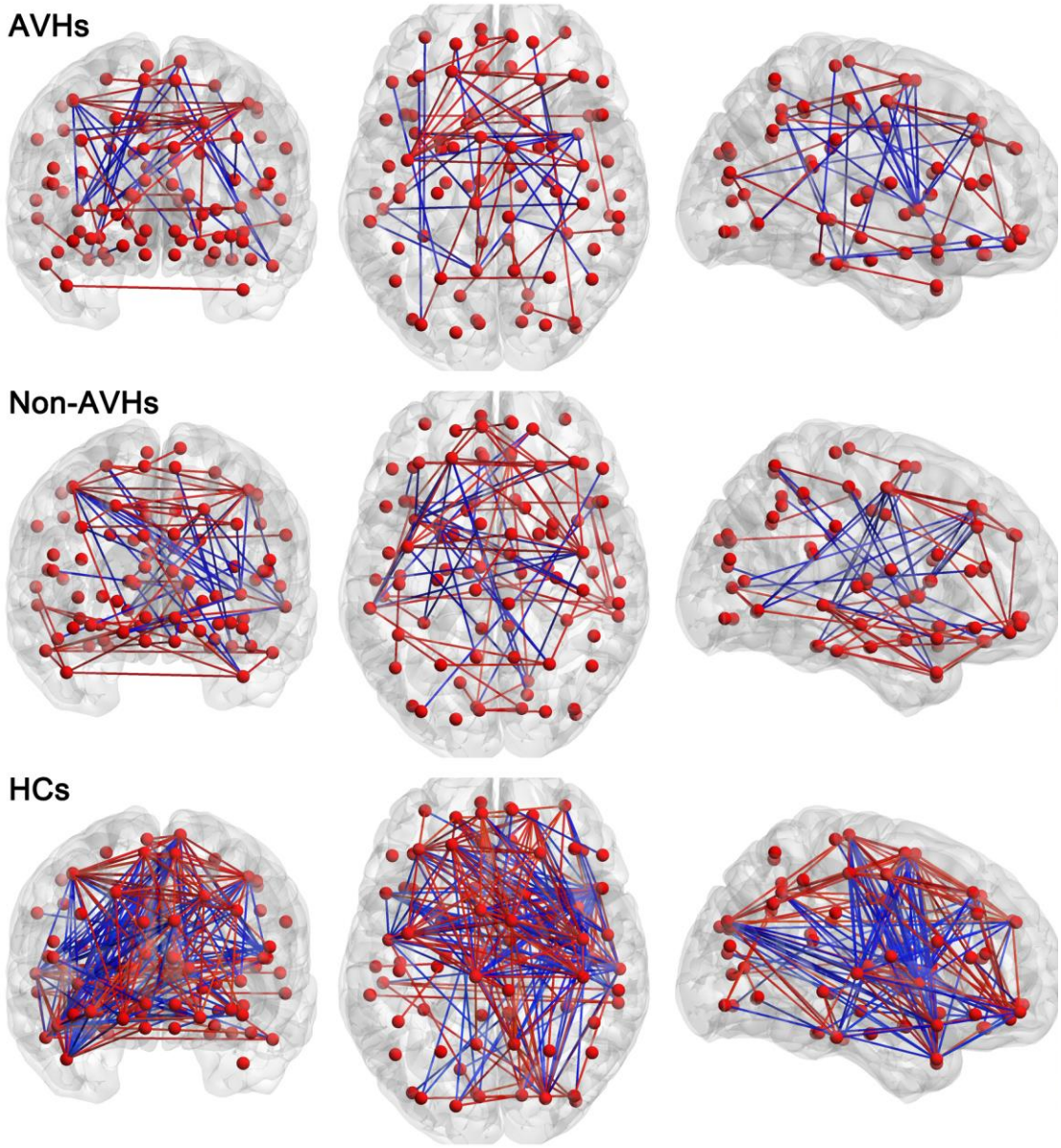

图 1-3 每组的 CBF 连接

Fig. 1-3 CBF connections of each group

The CBF networks showing connections with correlation coefficient value larger than 0.6

or less than −0.6. Line color indicates the positive (red) or negative (blue) coefficient.

表 1-5 言语性幻听与非幻听患者之间 CBF 存在差异脑区的显著连接的 *z* 值

Table 1-5 *z* values of significantly different connectivity with regions of different CBF between AHVs and Non-AVHs patients

Connectivity	***z* value**	***P* value**
Left SFG-left orbital SFG	2.9376	0.0107
Left SFG-left medial SFG	−3.2870	0.0036
Left SFG-left fusiform gyrus	2.8833	0.0125
Left SFG-right putamen	−3.0013	0.0088
Left SFG-left MTG	2.8012	0.0158
Right SFG-right putamen	−3.4944	0.0018
Left MFG-right MFG	−3.6714	0.0009
Left MFG-left insula	2.8746	0.0128
Right MFG-left insula	3.5115	0.0017
Right SMA-left PreCG	−3.6088	0.0012
Right SMA-right hippocampus	−3.0035	0.0088
Right SMA-left pallidum	3.2249	0.0044
Left medial SFG-right medial SFG	2.8878	0.0123
Left PostCG-left angular gyrus	−2.8430	0.0140
Right PostCG-right IOG	3.7866	0.0006

IOG, inferior occipital gyrus; MFG, middle frontal gyrus; MTG, middle temporal gyrus; PreCG, precentral gyrus; PostCG, postcentral gyrus; SFG, superior frontal gyrus; SMA, supplementary motor area; SPG, superior parietal gyrus.

值得注意的是，与非幻听患者相比，SZ 言语性幻听患者特征路径长度较长、聚类系数较小、局部效能较低，全局效能相对较高（图 1-4）。总体而言，两个 SZ 患者组比 HCs 网络内的连接降低。

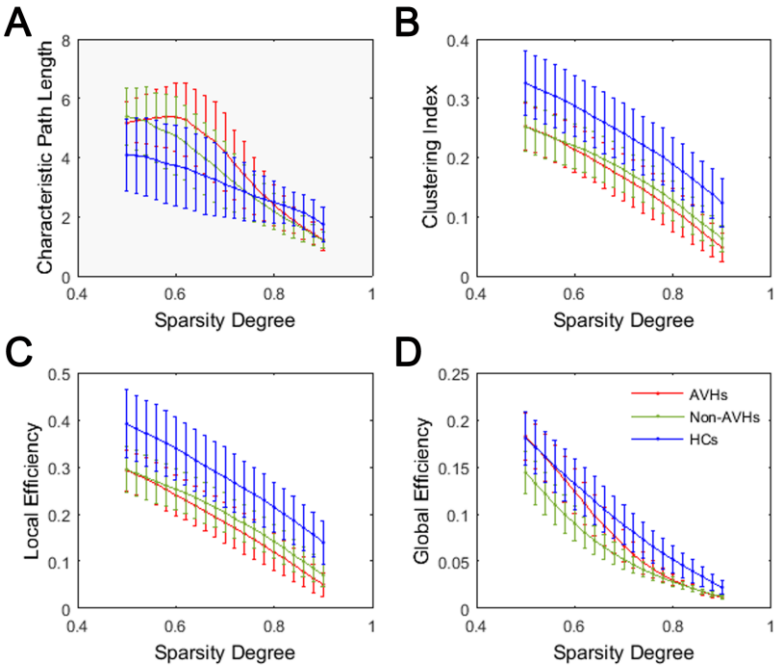

图 1-4 全局网络特性

Fig. 1-4 Global network properties

The characteristic path length, clustering index, local efficiency, and global efficiency decrease as the sparsity degree increases.

1.4 讨论

在本实验中，与非幻听患者相比，我们在 SZ 言语性幻听患者双侧 DLPFC 检测到更低水平的 CBF，这与最具影响力的认知模型之一较为一致，该模型提出对内部言语的自我监控受损导致将言语思维错误的辨识为外部来源[127]。然后，我们还发现 CBF 降低位于左侧补充运动区与双侧中央后回，它们参与言语想象（补充运动区）[8, 128]和产生（中央后回）[129]。此外，根据 ROC 分析，CBF 值可能是判断 SZ 言语性幻听易感性的有效指标。复杂网络分析证明 SZ 言语性幻听患者 CBF 连接功能障碍。以上发现在两个方面拓展了当前对于言语性幻听的认识：一是将言语想象脑区（补充运动区）与 SZ 言语性幻听联系起来，二是检测到言语性幻听的 CBF 连接模式介于 HCs 与非幻听之间的水平。

一些前期的研究已经将 ASL 应用到 SZ 患者 CBF 特征[117, 119, 130, 131]以及 TMS 改变 SZ 言语性幻听患者 CBF[56]的研究当中。在本实验中，两个患者组均显示出左侧

额中回 CBF 水平降低，这也是 Zhu 等、Scheef 等、Kinder 等在 SZ 患者中检测到的结果[117, 119, 130]。除了左侧额中回以外，Zhu 等发现左侧岛叶 CBF 降低[117]，这也是本实验在 SZ 言语性幻听患者与 HCs 比较中的发现。除此之外，这些研究中还有一些不完全一致的发现。本实验中基于症状的亚分型（即言语性幻听与非幻听）和被试的临床异质性可能引起了这些矛盾；另一个可能的因素是所采用的序列，即本实验是 pASL 而他们的研究是伪连续 ASL（pseudocontinuous ASL，pcASL）。根据《*ASL 白皮书*》中达成的共识，pcASL 的信噪比（signal-to-noise ratio，SNR）比 pASL 更高，而 pASL 则是用单个短脉冲或者数量有限的脉冲即可将血液作为标记进行灌注成像，这在高场强的磁场中更优[132]。另外，Zhu 等和 Liu 等用更大样本量的 SZ 患者做了被试的 CBF 连接分析[117, 133]，但是它们并未基于症状对患者进行分组。

再回到本实验的发现上来，首先，我发现在 SZ 言语性幻听患者双侧 DLPFC 中广泛的 CBF 降低。PFC 几乎直接连接每个脑功能单元[134]，这些特殊的连接使它更适宜协调并整合其他脑区的功能[135]。DLPFC 是 PFC 的重要组成部分，可能发挥监控语言处理中言语产生的作用，尤其是在 SZ 言语性幻听患者当中[136]。越来越多的 fMRI 研究已经表明 DLPFC 功能异常与言语性幻听有关[51, 69, 137-139]，前期的研究已经证明了 DLPFC 与 SZ 言语性幻听之间的关联。除此之外，神经活动伴随着代谢改变，PET 可以通过监测各脑区代谢情况来反映脑功能的变化，是在生理状态下直接观察脑功能的成像技术。Horga 等[107]的一项 PET 研究中纳入了处于急性发作期具有严重幻听的 SZ 患者，在 PET 扫描时采取两种模式，静息状态和给予类似幻听的声音刺激，结果显示患者边缘系统、边缘旁系统和左侧杏仁核在施加刺激时显著激活。研究还发现 SZ 幻听患者杏仁核与听觉皮层和丘脑的连接增强，伴随杏仁核与内侧前额叶皮层的连接减弱。

运用 FC 分析，Lawrie 等发现 SZ 执行语言任务时左侧 DLPFC 与颞上/中回连接减弱，该连接与言语性幻听的严重性呈负相关[51]。静息状态下，SZ 言语性幻听患者比非幻听患者比左侧 DLPFC 与 Wernicke 区的连接明显增强[69]。此外，Sommer 等发现左侧 DLPFC 与额下回（代表 Broca 区）连接减弱[137, 138]。采用脑磁图分析，Kawaguchi 等也证明 SZ 言语性幻听中左侧 DLPFC 存在功能障碍[139]。与这些无外部干预的前期发现一致，DLPFC 也受下述提及的 tDCS 或 TMS 调节。

临床中，运用最常用的方式 tDCS 能够明显减弱 SZ 患者的难治性言语性幻听[136, 140-142]，即将阳极置于左侧 DLPFC、阴极置于左侧颞顶联合区[143]。另外一个治疗 SZ 的工具是 rTMS。一方面，通过 FC 分析，tDCS 和 rTMS 都能增强左侧颞顶联合区与 DLPFC 之间的连接[136, 144]。另一方面，rTMS 增强 SZ 言语性幻听患者左侧 DLPFC 的局部活动[145]，上述发现为这些方法治疗 SZ 幻听效果的可能机制提供了证据。曾经有推测 SZ 易患幻听是言语产生和监控之间失去联系的结果，分别涉及补充运动区和 DLPFC[138]。在 CBF 方面，本实验证明 SZ 言语性幻听患者针对内部言语的自我监控系统（DLPFC）活动减弱。

然后，与非幻听患者相比，本实验中的 SZ 言语性幻听患者右侧补充运动区 CBF 降低。尽管尚无关于功能成像研究比较无幻听时言语性幻听相关脑区活动中补充运动区活动的典型报道[83, 146]，然而在 McGuire 等的一项语义研究中[8]，言语想象时 SZ 幻听患者补充运动区活动较 HCs 减弱。另外，Raij 等发现 SZ 言语性幻听患者幻听时比言语想象时补充运动区的活动更弱[128]。因此，有关补充运动区 CBF 的结果强烈提示了它的功能缺陷可能与 McGuire 等解读的“the loss of the sense that the inner speech is self-generated”[8]相关。

最后，在本课题组前期的体素镜像同伦连接研究中，SZ 言语性幻听患者双侧顶上小叶、前扣带皮层之间的连接减弱，且该连接与 PANSS 阳性症状积分呈负相关[53]，而本实验中，CBF 水平在双侧中央后回对称性降低。换言之，用不同的序列和数据分析方法，在 SZ 言语性幻听患者的双侧同伦脑区都发现了功能变化。此外，MRI 的体积研究表明双侧中央后回体积降低与 SZ 言语性幻听的严重性具有相关关系[34, 147]。除了结构异常，上述结果进一步为 SZ 言语性幻听患者双侧中央后回功能异常提供了证据。通过纳入比较经历幻听与无幻听状态的研究，Kühn 等的一项荟萃分析[84]建立了 SZ 言语性幻听与双侧中央后回活动的关联，而中央后回是无声言语（默读）相关脑区[148]，因此也被认为参与言语产生。

采用上述提及的方法，我们做了 CBF 连接并分析了网络特性。与采用受到多种生理参数影响的 BOLD 数据的 FC 相比，CBF 连接则具有更为确切的生理意义，且仅受 rCBF 调节。计算得到的网络特性，包括聚类系数、特征路径长度、局部效能及全局效能，表明 SZ 患者无法在脑功能网络内有效地进行信息传递，且较 HCs 网络的抗干扰能力降低[149]。同样，SZ 言语性幻听患者的三个网络特性的数值接近于非幻

听患者。更为重要的是，他们还有一个特性，即全局效能，则介于 HCs 和非幻听患者之间的水平，提示了一种更大更宽网络内较为活跃的整合能力[150]。该研究为脑区之间 CBF 网络拓扑性质提供了综合性描述。

当然，本实验的一些不足也需承认。首先，CBF 值与 AHRS/PANSS 阳性症状积分无相关性，仅能提示与幻听特质相关的脑功能障碍，而与幻听严重性无关。为了检测到 SZ 亚型的微弱差异，也就是本实验中的言语性幻听，机器学习法可能会是更好的选择[151]。其次，本实验中治疗的相关信息（例如药物、剂量、疗程）不足 ，以至于无法评估抗精神病药物对患者脑功能造成的影响。尽管如此，仍要建议探索 SZ 言语性幻听背后的神经机制十分重要，在患者临床获益之前这需要更大的努力与投入。

总而言之，本实验证明，与非幻听患者相比，SZ 言语性幻听患者 CBF 异常脑区包括双侧 DLPFC（内部言语监控）与中央后回（言语产生），以及右侧补充运动区（言语想象）。另外，由 CBF 网络显示的复杂网络测量表明 SZ 言语性幻听中不同功能单元之间的通讯模式异常。

实验二　首发精神分裂症言语性幻听大尺度脑网络紊乱：结构连接的 rich club 组织研究

Long-Biao Cui, Yongbin Wei, Martijn P. van den Heuvel, René S. Kahn, Hong Yin

In preparation

人脑是由结构上与功能上相互连接的脑区构成的复杂网络，实验一从一定程度上再次证明了这一现象。人脑连接组[152, 153]以及比较连接组学[154]的提出也正强调了脑作为整体的网络组织特性，人脑功能的发挥便是依赖于此，相反，其功能障碍可能就是脑网络信息传递异常的最终结果[155]。随着研究的不断积累与深入，这种大尺度脑网络与神经系统微观尺度的发现联系越来越紧密[156]。某些高度连接的重要脑区，即 hub 节点，在全脑网络的拓扑学中至关重要[157, 158]，它们在正常的脑中共同形成 rich club[159]，而正是这些 rich club 连接在脑区间的通讯中发挥重要作用[160]。

van den Heuvel 等前期研究发现，SZ 存在结构网络 rich club 组织受损，并扰乱脑功能动力学[104]，这一重要的 rich club 的信息传输紊乱可能参与 SZ 的病理生理学。那么，作为 SZ 主要症状的言语性幻听，它的结构网络又将呈现出怎样的 rich club 特征值得深入探究。因此，继实验一对 SZ 言语性幻听患者 CBF 及其连接的分析之后，本实验将检测 SZ 患者结构网络的 rich club 组织、rich club/feeder/local 连接密度，并进一步分析言语性幻听患者与非幻听患者之间的差异。需要指出的是，为了减小治疗对于患者的干扰和疾病慢性化的影响，在后续实验中，均采用首发未经治疗的 SZ 患者。

2.1 材料

2.1.1 被试

本研究由第四军医大学第一附属医院药物临床试验伦理委员会批准，所有参与者均提供了书面知情同意。本实验数据来自未经治疗的首发患者，与实验一的被试存

在部分重叠，自 2011 年 5 月至 2013 年 9 月累计 15 名首发 SZ 言语性幻听患者、27 名首发 SZ 非幻听患者、48 名 HCs 纳入本实验。其余纳入标准与排除标准同实验一，具体参见 1.1.1。样本的人口学与临床特征的全部描述见**表 2-1**。

2.1.2 仪器设备

同实验一，具体参见 1.1.2。

2.2 方法

2.2.1 图像采集

所有影像学数据均在西京医院放射科获取。高分辨 T1 加权 3D 解剖数据运用 3D MPRAGE 序列采集，同实验一，具体参见 1.2.1。DTI 数据扫描参数如下：TR：7000 ms；TE：91 ms；视野：256 mm ×256 mm；矩阵：128 ×128；层厚：3 mm；层间距：0 mm；层数：50；方向：64；b 值：0/1000 s/mm^2。

2.2.2 数据预处理

后续分析依照 van den Heuvel 前期一项研究[104]的路线与方法进行。首先，采用 FreeSurfer 软件（https://surfer.nmr.mgh.harvard.edu/）将灰质分割成不同脑区，其中包括 68 个皮层脑区。其次，对 DTI 数据进行重设原点及校正运动干扰，并进行白质纤维的追踪重建。

2.2.3 构建结构网络

将重建的纤维束与每个分割图结合创建结构网络，该网络包含一组节点和连接，先构建一个由 68 个皮层脑区组成的结构网络。除了分析基于 NOS（number of streamline）绝对值的加权网络，进一步分析代表连接权重的 streamline 密度，即 NOS 除以两个相互连接的感兴趣区（regions of interest，ROIs）的体积。

2.2.4 结构连接组拓扑学的图论分析

检测指标全部基于个体加权网络。结构网络的 rich club 组织分析采用加权的 rich club 行为进行评估，进一步通过对比 1000 次随机网络得到标准化 rich club 系数 $\Phi^{w}norm(k)$。在一定的 k 值范围内 $\Phi^{w}norm(k)$大于 1 则表明该网络具有 rich club 组织。另外，本实验中 rich club 点是将 rich club 水平设定为 $k > 17$ 并基于皮层脑区网络选取的。根据网络节点分为 rich club 脑区与非 rich club 脑区的分类，网络中的边分为

rich club 脑区与 rich club 脑区之间的 rich club 连接、rich club 脑区与非 rich club 脑区之间的 feeder 连接、非 rich club 脑区与非 rich club 脑区之间的 local 连接。

2.2.5 统计学分析

对 rich club 系数、rich club 连接、feeder 连接、local 连接行非参数置换检验（10000 次），即假设各组之间没有差异，观察实验指标是否超出假设的分布。统计学分析时未将年龄、性别、受教育程度作为协变量进行回归，$P < 0.05$ 则认为差异具有统计学意义。

2.3 结果

2.3.1 人口学与临床特征

表 2-1 总结了被试的人口学与临床特征。除 SZ 非幻听患者与 HCs 的受教育年限以外，SZ 言语性幻听、非幻听患者与 HCs 人口学特征的差异无统计学意义。

表 2-1 被试人口学与临床特征

Table 2-1 Demographical and clinical characteristics of subjets

Characteristic	AVHs (n = 15)	Non-AVHs (n = 27)	HCs (n = 48)
Age (y)	24 ± 7	26 ± 6	26 ± 4
Gender (M/F)	8/7	15/12	22/26
Education level (y)	14 ± 2	13 ± 2*	15 ± 2
Duration of illness (mon)	10 ± 12	12 ± 16	—
PANSS score			
Total score	107 ± 15	92 ± 18	—
Positive score	30 ± 7	21 ± 7	—
Negative score	26 ± 4	22 ± 9	—
General score	51 ± 9	49 ± 9	—
AHRS score	26 ± 8	—	—

Data are mean ± standard deviation (SD). *$P < 0.05$ versus HCs. PANSS, Positive and Negative Syndrome Scale; AHRS, Auditory Hallucination Rating Scale.

2.3.2 rich club 组织

患者与 HCs 的结构网络均展现出 rich club 组织属性，图 2-1 显示了被试的组平均 $\Phi^{w}norm(k)$曲线（基于 NOS 获得），SZ 患者比 HCs 皮层网络的 rich club 组织明显降低（k 值为从 6 到 14、16 到 22，$P < 0.05$）。进一步采用 HCs 组分析脑内 rich club 点（设定为 $k > 17$）发现，rich club 脑区包括双侧楔前叶、额上回、顶上回、岛叶及枕外侧皮层（图 2-2）。

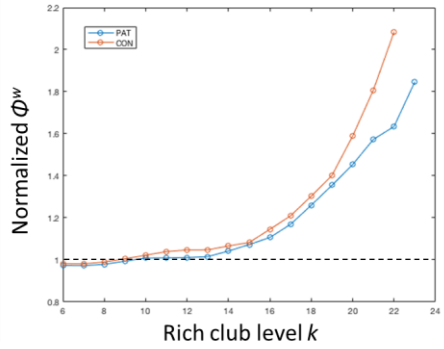

图 2-1 组平均 rich club 曲线

Fig. 2-1 Group-averaged rich club curve

As compared with HCs, SZ patients had a significantly decreased rich club organization for the range of k = 6-14 and 16-22 (P < 0.05, 10000 permutations), reflecting hypoconnectivity between central hubs of the brain structural network, e.g., rich club regions. PAT, SZ patients; CON, HCs.

2.3.3 连接密度

图 2-2 展示了三种连接形式，包括 rich club 脑区与 rich club 脑区之间的 rich club 连接、rich club 脑区与非 rich club 脑区之间的 feeder 连接、非 rich club 脑区与非 rich club 脑区之间的 local 连接。如图 2-3 所示，在连接密度分析中，SZ 患者结构连接的 rich club 连接（rich club 脑区之间的连接）密度与 local 连接（非 rich club 脑区之间的连接）密度降低（$P < 0.05$），而 feeder 连接（rich club 脑区与非 rich club 脑区之间的连接）密度升高（$P < 0.05$）。

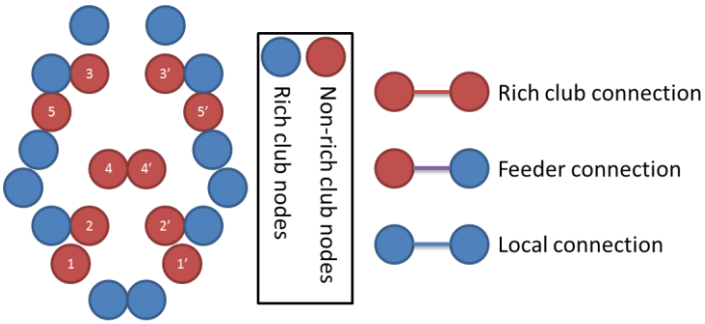

图 2-2 基于 HCs 皮层网络获得的 rich club 脑区

Fig. 2-2 Rich club regions obtained based on cortical network of HCs

Confirming previous findings, rich club regions included bilateral precuneus, superior frontal gyri, superior parietal gyri, insula and lateral occipital cortices (at a rich club level of $k > 17$). 1/1', left/right lateral occipital cortex; 2/2', left/right precuneus; 3/3', left/right superior frontal gyrus; 4/4', left/right superior parietal gyrus; 5/5', left/right insula.

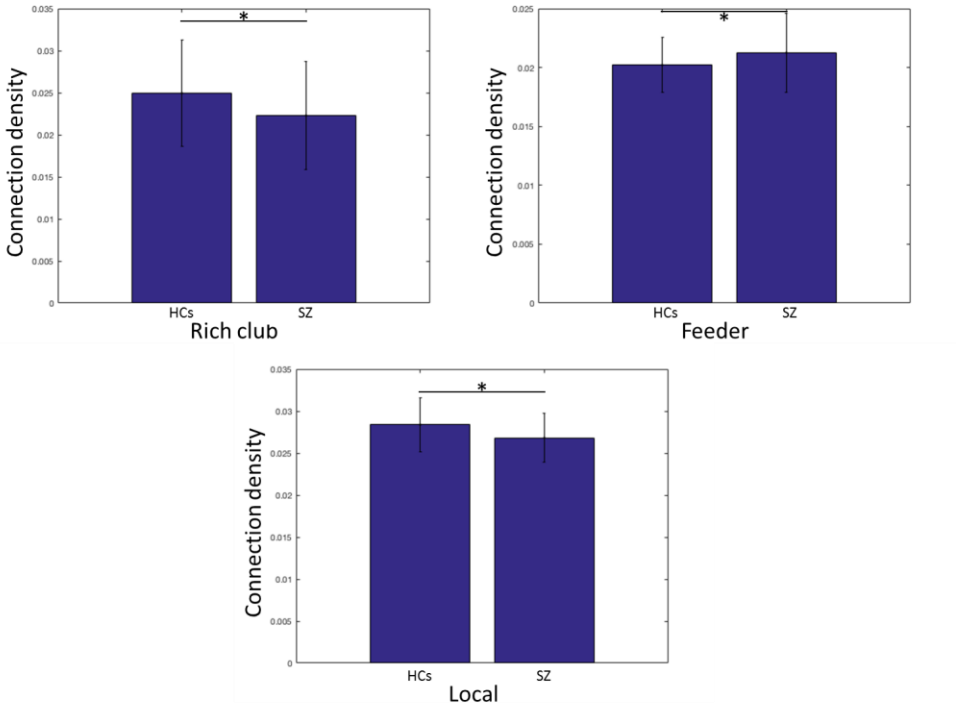

图 3-3 Rich club/feeder/local 连接密度

Fig. 3-3 Density of rich club/feeder/local connection

Examining the density of rich club, feeder and local connections between SZ patients and HCs showed a significant reduction in rich club and local density in patients ($P < 0.05$,

10000 permutations) but significant increase in feeder density ($P < 0.05$, 10000 permutations). *, $P < 0.05$.

2.3.4 SZ 言语性幻听相关结果

图 2-5 展示了 SZ 言语性幻听 rich club 组织的相关结果。首先，SZ 言语性幻听患者的结构网络依然具有 rich club 组织特性，并且 SZ 言语性幻听患者与 HCs 相比皮层网络的 rich club 组织水平降低，而与非幻听患者相比 rich club 组织水平并无差异。其次，与 HCs 相比，SZ 言语性幻听患者结的 local 连接密度降低（$P < 0.05$），而 rich club 连接密度和 feeder 连接密度并无改变（$P > 0.05$）。再次，与非幻听患者相比，SZ 言语性幻听患者结构连接的 local 连接密度降低（$P < 0.05$），而 rich club 连接密度与 feeder 连接密度并无改变（$P > 0.05$）。

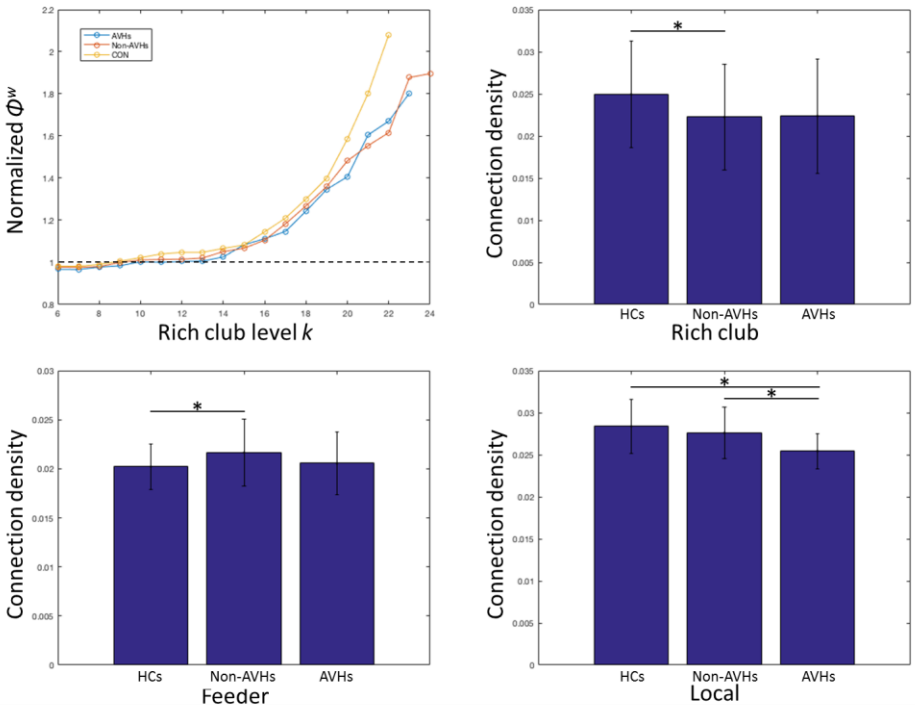

图 2-5 SZ 言语性幻听 rich club 组织及连接密度

Fig. 2-5 Rich club organization and connection density in SZ patients with AVHs

As compared with SZ patients without AVHs, AVHs patients had no significantly different rich club organization and the density of rich club or feeder connection ($P > 0.05$, 10000 permutations), but the density of local connection showed a significant reduction ($P < 0.05$, 10000 permutations). CON, HCs. *, $P < 0.05$.

2.4 讨论

本实验的主要发现是 SZ 患者的脑网络依然保存着 rich club 现象，且 rich club 组织较 HCs 明显降低，反映出其脑内 hub 节点之间的连接水平降低，而 SZ 言语性幻听患者 rich club 组织水平与非幻听患者相比并无变化，从结构网络的 rich club 组织水平上来讲，言语性幻听作为 SZ 的主要症状并未体现出与其他非幻听患者的明显区别。进一步的分析发现，与非幻听患者相比，SZ 言语性幻听患者 rich club 连接密度与 feeder 连接并未改变，而 local 连接的密度降低，表明皮层 rich club 脑区之间的连接以及 rich club 脑区与非 rich club 脑区同 SZ 言语性幻听并无直接的相互影响，非 rich club 脑区之间的网络与 SZ 言语性幻听的关系更为密切。

近年来，白质损伤的重要性已经得到了 SZ 研究的关注[161]，而幻听作为 SZ 的核心症状也很有可能是由较大尺度的脑区整合异常引起的。前期关于 SZ 结构连接的研究结果并不完全一致[162]，其中一个原因就是 SZ 显著的临床异质性。因此，将 SZ 进行基于症状的亚分型便成为一种具有临床意义的研究对策[163]。另外，研究发现，DTI 研究中的 FA 值降低、RD 值升高反映在神经解剖学/神经生物学层面的问题就是脱髓鞘[164, 165]。因此，基于白质的结构连接分析结果体现了 SZ 患者髓鞘存在异常改变。

在本课题组前期的 DTI 研究[39]中，ANOVA 分析结果发现，首发 SZ 言语性幻听、非幻听及 HCs 中 FA 值存在差异的白质纤维主要包括右侧内囊前肢与前放射冠，进一步比较发现 SZ 言语性幻听患者较非幻听患者具有更多的 FA 降低脑区，包括扣带束及左侧上/后放射冠；三组中 RD（radial diffusivity）值存在差异的是胼胝体、内囊、放射冠、外囊，且 SZ 言语性幻听患者扣带束 RD 值升高，但非幻听患者中并无此发现；最后，将 FA 图与 RD 图重叠时，发现 SZ 言语性幻听患者右侧放射冠与内囊前肢的 FA 值最低、RD 值最高，非幻听患者则介于幻听患者与 HCs 之间。

相反，本实验则是以白质结构连接为基础，并不直接探讨存在异常改变的白质所在的具体纤维束，而是从网络水平检测 SZ 言语性幻听患者结构网络的变化。当然，这些改变的基础仍然是某些特定白质纤维束异常的综合效应。具体而言，内囊前肢与前放射冠中包含钩状束、额枕束以及丘脑辐射，这些纤维束均是连接大脑皮层执行语言功能脑区的基础。另人兴奋的是，本实验中获取的 rich club 脑区，即双侧楔

前叶、额上回、顶上回、岛叶及枕外侧皮层恰恰位于上述纤维束连接的部位。这种计算神经科学领域的结构连接与神经解剖学领域的白质纤维束的高度契合大大提高了本实验结果的证据级别，也足以说明大尺度脑网络与微观尺度的发现存在紧密的联系。

需要指出的是，从方法学的角度来讲，目前的数据分割中使用的最佳分辨率尚无定论。虽然已有研究提倡高分辨率分割模板处理数据[159]，但是过于精细的分割模板会使个体差异更加明显[166]；然而，分辨率过低也会使较小的连接在空间平均时丢失。本实验的不足即体现在对脑网络的探究采用的是相对较低的分辨率，这可能会对观察到的 rich club 组织产生一定影响。毕竟分辨率的高低问题仍然属于数据分割中的双刃剑，如何选择本身也是需要研究的问题。

总之，从结构网络的 rich club 组织水平上来讲，言语性幻听作为 SZ 的主要症状并未体现出与其他非幻听患者的明显区别，且皮层 rich club 脑区之间以及 rich club 脑区与非 rich club 脑区的连接和 SZ 言语性幻听并无直接的相互影响，非 rich club 脑区之间的网络与 SZ 言语性幻听的关系才更为密切。由于 rich club 连接是构成脑内通讯的骨干力量，本实验的结果提示 SZ 言语性幻听脑内通讯的结构完整性受损，在此基础上，SZ 言语性幻听患者非 rich club 脑区之间的连接进一步遭到破坏，该系统的完整性降低可能导致脑内不同系统之间信息整合紊乱。

实验三　首发精神分裂症言语性幻听信息滤过、语言与听觉处理失衡：静息态网络研究

Long-Biao Cui, Lin Liu, Fan Guo, Yun-Chun Chen, Gang Chen, Min Xi, Wei Qin, Jin-Bo Sun, Chen Li, Yi-Bin Xi, Hua-Ning Wang, Hong Yin

Radiology, 2017; 283(3):810-819.

言语性幻听被认为是 SZ 最主要的特征之一[12]，理解言语性幻听的机制对于更好的控制其不良后果以及揭示正常感觉体验至关重要[31]。实验二的结果说明 SZ 言语性幻听患者脑结构与功能动力学耦联紊乱，那么，具体的脑功能网络如何变化仍需接下来的实验予以阐明。RSNs（静息态网络）指的是静息状态下自发活动时相互连接的脑区，研究指出 RSNs 改变可能参与 SZ 的精神病理学基础[167]。静息态 fMRI 研究显示 SZ 患者 DMN[79, 119, 168-171]及其他 RSNs[170, 172, 173]明显异常。此外，SZ 言语性幻听也可能与 RSNs 异常相关：（1）初级听觉皮层的静息态活动异常增高，（2）言语处理系统（例如额下回）功能性相互作用紊乱，以及（3）DMN 相关的功能障碍[12]。证据显示，包括听觉网络（听觉皮层与岛叶）、DMN（内侧前额叶、前后扣带皮层、楔前叶、角回与海马）、执行网络（DLPFC 与丘脑）、运动网络（中央前回、补充运动区与壳核）以及额顶网络（Broca 区与 Wernicke 区）在内的 RSNs 中的众多脑区局部异常[57, 63-65, 83]以及相互作用改变[53, 66-75]均在言语性幻听中有所体现。

分析 RSNs 的一种方法就是 Beckmann 等研发的 ICA（独立成分分析）[174]。ICA 将数据分解为时间与空间成分，当用于静息态 BOLD-fMRI 数据时，ICA 可发现具有相似 BOLD 信号-时间序列的脑区。ICA 输出的是一组行为学[175]以及临床[176]相关的网络，前期曾用于检测 SZ 患者静息态或任务态下的 RSNs 变化[119, 170, 172, 173, 177-179]，并发现了 DMN、感觉运动网络、执行网络与突显网络的异常。通过 ICA，Escart í等观察到 SZ 慢性言语性幻听患者边缘网络内杏仁核与海马旁回的活动增强[65]；其后，Wolf 等证实言语相关网络的内部连接紊乱可能是 SZ 患者顽固性与难治性幻听的基

础[73]。识别在 SZ 发病机制中发挥重要作用的特征性脑区有助于指导治疗中采取适当的策略。例如，左侧颞顶联合区曾被选为靶区，TMS[64]或者 tDCS[136]采用此脑区在临床实践中可有效降低言语性幻听的严重性。然而，根据上述所提及研究的散在证据，这些 RSNs 在首发 SZ 言语性幻听患者中的变化模式并未完全建立。

本实验采用 ICA 揭示首发未经治疗的 SZ 言语性幻听患者前期报道过的 SZ 相关 RSNs 的特征，运用反应局部场自发神经活动的 ALFF[180-182] 探索 RSNs 内的局部脑功能，推测 RSNs——特别是言语性幻听相关的 RSNs——可能在该组患者中出现紊乱。

3.1 材料

3.1.1 被试

本研究由第四军医大学第一附属医院药物临床试验伦理委员会批准，所有参与者均提供了书面知情同意。被试来自 1.1.1 中去除非首发的 SZ 患者，另外，排除 MRI 扫描中头动大于 2.5 mm（横移）和/或 3.0°（旋转）的被试。样本的人口学与临床特征的全部描述见**表 3-1**。

3.1.2 仪器设备

同实验一，具体参见 1.1.2。

3.2 方法

3.2.1 图像采集

被试接受扫描，所有影像学数据均在西京医院放射科获取。高分辨 T1 加权 3D 解剖数据运用 3D MPRAGE 序列采集，同实验一，具体参见 1.2.1。BOLD 数据运用平面回波成像（echo planar imaging，EPI）序列采集（TR：2000 ms；TE：30 ms；翻转角：90°；视野：220 mm ×220 mm；矩阵：64 ×64；层厚：4 mm；层间距：0.6 mm；层数：33），该序列有效地包含了全脑。采集 240 幅图像，其中前 4 幅图像被丢弃。

3.2.2 数据预处理

采用 FSL（Functional MR Imaging of the Brain or FMRIB，Software Library）（www.fmrib.ox.ac.uk/fsl）MELODIC（Multivariate Exploratory Linear Optimized Decomposition into Independent Components）软件[174]进行预处理，包括 EPI 图像校正以去除运动干扰、 提取脑、高斯核空间平滑（6 mm FWHM）、采用 150 s 截断频率高通滤波（0.007 Hz）。采用相应被试的结构像，运用 FLIRT（FMRIB's Linear Image Registration Tool）将 fMRI 像配准到标准 MNI 空间模板。每位被试预处理的功能数据包括 236 个时间点，最后存储为 4D 数据文件。

3.2.3 双回归

根据 Filippini 等，数据分析在 FSL 工具（www.fmrib.ox.ac.uk/fsl）中进行[183]，行双回归用于被试间分析。首先，采用 ICA 分解 fMRI 数据，在此应用 25 个成分。采用空间相关性比照一套近期界定的网络图[184]选出感兴趣的 RSNs（图 3-1）。其次，双回归方法用于发现被试特异的时间动力学及其 fMRI 数据内的空间图。然后，比照相关的 fMRI 数据，采用线性模型拟合（时间回归）的时间序列矩阵估计被试特异的空间图。最后，将不同的成分图合成单个的 4D 文件，行非参数置换检验（5000 次）[185]，假设检验基于前期工作中的 Gaussian/gamma mixture 模型[174]且检验水准为经 FDR（false-discovery rate）校正 $P < 0.05$。

3.2.4 低频振幅分析

在 SPM8 中预处理之后去除线性趋势，然后对 fMRI 数据行带通滤波（0.01-0.08 Hz）。采用 Matlab 软件行 ALFF 分析[186]。在本实验中，采用每个 RSNs 的时间序列（而不是每个体素的时间序列）变换为频域的每个体素，并获取功率谱。由于特定频率的功率与该频率成分的振幅的平方呈正比，在功率谱的每个频率计算出平方根，并在每个 RSNs 获得 0.01-0.08 Hz 的平均平方根。最后，在 Z 图上行空间平滑（6 mm FWHM）。

3.2.5 统计学分析

在 ALFF 分析中，采用两样本 *t* 检验比较言语性幻听与非幻听患者的差异（$P < 0.05$，FDR 校正）。为了检测脑功能测量值与症状严重性之间的相关性，分别计算每组患者的 Pearson 相关系数。另外，ROC 分析用于评估这些影像学测量值区分 SZ 言语性幻听与非幻听患者的诊断能力。采用 SPSS 软件（version 13.0）进行相关性与 ROC 分析，$P < 0.05$（相关性分析中需多重比较校正）时差异被认为具有统计学意义。

3.3 结果

3.3.1 人口学与临床特征

表 3-1 总结了被试的人口学与临床特征。SZ 言语性幻听、非幻听患者与 HCs 在年龄、性别、利手或受教育年限上差异无统计学意义。

表 3-1 AVHs 患者（n = 17）、非幻听患者（n = 15）以及 HCs（n = 19）的人口学与临床特征

Table 3-1 Demographic and clinical characteristics of patients with AVHs (*n* = 17), patients without AVHs (*n* = 15), and HCs (*n* = 19)

Characteristics	AVHs patients	Non-AVHs patients	HCs
Age (years)	21.24 ±3.85	22.53 ±4.07	23.79 ±3.75
Sex (male/female)	10/7	8/7	10/9
Handness (right/left)	17/0	15/0	19/0
Education (years)	13.71 ±1.93	13.40 ±1.55	14.74 ±2.26
Handedness (right/left)	17/0	15/0	19/0
Duration of illness (months)	6.51 ±6.01	10.20 ±18.15	—
PANSS Total Score	106.24 ±13.94*	88.07 ±26.19	—
PANSS Positive Score	31.12 ±7.13*	17.93 ±9.28	—
PANSS Negative Score	25.53 ±3.84	22.73 ±10.70	—
PANSS General Psychopathology	49.59 ±9.33	47.40 ±10.38	—
AHRS Score	26.12 ±8. 43	—	—

The three groups were matched for demographic characteristics. Data are mean ± standard deviation (SD). *$P < 0.05$ versus Non-AVHs patients. PANSS, Positive and Negative Syndrome Scale; AHRS, Auditory Hallucination Rating Scale.

3.3.2 RSNs

提取的六个 RSNs 分别是听觉网络[174]、DMN[183]、执行控制网络[174]、运动网络[174]，以及双侧额顶网络[175, 187]（图 3-1）。（1）听觉网络：听觉皮层、颞上回、后岛叶、前扣带皮层与前缘上回等；（2）DMN：前额皮层、前/后扣带、顶外侧部、颞中/下回、小脑，以及丘脑延伸至颞叶内侧区等；（3）执行网络：前额皮层上/中部、前扣带与扣带旁回、前额皮层腹外侧部，以及丘脑连接到前额皮层的区域等；（4）运动网络：中央前回与补充运动区等；（5）右侧额顶网络：右侧额上/中回与顶下小叶等；（6）左侧额顶网络：左侧额中回与顶上小叶等。

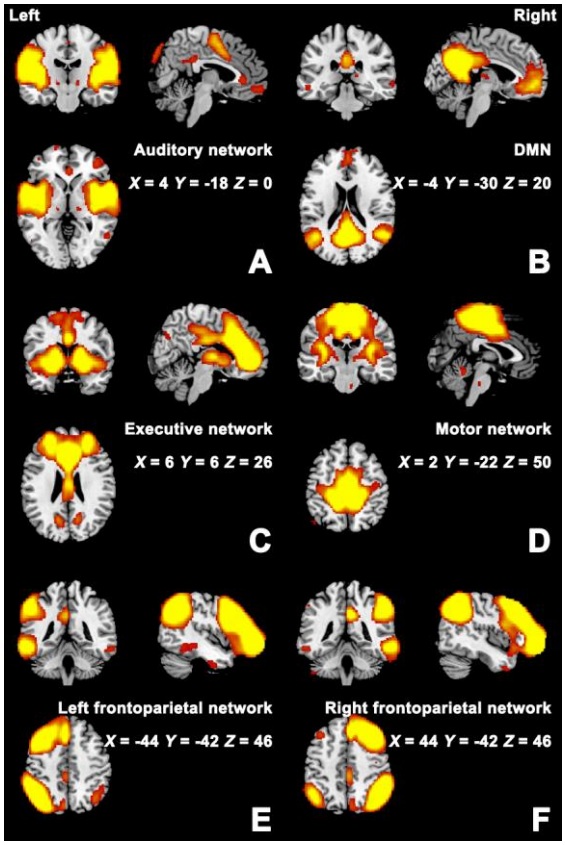

图 3-1 提取的 RSNs

Fig. 3-1 The RSNs extracted

MELODIC ICA generated resting state networks from our data. Group mean (A) auditory, (B) default mode, (C) executive, (D) motor, (E) left frontoparietal, (F) right frontoparietal networks. DMN, default mode network.

通过估计单独的网络图分析这些 RSNs 内的组间差异，表 3-2 列出了患者组 RSNs 内的信号强度，图 3-2 到 3-7 展示了这些 RSNs 中共活动变化的区域（$P < 0.05$，FDR

校正）。SZ 言语性幻听与非幻听患者相比，听觉网络内显著增强的共活动程度（采用双回归方法中的回归系数测量）位于右侧听觉皮与双侧岛叶（图 3-2）。与非幻听比较，在言语性幻听中 DMN 的双侧内侧前额皮层、前/后扣带皮层、角回与右侧顶上回发现了更高的信号幅度（图 3-3）。在执行网络内，与非幻听比，言语性幻听中观察到的活动增强的区域包括双侧前额皮层、尾状核、壳核、苍白球、左侧丘脑，但无活动降低区（图 3-4）。运动网络中言语性幻听共活动增强的脑区为双侧补充运动区，减弱的脑区为双侧丘脑、左侧中央前回、壳核与苍白球（图 3-5）。言语性幻听患者额定网络中 Broca 区与 Wernicke 区及其右侧半球的同伦脑区显示出比非幻听患者更高水平的共活动（图 3-6 与 3-7）。

表 3-2 患者组 RSNs 内的信号强度

Table 3-2 Signal Intensities within RSNs in Patient Groups

RSNs	AVHs Patients (Mean ± SD)	Non-AVHs Patients (Mean ± SD)	*T*	*P*
Increased				
Auditory network	4.81 ± 0.67	4.06 ± 0.78	2.92	0.01
DMN	4.64 ± 0.92	3.36 ± 0.79	4.17	0.0002
Executive network	4.06 ± 1.41	3.15 ± 0.36	2.42	0.02
Motor network	4.04 ± 0.71	3.11 ± 0.77	3.56	0.001
Left FPN	5.32 ± 0.88	4.27 ± 0.87	3.41	0.002
Right FPN	3.26 ± 0.74	2.37 ± 0.68	3.54	0.001
Decreased				
Auditory network	2.10 ± 0.69	3.10 ± 0.95	−3.42	0.002
DMN	0.85 ± 2.10	3.16 ± 2.34	−2.94	0.01
Executive network	0.59 ± 1.82	1.83 ± 0.97	−2.36	0.03
Motor network	2.38 ± 0.99	3.15 ± 0.77	−2.45	0.02

Left FPN	1.77 ±1.29	3.21 ±0.78	−3.75	0.001
Right FPN	1.79 ±0.67	2.74 ±0.55	−4.35	0.0001

SD, standard deviation; DMN, default mode network; FPN, frontoparietal network.

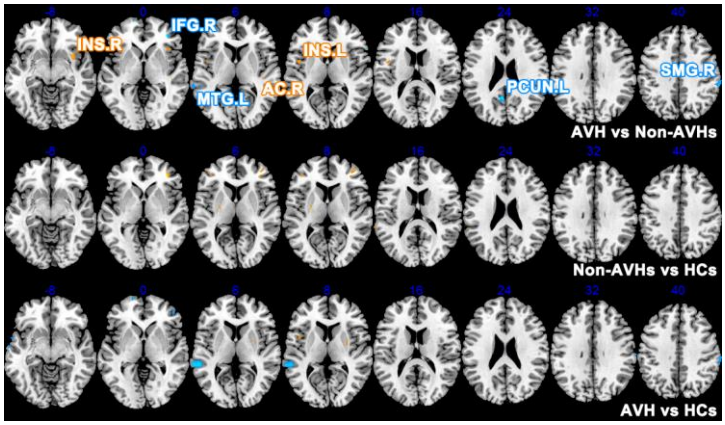

图 3-2 听觉网络双回归分析显示的组间差异

Fig. 3-2 Dual regression analysis in the auditory network showing differences between groups

Changes overlaid on template with coordinate planes in blue. Color encoding of increased signal amplitude in hot color and decreased in cold. AC, auditory cortex; IFG, inferior frontal gyrus; INS, insula; MTG, middle temporal gyrus; PreC, precuneus; SMG, supramarginal gyrus; PCUN, precuneus.

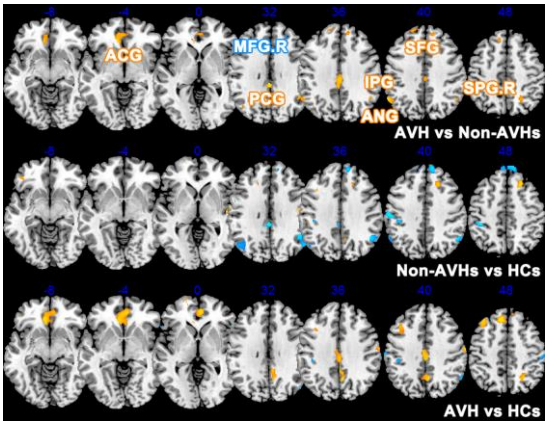

图 3-3 DMN 双回归分析显示的组间差异

Fig. 3-3 Dual regression analysis in DMN showing differences between groups

Changes overlaid on template with coordinate planes in blue. Color encoding of increased signal amplitude in hot color and decreased in cold. ACG, anterior cingulate gyrus; ANG, angular gyrus; IPG, inferior parietal gyrus; MFG, middle frontal gyrus; SFG, superior frontal gyrus; SPG, superior parietal gyrus; PCG, posterior cingulate gyrus.

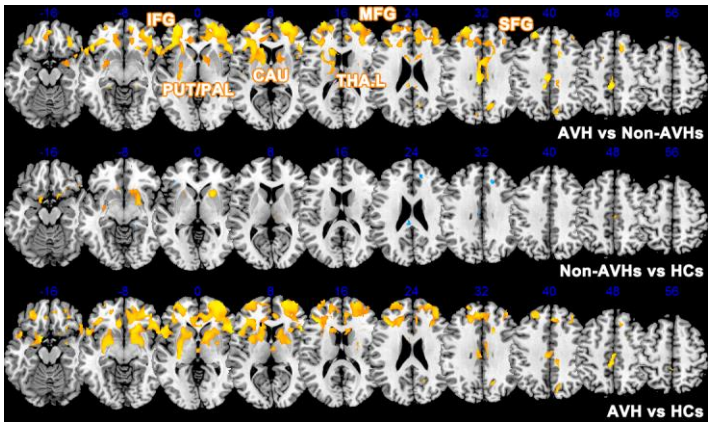

图 3-4 执行网络双回归分析显示的组间差异

Fig. 3-4 Dual regression analysis in the executive network showing differences between groups

Changes overlaid on template with coordinate planes in blue. Color encoding of increased signal amplitude in hot color and decreased in cold. CAU, caudate; IFG, inferior frontal gyrus; MFG, middle frontal gyrus; SFG, superior frontal gyrus; PAL, pallidum; PUT, putamen; THA, thalamus.

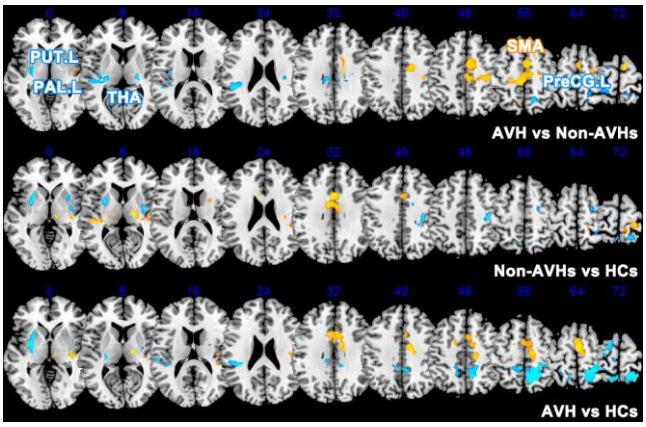

图 3-5 运动网络双回归分析显示的组间差异

Fig. 3-5 Dual regression analysis in the motor network showing differences between groups

Changes overlaid on template with coordinate planes in blue. Color encoding of increased signal amplitude in hot color and decreased in cold. PAL, pallidum; PreCG, precentral gyrus; PUT, putamen; SMA, supplementary motor area; THA, thalamus.

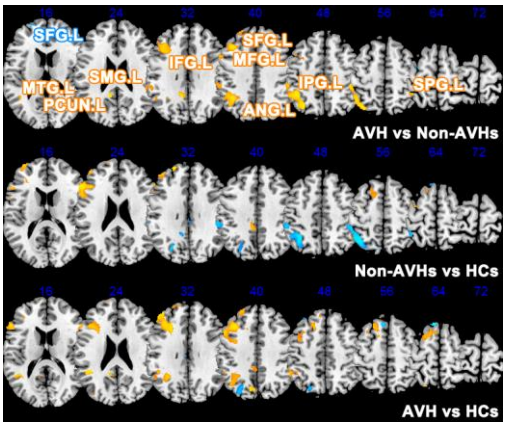

图 3-6 左侧额顶网络双回归分析显示的组间差异

Fig. 3-6 Dual regression analysis in the left frontoparietal network showing differences between groups

Changes overlaid on template with coordinate planes in blue. Color encoding of increased signal amplitude in hot color and decreased in cold. SMG, supramarginal gyrus.

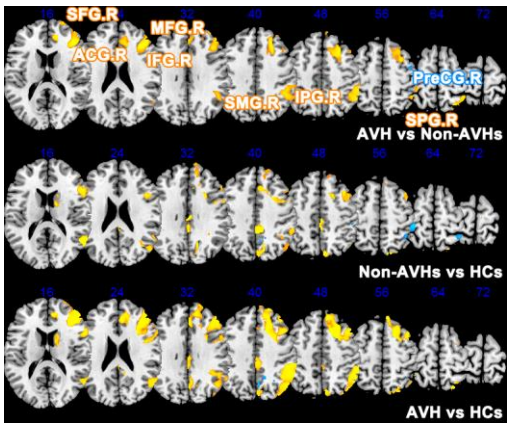

图 3-7 右侧额顶网络双回归分析显示的组间差异

Fig. 3-7 Dual regression analysis in the right frontoparietal network showing

differences between groups

Changes overlaid on template with coordinate planes in blue. Color encoding of increased signal amplitude in hot color and decreased in cold.

3.3.3 低频振幅

与双回归分析的结果相似，言语性幻听患者与非幻听患者相比 ALFF 变化的脑区位于听觉皮层、缘上回、岛叶、壳核、DLPFC、角回、楔前叶，以及丘脑（$P < 0.05$，FDR 校正）。

3.3.4 相关性分析

然后，计算 AHRS 积分与影像学测量值（ICA 构建的 RSNs 内的信号强度）之间的相关系数。SZ 言语性幻听患者中，AHRS 积分与运动网络内的信号强度呈正相关（$r = 0.67$，$P = 0.003$）。同时，AHRS 积分与听觉网络（$r = 0.60$，$P = 0.01$）以及执行网络（$r = -0.51$，$P = 0.04$）内的信号强度呈相关趋势。

3.3.5 ROC 分析

听觉网络（平均值±标准误：0.76 ±0.08，0.78 ±0.08）、DMN（0.85 ±0.07，0.85 ±0.08）、执行网络（0.79 ±0.08，0.76 ±0.09）、运动网络（0.80 ±0.08，0.80 ±0.08）、右侧额顶网络（0.82 ±0.07，0.90 ±0.06）、左侧额顶网络（0.79 ±0.08，0.86 ±0.07）的升高与降低的活动程度的 ROC 曲线下面积均大于 0.75.

3.4 讨论

本实验采用 ICA 探讨了首发未经治疗的 SZ 言语性幻听患者的 RSNs 模式，以及验证 ICA 结果的每个网络内的 ALFF。他们主要表现为多个网络内的共活动增强，即听觉网络、DMN、执行网络、运动网络，以及额顶网络，ALFF 分析进一步从局部脑功能层面证实了上述发现。我们还观察到运动网络的信号强度与言语性幻听的严重程度呈正相关。SZ 言语性幻听患者主要表现为听觉/语言处理与感觉信息滤过的共活动增强，为 SZ 言语性幻听的病理生理学关联性提供了更好的理解。此外，所有功能测量值的 ROC 曲线下面积均大于 0.75，显示了 RSNs 区分言语性幻听与非幻听患者的价值。另外，扫描期间无报告经历幻听的患者，由此我将本实验界定为 Jardri

等描述的特质研究（trait-study）[83]，即探索 SZ 患者言语性幻听易感性的神经基础。上述发现可能主要是言语性幻听的特质效应。我们的结果较既往发现的优势在于：一是为 SZ 言语性幻听特异的功能障碍提供了脑网络水平的观测，二是通过招募首发患者降低了临床异质性和治疗等混杂因素。

3.4.1 听觉网络共活动增强

听觉网络包含初级与次级听觉皮层，以及前扣带皮层、缘上回前部和丘脑[174]。一系列证据高度提示听觉网络与 SZ 言语性幻听关系密切。Jardri 等与 Kompus 等的荟萃分析曾发现 SZ 言语性幻听的听觉皮层活动增强[83, 85]。同样，ASL 也曾成功地证实了 SZ 言语性幻听患者听觉皮层 CBF 水平升高[57, 64]。在本实验中，与前期发现一致的是，我观察到言语性幻听患者显示出右侧听觉皮层共活动显著增强。如前所述，初级听觉皮层异常增高的静息态活动可能促进了 SZ 言语性幻听的出现。本实验显示 SZ 言语性幻听的特征是听觉网络活动增强。

此外，幻听作为 SZ 中较为严重的症状，也涉及双侧听觉皮层间的通讯障碍。SZ 言语性幻听患者初级与次级听觉皮层半球间的 FC 明显降低[92]。从白质的角度来讲，它们也显示出连接双侧听觉皮层的半球间听觉纤维 FA 值升高[91]。因此，基于结构连接与 FC 上的改变，连接双侧听觉皮层的半球间听觉通路参与 SZ 言语性幻听的病理生理学[88]。另外，除了局部活动增强，也曾有报道指出听觉皮层与其他脑区存在异常耦联。有证据表明颞上回（即听觉皮层）与包括额下回、海马与颞中回的语言/记忆相关脑结构之间的连接改变[69, 73, 137, 138]。所以，正如 Alderson-Day 等综述的那样，SZ 言语性幻听表现出颞上回的静息态连接紊乱[12]。本实验中观察到的听觉皮层活动增强可能同其与这些语言/记忆处理脑区之间的相互作用有关。

3.4.2 言语产生与监控脑区共活动异常

一方面，我们检测到执行网络中的壳核与听觉网络中的岛叶共活动增强。一般而言，壳核与岛叶均参与言语产生[188, 189]。以 SZ 为主的精神疾病言语性幻听患者左侧额下回与左侧岛叶之间的 FC 增强[138]。对 tDCS 敏感的 SZ 言语性幻听患者中，颞顶联合区与左侧前岛叶之间的 FC 明显降低，且与言语性幻听严重性的减弱相关[136]。结合本实验的 ICA 结果与那些 FC 分析结果，SZ 言语性幻听可能归因于岛叶的活动增强。另外，作为基底节的一部分，壳核参与涉及运动、执行/联合功能、情感/动机等多个方面的神经环路（如 Obeso 等在一幅示意图中所阐述的那样）[190]。此外，也

曾报道过言语产生涉及壳核[189]。在 SZ 言语性幻听患者中发现了壳核体积降低、连接增强[69, 191]。根据这一发现，本实验通过网络水平的分析进一步支持壳核活动异常。考虑到壳核这些结构与功能的变化，基于壳核涉及言语启动与执行的证据[189]，本实验结果提示壳核是 SZ 言语性幻听中可能的致言语性幻觉的脑区。

另外，在言语性幻听患者的双侧额顶网络中，Broca 区与 Wernicke 区及其右侧同伦脑区的共活动增强。它们通常被认为参与语言处理，是与言语相关的大脑皮层中重要的两个部分，涉及言语的产生。言语性幻听患者显示出活跃的言语产生也提示了语言处理相关脑区促进假性听觉感知的可能性，从而导致 SZ 言语性幻听。

另一方面，除了言语产生，内部言语监控脑区的功能障碍可能也在 SZ 言语性幻听的发病机制中发挥了重要作用。如本实验所展示，双侧楔前叶、DLPFC 与角回内广泛的共活动增强。采用 FC 分析，Lawrie 等发现接受语言任务时左侧 DLPFC 与颞上回之间的连接减弱，且与 SZ 言语性幻听的严重性呈负相关[51]。在静息状态下，与非幻听患者相比，SZ 言语性幻听患者左侧 DLPFC 表现出与 Wernicke 区的耦联显著增强[69]。此外，Sommer 等发现左侧额下回（代表的是 Broca 区）与 DLPFC 之间的连接减弱[137, 138]。DLPFC 似乎是发挥监控言语产生的功能。相似的是，楔前叶与角回组成 DMN 的节点，它们分别与语言[188]和记忆/自我指示（self-referential）[192]处理相关。因此，它们被认为是内部言语监控脑区。最近 Rotarska-Jagiela 等将楔前叶与 SZ 言语性幻听联系起来[193]。应用 ICA，曾有报道指出 SZ 言语性幻听患者显示出比 HCs 更弱的左侧楔前叶的内部连接[73]。接下来，tDCS 增强 SZ 言语性幻听患者左侧 DLPFC、角回、楔前叶与颞顶联合区作为种子点的 FC[136]。与这些前期结果一致的是，本实验所发现的前额叶与 DMN 共活动增强提示 SZ 言语性幻听患者内部言语监控脑区活动紊乱。

3.4.3 信息滤过脑区共活动异常——丘脑

丘脑在 SZ 中的特征是增强特定输入，而抑制其他输入，表现为丘脑从内部言语中滤过外部言语的功能受损[99-101]。我们前期的研究发现 SZ 言语性幻听患者的丘脑体积降低[36]。而本实验观察到 SZ 言语性幻听患者执行网络中左侧丘脑共活动水平升高、运动网络中双侧丘脑共活动水平降低。更为有趣的是，一项采用 SZ 小鼠模型的电生理学研究似乎尤为及时地提供了重要证据，建立起了丘脑-听觉皮层投射紊乱与幻听之间的关系。Chun 等发现丘脑多巴胺 D2 受体表达异常升高，由于谷氨酸释放

减少引起丘脑向听觉皮层投射的缺陷[95]。同时，左侧丘脑可能滤过由皮层预测的呈现于听觉皮层的信号[194]。所以，有人提出言语性幻听是丘脑将外部言语从内部言语中滤过的功能障碍的结果[100, 101]。因此，我们相信，通过结合基础与临床研究证据，执行网络中丘脑共活动的异常可能反映了丘脑中听觉信号滤过过程紊乱，从而促进了 SZ 中这一令人痛苦的症状。

当然，严格的纳入未经治疗的首发患者限制了本实验的样本量，这可能会影响统计力度并在一定程度上对结论的可靠性造成影响。尽管如此，探索 SZ 言语性幻听的神经机制十分重要，在临床获益之前仍然需要更多努力付出。下一步需要做的是评估前期以及当前研究的可重复性以及采用 fMRI 预测 SZ 言语性幻听患者预后的可能性。

总而言之，本实验的结果提示首发未经治疗的 SZ 言语性幻听患者多个 RSNs 的异常模式，包括听觉网络、DMN、执行网络、运动网络和额顶网络。该发现展示了一幅 SZ 言语性幻听脑区功能障碍的全景，涉及听觉处理（听觉皮层与缘上回）、言语产生（Broca 区、Wernicke 区、岛叶与壳核）和监控（DLPFC、角回与楔前叶）、感觉信息滤过（丘脑），从而诱发假性感知推断。基于这些 RSNs 之间的失衡，本实验可能为 SZ 言语性幻听提供新的诊断和治疗策略，对 SZ 的干预具有潜在的临床意义。

实验四　首发精神分裂症言语性幻听言语启动的网络功能缺陷：局部功能与功能连接研究

Long-Biao Cui, Kang Liu, Chen Li, Liu-Xian Wang, Fan Guo, Ping Tian, Yu-Jing Wu, Li Guo, Wen-Ming Liu, Yi-Bin Xi, Hua-Ning Wang, Hong Yin

Schizophr Res, 2016; 173(1-2):13-22.

明确 SZ 神经生物学基础的最大障碍在于本病中明显的临床异质性[22]。SZ 已经越来越被认为是一组表型相似的疾病或症状，将 SZ 划分为症状特异性亚组有可能降低这一疾病的异质性并有助于明确其发病机制[23]，但症状特异性生物标记物仍然缺乏。言语性幻听是 SZ 中最主要的症状之一，影响 60%-90%的患者[12]，反映其重要性的一个事实就是它是该病诊断标准中重要的一项内容[19]。阐明 SZ 言语性幻听的神经基础仍然是精神病领域的研究热点。

揭示 SZ 言语性幻听背后的神经机制对于治疗这一严重的精神疾病具有重要的临床意义。目前，言语性幻听与听觉处理缺陷有关，包括半球间听觉连接障碍与听觉活动自发性激活[88, 195, 196]，但 SZ 言语性幻听的神经认知与神经生物学机制尚未完全建立起来。另外，连接障碍假说提示 SZ 的症状与涉及不同脑区的神经连接异常相关[53, 79, 96, 97]。由于运用 fMRI 技术的现代神经影像学方法的进步，基于症状的 SZ 言语性幻听发病机制的研究在过去十年迅速增长。这些研究已经为涉及这一具有挑战性的症状的脑区或网络提供了初步的认识。根据目前的神经影像学发现，SZ 言语性幻听患者显示出脑结构紊乱[146]与脑活动改变[83, 105, 197]。

除了实验一采用的 CBF，作为另一种脑功能的生物标记物，BOLD-fMRI 信号不仅能够使我们评估局部脑功能，也可以研究脑网络内的 FC。实验三在功能网络水平展示了 SZ 言语性幻听的异常改变，这种改变是否以局部脑功能改变为基础则需要继续研究。探索局部脑功能的一种途径是 ALFF（低频振幅），它与局部场自发性神经活动相关，因此被认为具有生物学或生理学意义[180-182]。另一种方法是 ReHo（局部一致性），它假定当功能脑区涉及某一特定状态时，这个脑区内的特定体素具有时间

上的一致性[198]。采用 BOLD 信号的 ReHo 分析也可以用于分析局部神经活动。来自运用 ALFF、ReHo 或 FC 的 BOLD-fMRI 研究的结果曾在 SZ 中被报道[63, 97, 172, 173, 199]，支持 SZ 涉及多种功能的广泛的脑区内活动异常，以及脑网络内的连接障碍的结论。

除 SZ 之外，如 Alderson-Day 等所综述，通过 FC（功能连接）分析已经有针对性地研究了 SZ 言语性幻听[12]。在前期静息态[63, 67-70, 92, 200]与任务态[51, 52, 201]fMRI 研究中，已经在 SZ 言语性幻听中观察到异常的 FC。一般来说，SZ 言语性幻听紊乱的 FC 包括听觉/语言处理、内部言语监控，以及记忆脑区[68-70, 92]。对于局部脑功能，Chyzhyk 等提供了运用 ALFF、ReHo 与 FC 具有很强的 SZ 言语性幻听与非幻听患者的分类能力的支持[63]。然而，尚未采用包括 ALFF 与 ReHo 的局部活动测量值广泛地探索 SZ 言语性幻听患者的局部脑功能，尤其是静息态自发活动。另外，前期的研究也未探索 SZ 言语性幻听患者静息态功能改变的脑区是否与其他脑区具有异常的 FC，换言之，即静息状态下局部脑功能的神经整合能力。

本实验采用 fMRI 揭示未经治疗的首发 SZ 言语性幻听与非幻听患者的局部与网络功能，从而保证排除治疗的混杂因素。从方法学上来讲，类似于 Lui 等的研究策略[199]，本实验的连接分析采用数据驱动的方法，目的在于测定异常 ALFF 与 ReHo 的脑区是否与其他脑区之间的 FC 改变。分析按四步进行：第一，检测 ALFF 与 ReHo 以明确 SZ 言语性幻听与非幻听患者这两种指标共同的与不同的局部功能缺陷；第二，测定局部功能障碍的脑区是否与其他脑区之间的 FC 改变；第三，探索患者中观察到的功能异常是否与症状测量值相关；第四，行 ROC 分析评估这些影像测量值的诊断性能。

4.1 材料

4.1.1 被试

同实验三，具体参见 3.1.1。本研究由第四军医大学第一附属医院药物临床试验伦理委员会批准，所有参与者均提供了书面知情同意。

4.1.2 仪器设备

同实验一，具体参见 1.1.2。

4.2 方法

4.2.1 图像采集

同实验三，具体参见 3.2.1。采集 240 幅图像，其中前 10 幅图像被丢弃。

4.2.2 数据预处理

采用 DPARSFA（Data Processing Assistant for Resting-State fMRI Advanced Edition）V3.1（http://rfmri.org/DPARSF）进行数据预处理[202]。对于每个被试，fMRI 数据首先头动校正（排除标准：横移> 2.5 mm 和/或旋转> 3.0 °），重采样到 3 mm ×3 mm ×3 mm 的体素，运用 4 mm ×4 mm ×4 mm FWHM 高斯核进行空间平滑。ALFF 计算与 FC 分析进行数据平滑，但 ReHo 计算不做平滑。在协变量回归中，选择白质信号与脑脊液信号作为干扰因素。

4.2.3 ALFF 与 ReHo 计算

为了明确局部脑功能，运用DPARSFA软件测量BOLD信号的ALFF与ReHo[202]。ALFF分析中对数据行带通滤波（0.01-0.08 Hz）。然后，每个体素的ALFF除以全脑模板内的平均ALFF值。ReHo分析包括27个体素。类似于ALFF分析的标准化步骤，每个体素的ReHo除以全脑模板内的平均ReHo值。

4.2.4 FC 分析

运用 DPARSFA 中的种子点体素相关方法检测 FC。对于每个被试，ALFF 与 ReHo 均改变的脑区，即双侧壳核用作种子点脑区。采用 MNI 峰值坐标、制作半径 6 mm 的 ROI。ALFF 与 ReHo 结果的 MNI 坐标并不完全相同，由于 ALFF 的发现对言语性幻听相对特异，从而选择 ALFF 的结果（左侧壳核：X = −27，Y = 3，Z = 0；右侧壳核：X = 24，Y = 12，Z = 3）制作 ROIs。对于每个 ROI，计算种子点与种子点外的全脑体素的时间序列之间的相关性。最后，Fisher *z* 变换用于将相关系数变换为 *z* 值。

4.2.5 统计学分析

在开源软件 REST V1.8（http://restfmri.net/forum/REST_V1.8）[126]中，运用单因素方差分析（one-way analysis of variance，ANOVA）与配对 *t*-检验行 ALFF、ReHo、FC 测量值体素水平的比较，并将头动作为协变量。阈值设为 *P* 值低于 0.01（AlphaSim 校正），根据 REST 中的 Correction Threshold by AlphaSim 模块 cluster 阈值为 19。

为了检测脑功能测量值（ALFF、ReHo、FC 值）与症状严重性（AHRS 与 PANSS 积分）之间的相关性，分别计算每个患者组异常脑区与连接的 Pearson 相关系数（多重比较经 Bonferroni 校正）。在 SZ 言语性幻听患者中，与非幻听患者和 HCs 相比发生变化的测量值用于相关性分析；在 SZ 非幻听患者中，较 HCs 变化的测量值用于相关性分析。另外，ROC 分析用于评估这些影像学测量值区分 SZ 言语性幻听与非幻听患者（言语性幻听与非幻听患者之间存在差异的测量值）、SZ 非幻听患者与 HCs（非幻听患者与 HCs 之间存在差异的测量值）的诊断能力。采用 SPSS（version 13.0）进行相关性与 ROC 分析，BrainNet Viewer（http://www.nitrc.org/projects/bnv/）Matlab 工具箱用于脑网络可视化[203]。*P* 值低于 0.05 被认为差异具有统计学意义。

4.3 结果

4.3.1 ALFF

表 4-2 总结了全脑分析中 ALFF 值变化的区域。ANOVA 显示双侧壳核、左侧后扣带皮层、右侧额中回与右侧楔前叶 ALFF 的差异具有统计学意义（图 4-1）。与 SZ 非幻听患者相比，SZ 言语性幻听患者显示出左侧壳核 ALFF 明显降低，与 HCs 相比右侧壳核 ALFF 升高、右侧中央后回 ALFF 降低。此外，与 HCs 相比，在 SZ 非幻听患者中有检测于双侧壳核的两个区域 ALFF 增加和观测于右侧海马旁回的一个区域 ALFF 降低。

4.3.2 ReHo

ANOVA 显示双侧壳核、右侧颞下回、右侧额中回眶部与双侧额中回 ReHo 差异具有统计学意义（图 4-2）。直接比较显示 SZ 言语性幻听患者包含 DLPFC 的右侧额中回 ReHo 比非幻听患者更高。与 HCs 相比，SZ 言语性幻听患者显示出双侧壳核与左侧俄中回的 ReHo 升高，而 SZ 非幻听患者也显示出双侧壳核的 ReHo 增加。关于这些发现的定位细节展示在表 4-3 中。对于 ALFF 与 ReHo，壳核均被发现存在双侧性改变从而用作连接分析中的两个种子点。

表 4-2 全脑分析中 ALFF 值变化的区域

Table 4-2 The regions where ALFF values were altered in the whole-brain analysis

Location	Peak MNI coordinate			Cluster size	*P*	Mean ALFF value (SD)		
	X	Y	Z			AVHs	Non-AVHs	HCs
ANOVA analysis								
Right putamen	24	12	3	203	*	0.75 (0.09)	0.87 (0.16)	0.67 (0.09)
Left PCC	-3	-45	12	24	*	1.43 (0.26)	1.49 (0.24)	2.10 (0.49)
Left putamen	-27	3	0	163	*	0.69 (0.08)	0.82 (0.13)	0.65 (0.10)
Right MFG	36	30	30	20	*	0.10 (0.21)	0.73 (0.18)	0.71 (0.15)
Right precuneus	3	-63	63	23	*	2.14 (0.51)	2.41 (0.36)	3.11 (0.54)
AVHs < Non-AVHs								
Left putamen	-27	3	3	33	*	0.64 (0.07)	0.82 (0.15)	
AVHs > HCs								
Right putamen	15	9	-9	36	*	0.94 (0.13)		0.75 (0.10)
AVHs < HCs								
Right PoCG	45	-12	33	24	*	0.81 (0.14)		1.21 (0.30)
Non-AVHs > HCs								
Right putamen	24	12	0	155	*		0.90 (0.17)	0.68 (0.09)
Left putamen	-27	-3	-9	106	*		0.87 (0.14)	0.67 (0.11)
Non-AVHs < HCs								
Right ParaHC	18	-27	-12	34	*		0.86 (0.12)	1.20 (0.19)

MFG, middle frontal gyrus; ParaHC, parahippocampus; PCC, posterior cingulate cortex; PoCG, postcentral gyrus; SD, standard deviation. $^{*}P < 0.01$ (correction thresholds by AlphaSim).

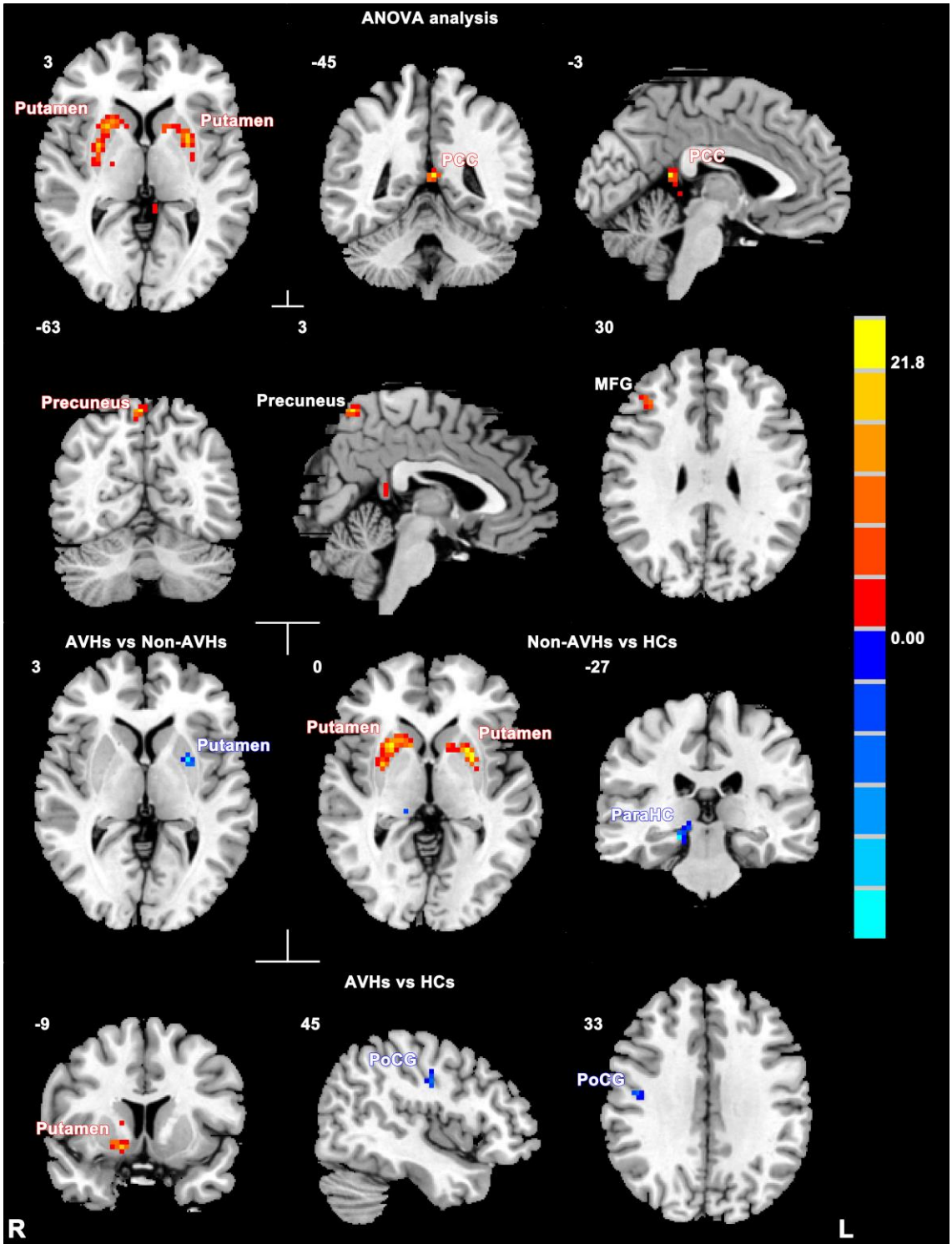

图 4-1 SZ 言语性幻听患者、SZ 非幻听患者与 HCs 之间 ALFF 的比较（*P* < 0.01，AlphaSim 校正）

Fig. 4-1 Comparisons of ALFF among SZ patients with AVHs, SZ patients without AVHs, and HCs (*P* < 0.01, AlphaSim corrected)

As compared with the latter group, the red and blue areas indicate higher and lower ALFF

in the former group, respectively. The slice location is marked in the upper-left. The color bar on the right indicates the F values. ParaHC, parahippocampus; PCC, posterior cingulate cortex; PoCG, postcentral gyrus; STG, superior temporal gyrus.

表 4-3 全脑分析中 ReHo 值变化的区域

Table 4-3 The regions where ReHo values were altered in the whole-brain analysis

	Peak MNI coordinate			Cluster		Mean ReHo value (SD)		
Location	**X**	**Y**	**Z**	**size**	***P***	**AVHs**	**Non-AVHs**	**HCs**
ANOVA analysis								
Right ITG	46	2	-39	29	*	1.00 (0.15)	0.87 (0.10)	0.77 (0.08)
Left putamen	-15	12	0	86	*	1.19 (0.11)	1.25 (0.14)	1.02 (0.10)
Right OMFG	30	54	-12	20	*	1.20 (0.19)	1.22 (0.16)	0.95 (0.17)
Right putamen	18	12	-6	148	*	1.19 (0.10)	1.21 (0.12)	0.99 (0.11)
Left MFG	-30	51	9	73	*	1.15 (0.10)	1.08 (0.07)	0.93 (0.10)
Left MFG	-39	21	39	36	*	1.21 (0.18)	0.98 (0.18)	0.93 (0.16)
Right MFG	36	36	21	22	*	1.22 (0.13)	0.93 (0.16)	0.97 (0.17)
AVHs > Non-AVHs								
Right MFG	42	36	27	28	*	1.29 (0.13)	0.98 (0.15)	
AVHs > HCs								
Right putamen	15	9	-9	36	*	1.34 (0.12)		1.08 (0.18)
Left putamen	-15	12	0	27	*	1.31 (0.13)		1.09 (0.11)
Left MFG	-30	51	9	49	*	1.11 (0.11)		0.87 (0.09)
Non-AVHs > HCs								
Right putamen	18	15	-3	110	*		1.21 (0.12)	0.96 (0.11)

Left putamen	-27	0	0	59	*	1.26 (0.15)	1.02 (0.11)

ITG, inferior temporal gyrus; MFG, middle frontal gyrus; OMFG, orbital middle frontal gyrus. *P < 0.01 (correction thresholds by AlphaSim).

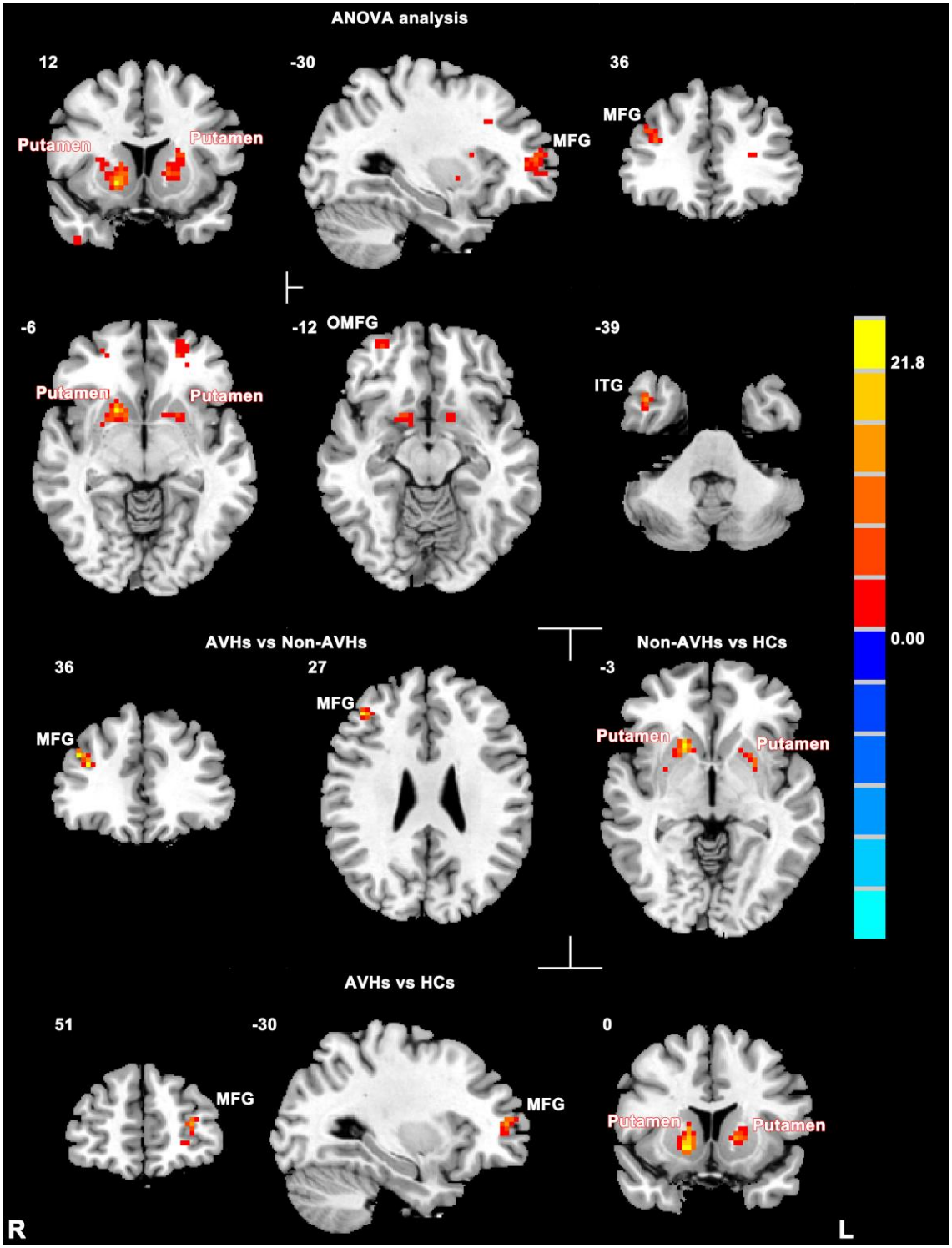

图 4-2 SZ 言语性幻听患者、SZ 非幻听患者与 HCs 之间 ReHo 的比较（*P* < 0.01，

AlphaSim 校正）

Fig. 4-2 Comparisons of ReHo among SZ patients with AVHs, SZ patients without AVHs, and HCs (*P* < 0.01, AlphaSim corrected)

As compared with the latter group, the red areas indicate higher ReHo in the former group. The slice location is marked in the upper-left. The color bar on the right indicates the F values. ITG, inferior temporal gyrus; MFG, middle frontal gyrus; OMFG, orbital middle frontal gyrus.

4.3.3 FC

多个脑区与种子点之间的 FC 发生改变（图 4-3 与表 4-4）。在 SZ 言语性幻听患者中，与 SZ 非幻听患者相比增强的 FC 见于右侧壳核与左侧额下回、额中回（DLPFC 与 Broca 区）之间。与 HCs 相比，在 SZ 言语性幻听患者中降低的 FC 见于右侧壳核与（1）双侧小脑、（2）右侧梭状回、（3）左侧枕下回、（4）左侧楔前叶、（5）双侧中央后回之间，以及左侧壳核与（1）双侧小脑、（2）右侧枕下回、（3）双侧中央后回、（4）右侧中央前回之间。此外，与 HCs 相比，SZ 非幻听患者中降低的 FC 见于右侧壳核与左侧额下回、额中回之间，以及左侧壳核与（1）双侧小脑、（2）双侧颞下回、（3）右侧 gyrus rectus、（4）双侧额下回、（5）左侧颞中回、（6）双侧中央后回、（7）左侧补充运动区、（8）右侧中央前回、（9）左侧中央旁小叶之间。

表 4-4 患者中与两个种子脑区 FC 有统计学意义的变化

Table 4-4 Significant alterations of FC with the two identified seed regions in patients

Seed area	Area with altered FC	*P*	Peak MNI coordinate			Cluster size
			X	Y	Z	
AVHs > Non-AVHs						
Right putamen	Left IFG, triangular part	*	-36	33	0	23
	Left MFG	*	-42	45	0	30
AVHs < HCs						

Right putamen	Cerebellum (Cerebellum_8_L)	*	-24	-57	-60	26
	Cerebellum (Cerebellum_4_5_L)	*	-9	-51	-15	709
	Cerebellum (Cerebellum_4_5_R)	*	21	-42	-24	38
	Right fusiform gyrus	*	27	-60	-3	19
	Left IOG	*	-33	-75	-3	38
	Left precuneus	*	-6	-54	69	105
	Left PoCG	*	-42	-36	66	23
	Right PoCG	*	24	-30	75	115
Left putamen	Cerebellum (Cerebellum_8_L)	*	-18	-54	-57	73
	Cerebellum (Cerebellum_8_R)	*	21	-60	-54	1477
	Cerebellum (Cerebellum_4_5_R)	*	21	-45	-24	197
	Right IOG	*	48	-81	-12	31
	Right PoCG	*	21	-45	63	1624
	Left PoCG	*	-45	-24	27	21
	Right PrCG	*	57	9	36	19
	Left PoCG	*	-42	-36	66	147
Non-AVHs < HCs						
Right putamen	Left IFG, triangular part	*	-36	33	0	46
	Left MFG	*	-45	48	0	33
Left putamen	Cerebellum (Cerebellum_Crus2_R)	*	9	-84	-42	23
	Right ITG	*	48	0	-45	64
	Cerebellum (Cerebellum_6_L)	*	-9	-66	-15	89
	Left ITG	*	-54	-45	-24	20

Right gyrus rectus	*	6	27	-18	30
Left IFG, orbital part	*	-48	24	-12	47
Left MTG	*	-51	-63	12	58
Right PoCG	*	57	-15	33	21
Right IFG, triangular part	*	60	21	24	19
Right PrCG	*	57	12	36	65
Left PoCG	*	-45	-24	27	71
Left IFG, opercular part	*	-60	9	24	34
Left SMA	*	-9	-3	51	25
Right PreCG	*	18	-24	78	44
Left PCL	*	-12	-39	78	50

IPG, inferior parietal gyrus; ITG, inferior temporal gyrus; MFG, middle frontal gyrus; MTG, middle temporal gyrus; PCL, paracentral lobule; PHG, parahippocampal gyrus; PreCG, precentral gyrus; PoCG, postcentral gyrus; SFG, superior frontal gyrus; SMA, supplementary motor area; SMG, supramarginal gyrus. $^{*}P < 0.01$ (correction thresholds by AlphaSim).

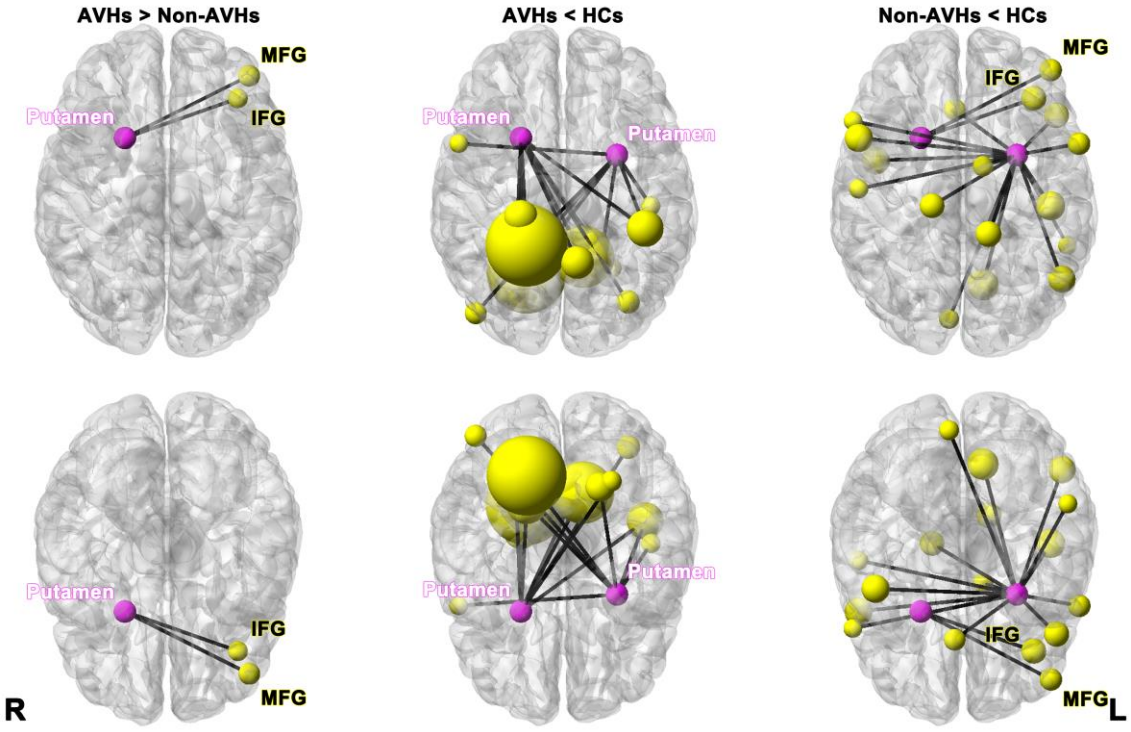

图 4-3 SZ 言语性幻听患者、SZ 非幻听患者与 HCs 之间 FC 的比较（*P* < 0.01，

AlphaSim 校正）

Fig. 4-3 Comparisons of FC among SZ patients with AVHs, SZ patients without AVHs, and HCs (*P* < 0.01, AlphaSim corrected)

Ball locations represent the peak MNI coordinate of differences within clusters, and the size indicates the cluster size. Upper panel, superior view; Lower panel, inferior view.

4.3.4 相关性分析

Allen 等推荐进行单独的影像测量值与幻觉的严重性的相关性分析[146]，因此本实验计算了 AHRS、PANSS 积分与影像测量值之间的相关性。然而，SZ 言语性幻听与非幻听患者的行为学积分（AHRS 与 PANSS 阳性症状积分）与影像测量值之间都无相关性。其他 PANSS 积分的相关性分析结果展示于图 4-4。在 SZ 言语性幻听患者中，左侧额中回的 ReHo 与 PANSS 一般精神病理积分（$r = -0.598$，$P = 0.011$）、总积分（$r = -0.654$，$P = 0.004$）相关。未经校正时，在 SZ 言语性幻听患者中右侧壳核与左侧额下回之间的连接强度与 PANSS 阴性症状积分可见正相关（$r = 0.526$，$P = 0.030$）。在 SZ 非幻听患者中，左侧壳核与右侧额下回之间降低的 FC 与阳性症状、一般精神病理、总积分相关（$r = 0.528$，$P = 0.043$；$r = 0.606$，$P = 0.017$；$r = 0.576$，$P = 0.025$）。

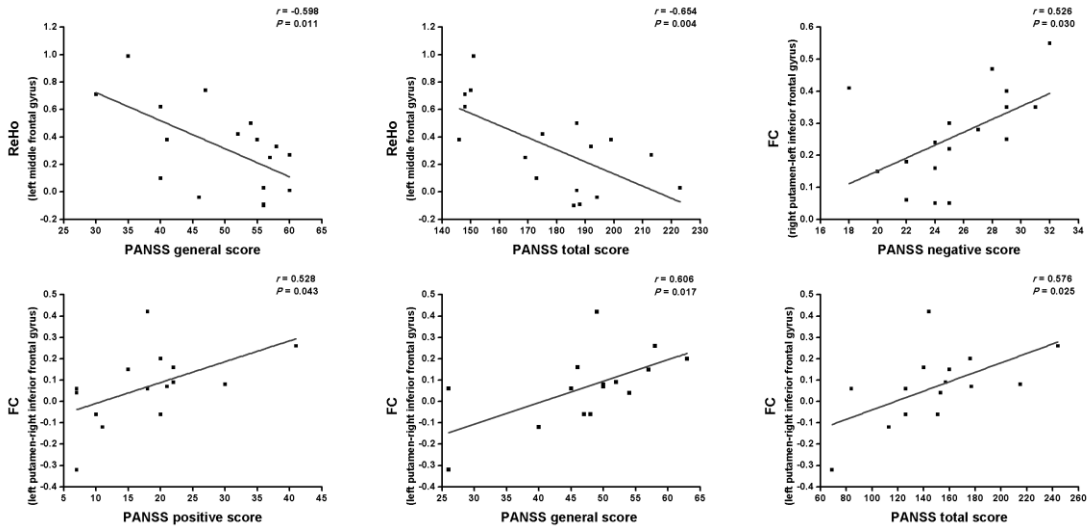

图 4-4 SZ 言语性幻听（上图）与非幻听（下图）患者影像测量值与 PANSS 积分之间的相关性分析

Fig. 4-4 Correlational analyses between the image measures and PANSS scores of SZ

patients with AVHs (upper panel) and without AVHs (lower panel).

4.3.5 ROC 分析

最后，采用 ROC 分析评价 ALFF、ReHo、FC 的诊断价值。表 3-5 列出这些影像测量值区分 SZ 言语性幻听与非幻听患者、区分 SZ 非幻听患者与 HCs 的 ROC 曲线下面积。在全部的分析中 ROC 曲线下面积均大于 0.80。

表 4-5 ROC 曲线下面积

Table 4-5 Area under ROC curve

			95% confidence interval	
Imaging measures		**Area under ROC curve**	**Lower bound**	**Upper bound**
Distinguishing SZ patients with AVHs from SZ patients without AVHs				
ALFF				
Left putamen		0.85	0.71	0.98
ReHo				
Right MFG		0.93	0.84	1.02
FC				
Seed area	**Area with altered FC**			
Right putamen	Left IFG, triangular part	0.90	0.79	1.00
	Left MFG	0.86	0.73	0.99
Distinguishing SZ patients without AVHs from HCs				
ALFF				

Right putamen		0.91	0.81	1.00
Left putamen		0.88	0.77	1.00
Right ParaHC		0.93	0.83	1.03
ReHo				
Right putamen		0.94	0.86	1.02
Left putamen		0.91	0.79	1.02
FC				
Seed area	**Area with altered FC**			
Right putamen	Left IFG, triangular part	0.91	0.80	1.01
	Left MFG	0.86	0.73	0.99
Left putamen	Cerebellum (Cerebellum_Crus2_R)	0.88	0.76	0.99
	Right ITG	0.92	0.81	1.02
	Cerebellum (Cerebellum_6_L)	0.89	0.78	1.00
	Left ITG	0.88	0.76	1.01
	Right gyrus rectus	0.86	0.74	0.98
	Left IFG, orbital part	0.88	0.75	1.00
	Left MTG	0.82	0.67	0.97
	Right PoCG	0.84	0.69	1.00
	Right IFG, triangular part	0.84	0.70	0.98

Right PrCG	0.87	0.74	0.99
Left PoCG	0.88	0.74	1.01
Left IFG, opercular part	0.86	0.73	0.99
Left SMA	0.82	0.66	0.98
Right PreCG	0.88	0.75	1.00
Left PCL	0.93	0.85	1.01

IPG, inferior parietal gyrus; ITG, inferior temporal gyrus; MFG, middle frontal gyrus; MTG, middle temporal gyrus; PCL, paracentral lobule; PHG, parahippocampal gyrus; PreCG, precentral gyrus; PoCG, postcentral gyrus; SFG, superior frontal gyrus; SMA, supplementary motor area; SMG, supramarginal gyrus.

4.4 讨论

本实验采用静息态 BOLD-fMRI 比较了未经治疗的首发 SZ 言语性幻听与非幻听患者的局部与网络功能。该结果显示，SZ 言语性幻听患者左侧壳核 ALFF 降低、右侧额中回 ReHo 升高，以及右侧壳核与左侧额中回、额下回的连接增强。换言之，SZ 言语性幻听壳核与前额叶皮层局部功能异常，以及它们之间的连接增强。此外，SZ 言语性幻听或非幻听患者皮层-纹状体-小脑网络内的连接障碍。

在后续的 FC 分析中选择双侧壳核作为种子点主要是考虑到以下三点：（1）有报道指出壳核参与言语产生[189]，并且在 SZ 言语性幻听患者中发现壳核体积降低、与壳核相关的连接增强[69, 191]；（2）本实验在双侧壳核中检测到三组被试之间 ALFF 与 ReHo 在的差异，而其他 ALFF 与 ReHo 的改变并无相同脑区；（3）根据本实验的发现，左侧壳核对言语性幻听相对特异。因此，根据 SZ 言语性幻听与语言处理脑区相关的证据[197]，考虑到壳核与 SZ 言语性幻听可能相关，于是最终选择双侧壳核作为种子点。

从解剖学上来讲，壳核是纹状体的一部分，投射到内侧苍白球与黑质网状部。皮层-基底节-丘脑皮层环路在运动、执行/关联功能、情感/动机等多个方面发挥重要作用[190]。本实验的结果表明，SZ 言语性幻听患者显示出异常的局部神经生理活动和脑区间整合，主要涉及壳核与前额叶。具体而言，与非幻听患者相比，SZ 言语性幻

听患者表现出左侧壳核 ALFF 降低、右侧额中回（代表 DLPFC）ReHo 升高，以及右侧壳核与左侧额中回、额下回（DLPFC 与 Broca 区）之间的 FC 增强。从结构与功能的角度来讲，壳核、DLPFC 以及 Broca 区以前也曾被联系到 SZ 言语性幻听。van Tol 等研究了全脑灰质体积，结果显示与非幻听患者相比，SZ 幻听患者左侧壳核灰质体积降低[191]。本实验所发现的局部与网络功能缺陷与体积研究是一致的。一项 Jardri 等的基于坐标的荟萃分析纳入了十项 PET 或 fMRI 研究，明确了 SZ 患者出现言语性幻听时的皮层活动，其中就包括左侧 Broca 区[83]。有趣的是，Hoffman 等[69]的 FC 研究中，当 SZ 言语性幻听患者与非幻听患者比较时壳核与左侧 Broca 区作为种子点的 FC 明显增强，表明无论以谁用作种子区，壳核与 Broca 区之间都有相互作用。与此同时，在该研究中还发现壳核与双侧 Wernicke 区作为种子点的 FC 增强，表明壳核与语言脑区的功能性相互作用异常可能促进 SZ 中的言语性幻听。

另外，ROC 曲线下面积等于一项分类器从阴性结果中发现阳性结果的准确性，ROC 曲线下面积越大提示诊断能力水平越高。在本实验中，ROC 分析证明这些影像测量值（ALFF、ReHo 与 FC）区分 SZ 言语性幻听与非幻听患者诊断价值的准确性大于 0.80。

显然，理解神经传递调控异常如何能够导致 fMRI 评估所发现的 SZ 中言语性幻听异常连接是非常重要的，尤其是在相互作用方面。失连接假说[204-206]表明 SZ 的症状与神经连接的异常相关，并强调治疗中的增益控制异常，特别是在幻觉期间异常或错误推断的预测编码模型中的编码准确性方面[108-110]。已经有学者指出 SZ 中“a failure to modulate the sensitivity of neurons responsible for passing sensory information of prediction errors up the visual cortical hierarchy”（用于传递预测错误的感觉信息到视觉皮层的神经元敏感性调控失败）[111]，SZ 中的言语性幻听似乎也具有对听觉/语言处理脑区相似的调控方式。Rolland 等研究 SZ 幻觉的多种感觉形式中伏隔核的 FC[70]。值得注意的是，SZ 幻视-幻听患者比单纯幻听患者表现出伏隔核与双侧壳核之间的 FC 明显增强。鉴于预测编码对语言处理具有潜在的重要作用，这种提议则与言语性幻听极其相关。简单来说，减弱感觉准确性的失败或者增益——皮层处理更高级水平的代偿性改变——可能是许多 SZ 症状与体征（例如，幻觉与不匹配阴性反应的减低）的原因。上述发现表明壳核与前额叶皮层（DLPFC 与 Broca 区）连接障碍。这种特殊形式的连接障碍可能表明壳核对从传递语言预测（即推测放电）的 DLPFC 与

Broca 区的前额叶输入的反应增益或敏感性增加，从而导致缺乏外部听觉刺激时产生言语知觉。

除了与 SZ 言语性幻听患者共有的 FC 变化，非幻听患者显示出壳核与广泛分布于额叶的脑区之间的 FC 减弱。另外，右侧壳核与左侧 DLPFC 与 Broca 区之间的 FC 在 SZ 言语性幻听患者中增强，但在非幻听患者中减弱。非幻听患者并未显示出言语性幻听患者中发现的右侧壳核与左侧楔前叶去耦联，表明言语性幻听语言启动（壳核）、产生（Broca 区）与监控（DLPFC、楔前叶）脑区之间的相互作用紊乱。表明这些改变可能使 SZ 非幻听患者免于这一症状。作为一种严重的精神疾病，SZ 涉及局部脑缺陷与脑区间连接紊乱[204, 206]，其中就包括我们前期发现的半球间通讯异常[53, 207]。就在最近这些年间，根据 fMRI 研究，涌现了大量了文献支持脑网络中的结构连接与 FC 障碍被认为是 SZ 及其显著的临床与神经病理学异质性背后的机制[23, 79, 96, 97, 208, 209]。在本实验中，与 HCs 相比，SZ 言语性幻听或非幻听患者均显示出某些相似的异常 FC 模式。他们显示出许多壳核与额叶-顶叶（感觉与运动区）、壳核与颞叶，以及壳核与小脑之间的 FC 减弱。与 Tu 等报道的结果一致，SZ 患者显示出广泛的双侧壳核与扣带-岛盖网络中其他皮层重要节点的 FC 改变[210]，为 SZ 皮层-纹状体通路功能障碍提供了证据。另外，从神经解剖学的角度讲该发现也是合理的。一方面，大脑皮层中皮层-基底节-丘脑皮层环路的额叶起源包含不同的功能分区：运动区（中央前回、旁中央小叶、补充运动区）、执行/联合区（前额叶），以及情感/动机区（前扣带皮层与内侧眶额皮层）[211]。另一方面，过去的结构与功能神经影像学研究已经提示 SZ 脑网络内连接障碍，尤其是 DMN[79, 96, 119, 168, 172, 173]与丘脑皮层通路[96, 173, 199, 208, 212]，构成了公认的 SZ 病理生理学基础。通过结合相关性与 ROC 分析，不难发现 SZ 患者额/顶/颞叶皮层-纹状体-小脑网络相对的连接减弱。因此，考虑到解剖学与影像学证据，推测皮层-纹状体-小脑连接障碍可能是 SZ 病理生理学的一个重要因素。

据我所知，这是第一个结合局部内部脑活动测量（ALFF 与 ReHo）与网络相互作用模式（FC）的研究——采用数据驱动方法进行评估——探究未经治疗的首发 SZ 患者中的言语性幻听。严格的纳入未经治疗的首发患者限制了本实验的样本量，希望继续扩大该研究的患者人群，将会提高统计效力和对更加细微改变的敏感性。相反，这一纳入标准使治疗的影响、队列效应与疾病相关的环境因素降到最低。本实验发现的异常可能反映了所比较的 SZ 亚组的同质性，有助于推断壳核相关缺陷对

SZ 中的言语性幻听的可能作用。因此，当根据症状亚分型研究 SZ 时该方法可能是有用的。此外，检测 FC 的数据驱动方法为在局部功能异常的脑网络水平功能相关性提供了直接评价[199]。但是，未来 SZ 言语性幻听的基础与临床研究应该评估除了本实验中的壳核之外其他相关脑区的 FC。

研究首发精神病患者的挑战之一便是疾病是动态演变的。一些在这一特定横断面时被认为“没有幻听”的患者如果有更长的观测时间可能会发展为言语性幻听。因此，言语性幻听与非幻听患者之间的界限比慢性患者更不清晰。另外，虽然 SZ 言语性幻听患者的 PANSS 积分与局部活动降低和功能性相互作用增强相关，却未能检测到患者中 AHRS 积分与影像测量值之间显著相关。

总之，本实验的结果表明壳核与前额叶异常局部功能以及它们之间的连接增强同 SZ 言语性幻听的关联。壳核与 DLPFC、Broca 区的功能性相互作用似乎对于 SZ 言语性幻听十分关键。另外，根据所发现的直接的在体证据，壳核相关的局部功能缺陷也可能反映了 SZ 言语性幻听神经调控失衡。在 SZ 患者中，存在广泛的皮层-纹状体-小脑网络内的连接减弱，也进一步支持了目前对于 SZ 失连接假说的观点。

实验五　首发精神分裂症言语性幻听丘脑-听觉皮层-海马连接信息流异常：有效连接研究

Baojuan Li, **Long-Biao Cui**, Yi-Bin Xi, Karl J. Friston, Fan Guo, Hua-Ning Wang, Lin-Chuan Zhang, Yuan-Han Bai, Qing-Rong Tan, Hong Yin, Hongbing Lu (co-first author)

Neurosci Bull, 2017; 33(3):281-291.

尽管 SZ 言语性幻听的神经认知与神经生物学机制在很大程度上尚不清楚，但是包括我们前期研究[36, 53]以及实验一、二、三、四在内的功能成像的发现表明听觉与语言处理相关脑区的局部活动改变可能与 SZ 言语性幻听密切相关。一项 Jardri 等的基于坐标的荟萃分析发现了，SZ 言语性幻听期间皮层活动增强的脑区包括左侧 Broca 区、中央前回、海马/海马旁回、颞上/中回、缘上回、右侧额叶岛盖以及双侧岛叶前部[83]，证明了言语性幻听与言语构成和感知、言语记忆之间的关联。他们进一步检测到经历一过性精神障碍的青少年 Broca 区活动增强[213]。对于 tDCS 或者 TMS 十分敏感的 SZ 言语性幻听患者，ASL 也曾成功地检测到包括听觉皮层和 Broca 区的额颞叶脑区 CBF 降低[57, 64]。

更重要的是，SZ 言语性幻听还涉及上述提及脑区之间的相互作用异常。采用 FC 分析，Lawrie 等发现左侧 DLPFC 与颞叶皮层之间的 FC 同 SZ 言语性幻听的严重性呈负相关[51]。与 SZ 听-视幻觉患者相比，言语性幻听患者表现为海马复合体与丘脑之间的 FC 增强[67]。曾有报道称，与非幻听患者相比幻听患者左侧听觉皮层与右侧海马复合体及丘脑背内侧核 FC 减弱、与左侧额顶区 FC 增强[68]，他们还表现为双侧初级、次级听觉皮层之间的半球间 FC 明显降低[92]。SZ 言语性幻听同非幻听患者相比时，作为种子点的 Wernicke 区与左侧额下回——包括 DLPFC——的 FC 明显增强[69]。最近，Rolland 等发现 SZ 言语性幻听患者显示出伏隔核与中脑边缘通路中的脑区 FC 明显增强[70]，而 Mondino 等证明 tDCS 减弱 SZ 患者言语性幻听与其调节涉及内部言

语监控脑区（左侧 DLPFC）的 FC 相关[136]。同时，结构连接分析证据为神经元之间的相互作用缺陷提供了支持。曾经有学者提出语言处理相关的额颞叶皮层之间的结构连接受损导致言语性幻听[146]，SZ 言语性幻听患者显示出各向异性分数（fractional anisotropy，FA）降低，并主要位于左侧弓状束[41-43, 90, 214-217]及左侧上纵束[44, 47, 214, 215]，而且相似的发现——左侧弓状束白质完整性受损——也在最近的一篇荟萃分析中报道[62]。弓状束是额、颞-顶言语脑区之间一个重要的解剖连接，涉及 Broca 区。而上纵束终止于 DLPFC，这是参与 SZ 发病机制的重要皮层区域，右侧 DLPFC-左侧海马结构连接障碍与 SZ 发病风险相关[209]。另外，左侧颞上回中白质增高的平均扩散性（mean diffusivity）也与 SZ 言语性幻听相关[61]，并且患者中连接双侧听觉皮层的半球间听觉纤维内的 FA 升高[91]。这些结果表明涉及听觉和语言处理的不同脑区之间的 FC 异常，而结构连接分析的证据也为这些神经元之间的相互作用缺陷提供了支持。

SZ 失连接假说[204]强调增益控制异常，特别是幻觉产生时，在异常或错误推测的预测性编码模型中，编码精度的敏感性控制出现异常[108-110]。前期在 SZ 中的动态因果建模（dynamic causal modeling，DCM）提示："a failure to modulate the sensitivity of neurons responsible for passing sensory information of prediction errors up the visual cortical hierarchy"[111]。既然语言处理中预测性编码具有潜在的重要性，这些说法特别适于言语性幻听。简而言之，无法削弱感觉精度或增益——高级皮层处理区域的代偿性变化——或许可以解释 SZ 的众多症状（例如，幻觉）。正如 Adams 等讨论过的[108]，把 SZ 言语性幻听视为无法削弱默读[218]或内部言语[219]（自我产生的活动）的听觉结果伴随放电（corollary discharge）可能更好理解。

虽然前期基于 FC 与结构连接分析的研究发现了部分与 SZ 言语性幻听相关的脑网络，实验一、二、三、四也从不同角度证明了 SZ 言语性幻听的脑网络异常，但是这些脑网络内的信息流向尚不清楚。相比之下，EC（有效连接）的定义是一个神经单元对另一个的因果（有向）影响。DCM 便是基于功能神经成像测量脑区间 EC 的技术[220]，DCM 不仅可使我们量化不同脑区间的连接强度，还能用于研究一个脑区到另一个脑区的信息流向。传统的确定性 DCM 曾被用于揭示 SZ 幻听患者言语网络内（仅关注了 Broca 区与 Wernicke 区及其右侧半球的同伦脑区）的 EC 变化[78]。与传统的确定性 DCM 相比，随机 DCM（stochastic DCM，sDCM）能够用于推断静息态 fMRI 数据的 EC[221]，并提供更为准确的参数估计[222]。最近的在体研究已经开始

采用 sDCM 揭示一些神经精神疾病的病理生理学机制[79, 223-225]。在一项近期的研究中，sDCM 显示首发 SZ 患者从后扣带皮层到 DMN 前额节点的 EC 减弱，这反映的是前额传入的突触后有效性降低[79]。更为重要是，采用频域 DCM，我们前期的研究发现 SZ 患者与 DMN 中的内侧前额叶相关的 EC 改变，提示海马-DLPFC-内侧前额叶连接减弱[223]。

在本实验中，采用 sDCM 探讨前期报道的基于 fMRI 数据得到的与言语性幻听相关的听觉和语言处理脑区之间的 EC，包括 DLPFC（内部言语监控）、听觉皮层（听觉处理）、海马（记忆处理）、丘脑（信息滤过）、Broca 区（言语产生），从而更好地理解 SZ 言语性幻听的病理生理学基础。语言功能（Broca 区）具有高度非对称性[226]，根据上述提及的研究，偏侧化，特别是左侧化，已知是与 SZ 言语性幻听相关的，涉及 DLPFC、海马、丘脑、听觉皮层。因此，推测 SZ 言语性幻听患者到听觉皮层的有向连接增强，从而在缺乏外部听觉刺激时易于出现假性知觉推断。

5.1 材料

5.1.1 被试

同实验三，具体参见 3.1.1。本研究由第四军医大学第一附属医院药物临床试验伦理委员会批准，所有参与者均提供了书面知情同意。

5.1.2 仪器设备

同实验一，具体参见 1.1.2。

5.2 方法

5.2.1 图像采集

同实验三，具体参见 3.2.1。采用 EPI 序列获取全部被试的静息态功能像。

5.2.2 数据预处理

预处理静息态 fMRI 图像。对于每位被试，首先配准 fMRI 图像以校正头动，头动排除标准：横移> 2.5 mm 和/或旋转> 3.0 °。然后将配准的图像标准化到 MNI 空间，最终用 8 mm FWHM 高斯核平滑。

5.2.3 广义线性模型

在被试水平，正如我前期研究中所描述的细节[223]，为每位被试构建广义线性模型（general linear model，GLM）。GLM 包括来自于配准步骤中的六个运动参数、一个常量回归量基线建模，以及余弦基函数。

5.2.4 选取 ROIs

如前所述，大部分结构与功能改变位于左半球。为每位被试选择五个 ROIs，包括左侧听觉皮层、DLPFC（包括 Frontal_Sup_L 与 Frontal_Sup_Medial_L）、海马、丘脑以及 Broca 区（包括 Frontal_Inf_Tri_L 与 Frontal_Inf_Oper_L）。采用 WFU PickAtlas Tool 和 AAL 图谱模板（Version 3.0.4, http://www.nitrc.org/projects/wfu_pickatlas/）[125] 为每个脑区制作一个 mask，提取被试每个 ROI 的特异性时间序列。mask 的位置与 ROIs 的时间序列展示于图 5-1。

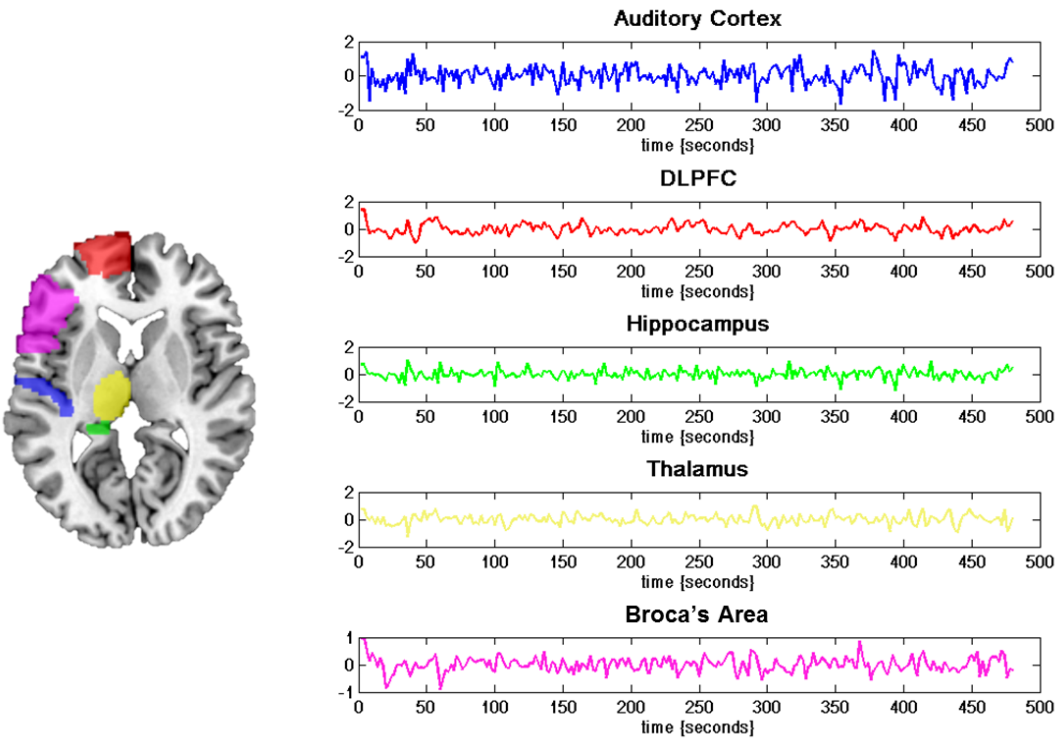

图 5-1 模板位置及提取的 ROIs 时间序列

Fig. 5-1 Locations of the masks and extracted ROIs time series

Yellow indicates the left thalamus; red indicates the left DLPFC; blue indicates the left auditory cortex; violet indicates the left Broca's area caudate; green indicates the left

hippocampus. DLPFC, dorsolateral prefrontal cortex.

5.2.5 sDCM

采用 sDCM 研究左侧 Broca 区、DLPFC、海马、丘脑，以及听觉平层之间的 EC。为每位被试构建全连接模型，然后用广义滤波转换该模型[227]。组间比较 *t* 检验时，将连接的估计作为经典随机效应推断的统计量。由于假设只关注 ROIs 之间的连接，因此组间比较采用未校正的 *P* 值。

5.2.6 统计学分析

ROC 分析用于评估影像测量值区分 SZ 言语性幻听与非幻听患者的诊断能力。另外，Allen 等[146]建议对影像测量值与幻觉严重性进行相关性分析，为了检测 EC 与幻觉严重性的相关性，计算言语性幻听患者中连接强度与 AHRS 积分之间的 Pearson 相关系数。经多重比较校正的 *P* 值小于 0.05 时被认为差异具有统计学意义。

5.3 结果

5.3.1 EC

在组水平显著的连接（单样本 *t* 检验 *P* 值 0.05，多重比较 Bonferroni 校正）展示于图 5-2 与表 5-1。在言语性幻听患者中，听觉皮层、DLPFC 以及 Broca 区形成了一个双向连接网络（图 5-2A）。相比而言，非幻听患者中检测到的连接更加分散（图 5-2B），除了 DLPFC 与 Broca 区之间、听觉皮层与 Broca 区之间的双向连接，还观察到了听觉皮层与海马之间、听觉皮层与丘脑之间的相互连接，以及从海马到 DLPFC 的单向连接。HCs 也显示出听觉皮层与 Broca 区之间、DLPFC 与 Broca 区之间的相互连接（图 5-2C）。

表 5-1 SZ 患者与 HCs 的连接强度（Hz）

Table 5-1 Strength (Hz) of Connections in SZ Patients and HCs

Connections	AVHs patients	Non-AVHs patients	HCs
auditory cortex-DLPFC[a]	−0.1161	−0.0946	−0.0634

auditory cortex-hippocampus[b]	0.0449[*]	0.2516	0.0664
auditory cortex-thalamus[b]	0.0658	−0.2112	−0.0203
auditory cortex-Broca's area[a,b,c]	0.1334	0.2413	0.1628
DLPFC-auditory cortex[a]	−0.2732	−0.0016	−0.1180
DLPFC-hippocampus[c]	0.1552	0.1698	0.2111
DLPFC-Broca's area[a,b]	0.3538	0.4347	0.3999
hippocampus-auditory cortex[b]	0.1378	0.3213	0.1288
hippocampus-DLPFC[b,c]	0.0967	0.2849	0.1583
hippocampus-thalamus[c]	0.0130	0.1362	0.3128
thalamus-auditory cortex[b]	0.0446[*]	−0.2738[#]	−0.0322
Broca's area-auditory cortex[a,b,c]	0.3543	0.3224	0.4199
Broca's area-DLPFC[a,b,c]	0.2910	0.3505	0.4051

Significant effective connectivity at the group level (P < 0.05, Bonferroni corrected) of AVHs ([a]), Non-AVHs ([b]), and HCs ([c]). [*]P < 0.05 versus Non-AVHs patients (uncorrected); [#]P < 0.05 versus HCs (uncorrected).

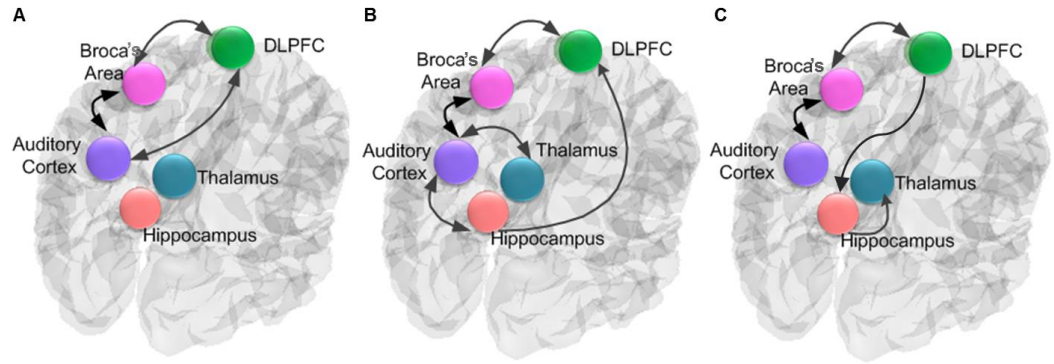

图 5-2 SZ 患者与 HCs 中 ROIs 之间显著的 EC（组内水平）

Fig. 5-2 Significant EC (at the group level) among ROIs in the SZ patients and HCs

Significant connections in the AVHs group (A), Non-AVHs group (B), and HCs (C).

两样本 *t*-检验（*P* 值设为 0.05，多重比较未校正）显示与非幻听患者相比，SZ 言语性幻听患者从丘脑到听觉皮层的 EC 增强（图 5-3A）。与 HCs 相比，从丘脑到听觉皮层的连接强度在非幻听患者中减弱（图 5-3B）。另外，言语性幻听患者中从听觉皮层到海马的连接减弱。

5.3.2 ROC 分析

丘脑-听觉皮层连接的曲线下面积为 0.79（95%置信区间，0.64-0.95），听觉皮层-海马连接的曲线下面积为 0.70（95%置信区间，0.51-0.88），显示出影像测量值具备区分 SZ 言语性幻听与非幻听患者的诊断能力（$P < 0.05$，图 5-3C）。

5.3.3 相关性分析

最后，对言语性幻听组行幻听严重性与连接强度的相关性分析。结果发现，AHRS 积分与丘脑到听觉皮层连接及听觉皮层到海马连接并无相关（图 5-3D 与 E），而 Broca 区到听觉皮层的连接强度与 AHRS 积分呈正相关（图 5-3F）。

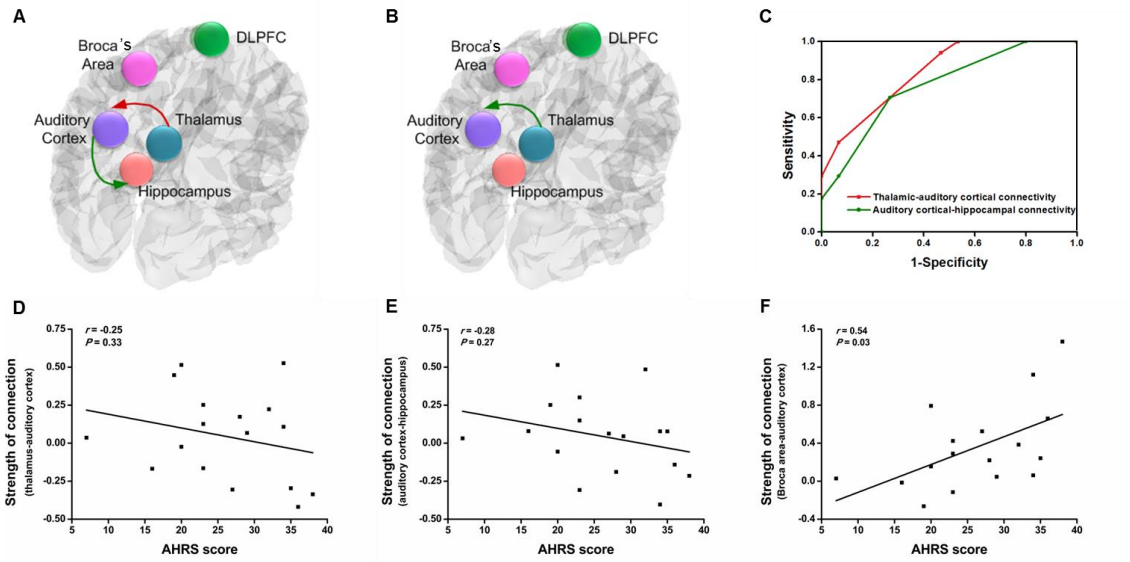

图 5-3 SZ 言语性幻听与非幻听患者之间显著的 EC（组间水平）、ROC 分析及相关性分析

Fig. 5-3 Significant EC (at the between group level) among ROIs between the SZ patients with and without AVHs, ROC analysis and correlation analysis

(A) Increased (red) and decreased (green) EC in the AVHs group as compared with Non-AVHs group. (B) Decreased (green) EC in the Non-AVHs group as compared with

HCs. (C) ROC analysis for distinguishing AVHs from Non-AVHs. (D-F) Correlations between the AHRS score and strength of connection from the thalamus to the auditory cortex, from the auditory cortex to the hippocampus, and from the Broca area to the auditory cortex.

5.4 讨论

运用 fMRI 与 sDCM，结果显示 SZ 言语性幻听患者与非幻听患者相比丘脑-听觉皮层连接增强与听觉皮层-海马连接减弱。有趣的是，SZ 言语性幻听患者与 HCs 之间的差异并无统计学意义。HCs 的丘脑-听觉皮层-海马连接强度介于 SZ 言语性幻听与非幻听患者之间，恰恰提示了言语性幻听患者在这种精神病理学状态下的脑功能紊乱，导致言语性幻听患者的连接强度与 HCs 相似。另外，扫描期间患者未经历幻听，因此该研究为 Jardri 等描述的特质研究[83]。

5.4.1 SZ 中言语性幻听的特异性发现：丘脑-听觉皮层连接增强

本实验的结果提示 SZ 言语性幻听患者表现出可由连接障碍解释的异常的神经生理活动，主要涉及听觉皮层。具体而言，SZ 言语性幻听患者丘脑-听觉皮层 EC 增强，提示减弱从丘脑到听觉皮层的兴奋性传入的相对失败。这一发现从神经解剖学角度也是合理的：从丘脑内侧膝状体投射到听觉皮层的突触前终末在靶区释放兴奋性神经递质，即谷氨酸，SZ 的确涉及丘脑皮层连接障碍[212]。在分子水平，SZ 被认为是神经发育障碍，其中谷氨酸与多巴胺系统可能是异常的。神经影像学研究已经发现 SZ 言语性幻听患者多巴胺能网络内的 FC 异常[70]。在 SZ 小鼠模型，Chun 等采用神经电生理学方法证实了丘脑-听觉皮层突触传递缺陷与幻听相关，Drd2 依赖的丘脑-皮层障碍可能代表了 SZ 言语性幻听的一种病理生理学机制[95]。这与本实验的发现较为一致，本实验采用在体 fMRI 发现 SZ 言语性幻听患者从丘脑到听觉皮层的连接异常。特别是 SZ 非幻听患者显示出丘脑-听觉皮层明显抑制，提示到听觉皮层的丘脑传入得到有效的增益控制，从而无幻听症状。相反，与非幻听患者相比，SZ 言语性幻听患者无法降低从丘脑到听觉皮层的兴奋性传入。这就提示了对丘脑到听觉皮层的上行输入调控失败，导致易于出现言语性幻听。综合考虑基础与临床证据，丘脑-听觉皮层连接障碍可能是 SZ 言语性幻听病理生理学机制中的重要因素。

5.4.2 预测编码、错误推断与 SZ 言语性幻听

由于异常神经调节，减弱听觉系统上行感觉信息的失败，造成了 Fogelson 等运用脑电图数据 DCM 的结果[111]。总体而言，本实验的结果与无法降低感觉（听觉）准确性以及相关皮层增益控制一致。从生理学角度而言，将这种失败解释为对非预测性刺激的特征性异常弱化（参见 Baldeweg 等[110]综述）；从功能的角度讲，这种增益控制异常已经被解读为在预测性编码中无法恰当解码上行感觉信息准确性。准确性的归因错误将对感觉推断产生深远的影响，很有可能导致幻觉以及继发的妄想（参见 Adams 与 Fletcher [108, 228]更为全面的讨论）。

丘脑可能通过不同的通路介导听觉皮层的反应。丘脑-听觉皮层投射来自于丘脑的多个核团，除了内侧膝状体之外还包括丘脑内侧及背侧部。言语性幻听中从丘脑到听觉皮层的连接增强，反映了丘脑对听觉皮层的总体效应（因为在 sDCM 中本实验把丘脑活动看作包含所有核团的单个脑区）。多种神经递质/神经调质（多巴胺、谷氨酸/谷氨酰胺、乙酰胆碱、去甲肾上腺素、五羟色胺及组胺）对丘脑相关网络的综合影响可能是 SZ 幻觉出现的原因[98]。另外，根据丘脑皮层 γ 活动接受外部感觉信息的调控受损，丘脑在 SZ 中增强特定输入、抑制其他输入[99, 102]。有人提出言语性幻听是丘脑将外部言语从内部言语中滤过的功能障碍的结果[100, 101]。该结果与专注丘脑-听觉皮层投射中谷氨酸能神经元的研究形成对照，Chun 等发现由于 *dgcr8* 基因编码的小 RNA 缺失，丘脑 Drd2 异常增加导致谷氨酸释放减少，引起丘脑皮层突触缺陷[95]。显然，理解调控行神经传递如何导致 fMRI 评估的 EC 异常将十分重要，特别是在丘脑-皮层与皮层-丘脑相互紧密作用的情况下。

5.4.3 言语性幻听中听觉皮层活动增强

听觉皮层对丘脑输入的敏感性增加可能解释了 SZ 言语性幻听患者听觉皮层活动增强，正如 ASL 研究检测到的听觉皮层 CBF 升高[57, 64]。水平升高可能反映了 SZ 言语性幻听患者听觉皮层的兴奋性升高。tDCS 或 TMS 治疗后，治疗有效的 SZ 言语性幻听患者幻听严重性降低，听觉皮层 CBF 明显降低。另外，一项包括 12 项功能神经影像学研究的荟萃分析表明在没有外部听觉刺激时 SZ 言语性幻听患者左侧听觉皮层活动增强[85]。将这些结果与本实验的发现综合起来，据此推测 SZ 听觉处理起源于丘脑-皮层连接障碍[212]，这也曾在认知性辨距障碍中被提出[229]。这些建议完全适合可能由准确性异常产生的各种连接障碍。

5.4.4 SZ 言语性幻听中听觉皮层-海马连接减弱

至于听觉皮层与海马之间的连接减弱，本实验发现 SZ 言语性幻听比非幻听患者兴奋性连接减弱。采用多模态分析，Amad 等报道了海马与 SZ 言语性幻听之间的联系，显示 SZ 单纯言语性幻听或幻视-幻听患者涉及海马与丘脑之间的 FC、白质连接（钩状束）、海马体积的不同模式[67]。虽然听觉皮层与海马之间并未从解剖上发现存在神经投射，本实验结果表明在 SZ 中它们之间可能存在功能性的相互作用。考虑到下纵束中的长纤维连接视觉区域与海马[230]，由此推测类似的“听觉皮层-海马投射”参与听觉信息处理。可能是微弱的听觉皮层-海马连接促进了 SZ 言语性幻听，这可能是异常增益控制的另一种表现。调控性增益控制往往表现出在不同的皮层水平相互改变。从预测编码的角度来讲，无法降低听觉皮层的听觉敏感性与更高水平（海马）的准确性相对降低完全一致。简而言之，这可能意味着听觉皮层的感觉水平对上行或下行传入更为敏感，而更高的水平（例如，海马）则不那么敏感。

听觉皮层对上行（丘脑）与下行（前额叶）传入敏感性可能相对升高。通过结合 SZ 言语性幻听与非幻听患者数据，三组之间 DLPFC、Broca 区与听觉皮层之间的连接差异无统计学意义。然而，本实验检测到 AHRS 积分与 Broca 区到听觉皮层的 EC 强度呈正相关，提示 SZ 患者言语性幻听的严重性与听觉皮层对 Broca 区传入的敏感性增加，言语性幻听 Wernick 区-Broca 区连接减弱[78]引起 Broca 区-听觉皮层连接增强的代偿性改变可能是合理的解释。

据我所知，这是首个采用 sDCM 评估基于症状的首发未经治疗的 SZ 患者 EC 研究。值得一提的是，采用 DCM，Ćurčić-Blake 等指出的从 Wernicke 区到 Broca 区为负性连接[78]；采用非线性确定性 DCM，Dauvermann 等发现 SZ 患者的一级或二级亲属言语流畅性处理任务下丘脑-皮层连接减弱[231]。采用 sDCM，本实验刻画了与言语性幻听直接相关的 EC 特征，发现首发未经治疗的 SZ 言语性幻听患者表现出三个脑区（丘脑、听觉皮层、海马）之间的连接障碍，即与非幻听患者相比丘脑-听觉皮层 EC 增强、听觉皮层-海马 EC 减弱。另外，在我们前期的体积研究中，发现首发未经治疗的 SZ 言语性幻听患者双侧丘脑体积降低[36]。换言之，SZ 言语性幻听患者由于丘脑体积降低代偿性增强从丘脑到听觉皮层的兴奋性传入，这可能 SZ 言语性幻听的机制之一（图 5-4）。

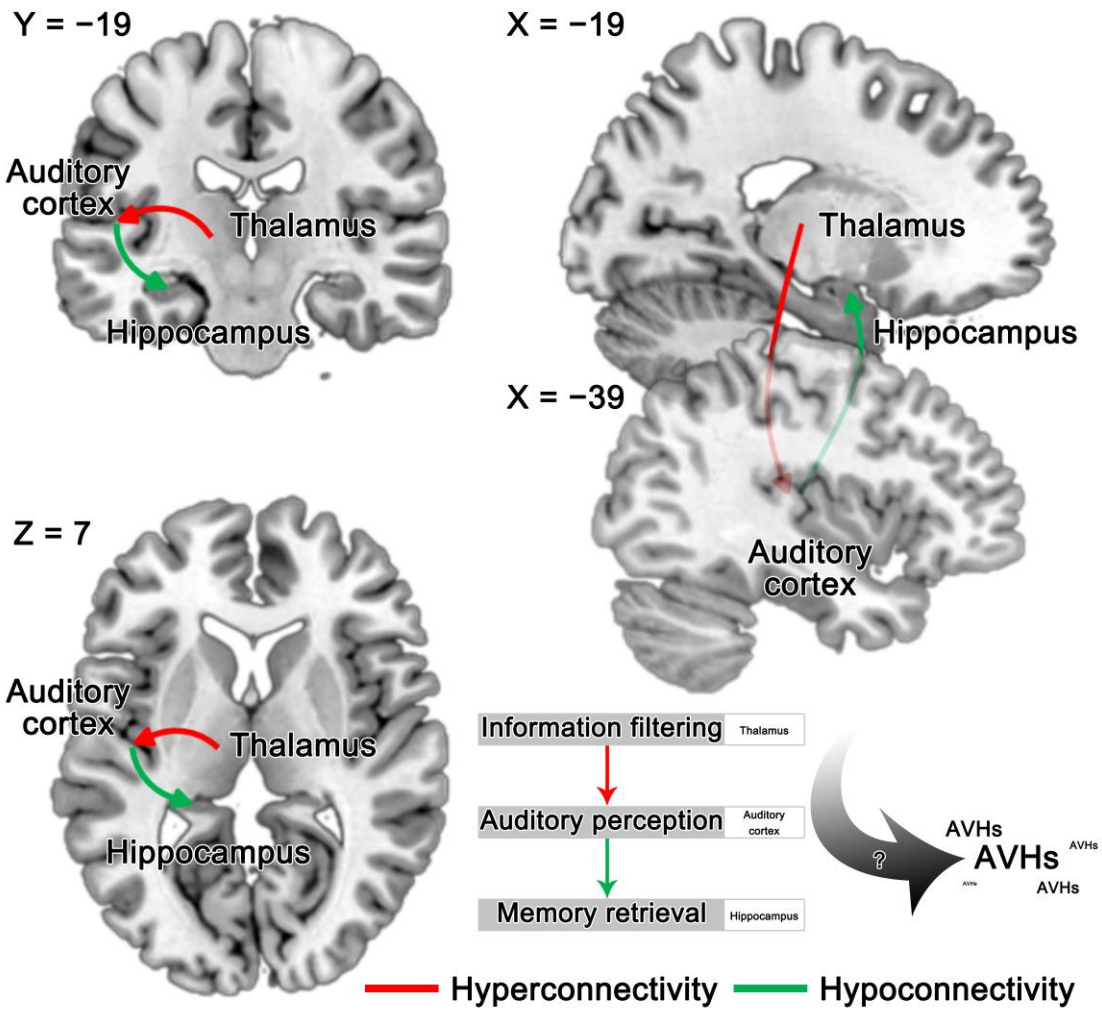

图 5-4 SZ 言语性幻听的可能机制

Fig. 5-4 Proposed mechanism responsible for AVHs in SZ

Disrupted interactivation among the sensory information filtering (thalamus), auditory perception (auditory cortex), and memory retrieval (hippocampus) might be involved in AVHs in SZ. Thalamic-auditory cortical-hippocampal dysconnectivity may lead to increased activation of the auditory cortex and false perceptual inference in the absence of auditory stimuli.

需要指出的不足是 fMRI 扫描通常需要被试较高的依从性，然而，这恰恰是多数未经治疗的 SZ 患者尤为缺乏的，这也进一步限制了该实验的样本量。在后续研究中，

仍需要进一步扩大样本量。

综上所述，本实验发现言语性幻听中从丘脑到听觉皮层连接增强、从听觉皮层到海马连接减弱。在 SZ 言语性幻听患者中听觉皮层对丘脑上行输入的敏感性降低失败，继而出现代偿性海马对听觉输入反应下调。这些发现与当前 SZ 是连接障碍综合征的想法一致，支持言语性幻听与听觉/语言处理区、DMN 脑区、其他网络（岛叶与纹状体）相关的连接障碍假说[12]。基于本实验所发现的在体证据，丘脑-听觉皮层-海马通路对 SZ 言语性幻听似乎十分重要。

小　　结

主要结论

（1）脑血流及其复杂网络研究：SZ 言语性幻听患者言语想象、产生、监控障碍（**Cui LB**, Chen G, Xu ZL *et al*. *Psychiatry Res Neuroimaging*, 2017; 260:53-61.）[232]；

（2）结构网络 rich club 组织研究：SZ 言语性幻听 rich club 组织水平降低，且非 rich club 脑区网络与其关系更为密切（**Cui LB**, Wei Y, van den Heuvel MP *et al*. In preparation）；

（3）静息态网络研究：首发 SZ 言语性幻听患者听觉处理、语言处理、信息滤过失衡（**Cui LB**, Liu L, Guo F *et al*. *Radiology*, 2017; 283(3):810-819.）[233]；

（4）局部脑功能与功能连接研究：首发 SZ 言语性幻听患者言语启动受损（**Cui LB**, Liu K, Li C *et al*. *Schizophr Res*, 2016; 173(1-2):13-22.）[234]；

（5）有效连接研究：首发 SZ 言语性幻听患者丘脑-听觉皮层-海马通路紊乱（Li BJ, **Cui LB**, Xi YB *et al*. *Neurosci Bull*, 2017; 33(3):281-291.）[235]；

以上结果显示，SZ（特别是首发 SZ）幻听患者的脑结构与功能具有特征性改变：大尺度脑网络结构紊乱，其中涉及听觉、语言、记忆、信息滤过的脑区明显异常。据此推测**由于 SZ 患者负责言语想象、启动、产生、监控等任务的语言相关脑区活动失衡，导致内部言语紊乱；同时，丘脑体积降低，出现内部言语滤过障碍，使其对听觉皮层的调节代偿性增强，致使听觉中枢异常活跃；另外，上述信息反馈至海马等记忆相关脑区，言语性回忆异常，进一步促进内部言语紊乱（图 1）。因此，涉及听觉、语言、记忆、信息滤过的脑区局部及相互作用明显异常，可能最终导致 SZ 患者在缺乏外部刺激时出现幻听。**这些脑结构与功能的改变可能是导致 SZ 幻听的神经影像学基础，为进一步探讨针对上述 SZ 幻听神经机制的特异性干预策略提供理论依据。

创新点

（1）首次提出涉及听觉、语言、记忆、信息滤过的脑区局部及相互作用明显异常，可能最终导致 SZ 患者在缺乏外部刺激时出现幻听这一相对完善的神经机制，具有理论创新性。

（2）基于多模态 fMRI 数据，综合采用复杂网络、rich club 组织、静息态网络、低频振幅、局部一致性、功能连接、有效连接等多种分析方法，高度整合结果，对 SZ 幻听的神经机制进行多角度探讨，具有分析思路创新性。

（3）通过横断面研究，对 SZ 幻听患者与非幻听患者脑结构与功能影像进行比较，分析两者与幻听症状变化的关系，揭示 SZ 幻听的神经影像学基础及其背后可能的神经机制；同时，为了减少治疗因素的干扰和疾病慢性化的影响，实验二、三、四、五仅纳入首发未经治疗的患者，具有研究策略创新性。

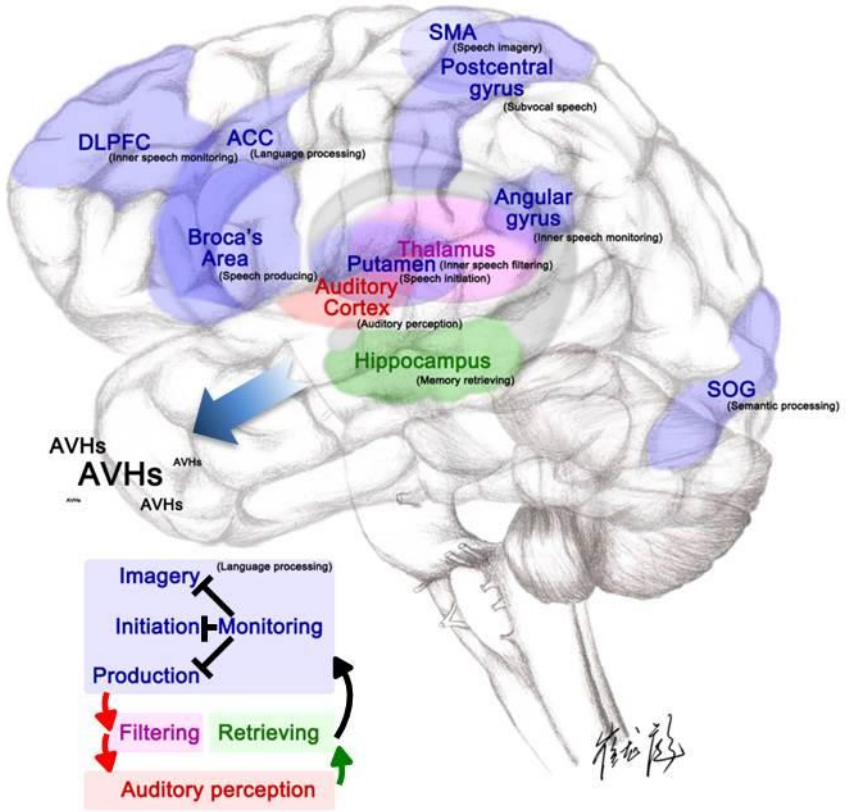

图 1 SZ 言语性幻听可能的神经机制

Fig. 1 Proposed neural mechanism responsive for the AVHs in SZ patients

Dysfunctional interaction of brain regions involving auditory processing, language producing and monitoring, sensory information filtering, and verbal memory retrieval

predisposes SZ patients to false perceptual inference, i.e., AVHs in the absence of external auditory stimuli. We hypothesize that language-related memory retrieving helps to provide the source of inner speech, and active speech imagery, initiation and production without appropriate monitoring yield excessive inner speech, inducing overmuch auditory input due to deficit information filtering. ACC, anterior cingulate cortex; DLPFC, dorsolateral prefrontal cortex; SMA, supplementary motor area; superior occipital gyrus.

局限性

本研究存在以下两点不足。第一，尽管本研究采用了高分辨 T1 图像、DTI、BOLD 功能图像，以及灌注图像等多模态 fMRI 数据，然而每个实验都是孤立地使用一种模态的数据进行分析，并未将多模态数据进行真正意义上的融合。各部分实验的结果之间既有相同点又有不同点，这在一定程度上对实验结果的阐述造成了影响。后续研究则应将灰质、白质、功能图像进行多模态融合分析，找出不同模态之间高度一致的 SZ 幻听特征性脑改变。第二，样本量较小也是其中一个不足之处，实验一的被试数目为 75 人，实验二为 90 人，而实验三、四、五则为 51 人。特别是后面四个实验，为了减少治疗因素的干扰和疾病慢性化的影响，仅纳入首发未经治疗的患者。但是，由于依从性相对较差，收集首发患者的 MRI 数据就显得尤为困难，从而导致样本量偏小。因此，目前也只能通过更长的时间积累更大量的宝贵数据。

研究展望

后续实验应将结构网络、白质网络、功能网络进行真正意义上的多模态融合分析，以期更加全面清晰地阐述 SZ 幻听特征性脑改变；同时，继续探讨已经发现的 SZ 幻听特异性脑区能否作为干预的靶区，从而指导 SZ 的临床治疗；另外，部分 SZ 幻听患者药物治疗效果不佳，通过对难治性 SZ 幻听患者进行前瞻性研究，深入了解难治性 SZ 幻听的神经病理机制，从而寻找筛查及预测生物标记物。通过开展横向及纵向研究，实现基于神经影像学基础的 SZ 诊疗全程的个体化精准指导。

参考文献

[1] Whiteford HA, Degenhardt L, Rehm J, Baxter AJ, Ferrari AJ, Erskine HE, Charlson FJ, Norman RE, Flaxman AD, Johns N, Burstein R, Murray CJ, Vos T. Global burden of disease attributable to mental and substance use disorders: findings from the Global Burden of Disease Study 2010. Lancet 2013;382:1575-86.

[2] Owen MJ, Sawa A, Mortensen PB. Schizophrenia. Lancet 2016;388:86-97.

[3] Gonzalez JC, Aguilar EJ, Berenguer V, Leal C, Sanjuan J. Persistent auditory hallucinations. Psychopathology 2006;39:120-5.

[4] Shergill SS, Murray RM, McGuire PK. Auditory hallucinations: a review of psychological treatments. Schizophr Res 1998;32:137-50.

[5] Hor K, Taylor M. Suicide and schizophrenia: a systematic review of rates and risk factors. J Psychopharmacol 2010;24:81-90.

[6] Penfield W. Some Mechanisms of Consciousness Discovered during Electrical Stimulation of the Brain. Proc Natl Acad Sci U S A 1958;44:51-66.

[7] Frith CD, Done DJ. Towards a neuropsychology of schizophrenia. Br J Psychiatry 1988;153:437-43.

[8] McGuire PK, Silbersweig DA, Wright I, Murray RM, David AS, Frackowiak RS, Frith CD. Abnormal monitoring of inner speech: a physiological basis for auditory hallucinations. Lancet 1995;346:596-600.

[9] Feinberg I. Efference copy and corollary discharge: implications for thinking and its disorders. Schizophr Bull 1978;4:636-40.

[10] Allen P, Freeman D, Johns L, McGuire P. Misattribution of self-generated speech in relation to hallucinatory proneness and delusional ideation in healthy volunteers. Schizophr Res 2006;84:281-8.

[11] Copolov DL, Seal ML, Maruff P, Ulusoy R, Wong MT, Tochon-Danguy HJ, Egan GF. Cortical activation associated with the experience of auditory hallucinations and

perception of human speech in schizophrenia: a PET correlation study. Psychiatry Res 2003;122:139-52.

[12] Alderson-Day B, McCarthy-Jones S, Fernyhough C. Hearing voices in the resting brain: A review of intrinsic functional connectivity research on auditory verbal hallucinations. Neurosci Biobehav Rev 2015;55:78-87.

[13] Alderson-Day B, Diederen K, Fernyhough C, Ford JM, Horga G, Margulies DS, McCarthy-Jones S, Northoff G, Shine JM, Turner J, van de Ven V, van Lutterveld R, Waters F, Jardri R. Auditory Hallucinations and the Brain's Resting-State Networks: Findings and Methodological Observations. Schizophr Bull 2016;42:1110-23.

[14] Bohlken MM, Hugdahl K, Sommer IE. Auditory verbal hallucinations: neuroimaging and treatment. Psychol Med 2017;47:199-208.

[15] Upthegrove R, Broome MR, Caldwell K, Ives J, Oyebode F, Wood SJ. Understanding auditory verbal hallucinations: a systematic review of current evidence. Acta Psychiatr Scand 2016;133:352-67.

[16] Vos T, Flaxman AD, Naghavi M, Lozano R, Michaud C, Ezzati M, et al. Years lived with disability (YLDs) for 1160 sequelae of 289 diseases and injuries 1990-2010: a systematic analysis for the Global Burden of Disease Study 2010. Lancet 2012;380:2163-96.

[17] Becker AE, Kleinman A. Mental health and the global agenda. N Engl J Med 2013;369:66-73.

[18] 国家卫生计生委. 2016 中国卫生和计划生育统计年鉴. 北京 2016: 中华人民共和国卫生和计划生育委员会.

[19] APA. Diagnostic and Statistical Manual of Mental Disorders. 5th ed. Washington, DC: American Psychiatric Association 2013:87-118.

[20] Freedman R. Schizophrenia. N Engl J Med 2003;349:1738-49.

[21] Hales RE, Yudofsky SC, Gabbard GO. The American Publishing Textbook of Psychiatry, 5th eded. Washington DC and London: American Psychiatric Publishing, Inc., 2008.

[22] Insel TR, Wang PS. Rethinking mental illness. JAMA 2010;303:1970-1.

[23] Voineskos AN, Foussias G, Lerch J, Felsky D, Remington G, Rajji TK, Lobaugh N, Pollock BG, Mulsant BH. Neuroimaging evidence for the deficit subtype of schizophrenia. JAMA Psychiatry 2013;70:472-80.

[24] Kjelby E, Sinkeviciute I, Gjestad R, Kroken RA, Loberg EM, Jorgensen HA, Hugdahl K, Johnsen E. Suicidality in schizophrenia spectrum disorders: the relationship to hallucinations and persecutory delusions. Eur Psychiatry 2015;30:830-6.

[25] Bucci S, Birchwood M, Twist L, Tarrier N, Emsley R, Haddock G. Predicting compliance with command hallucinations: anger, impulsivity and appraisals of voices' power and intent. Schizophr Res 2013;147:163-8.

[26] Sacks O. Hallucinationsed. London, UK: Pan Macmillan, 2012.

[27] Fenelon G, Mahieux F, Huon R, Ziegler M. Hallucinations in Parkinson's disease: prevalence, phenomenology and risk factors. Brain 2000;123 (Pt 4):733-45.

[28] Llorca PM, Pereira B, Jardri R, Chereau-Boudet I, Brousse G, Misdrahi D, Fenelon G, Tronche AM, Schwan R, Lancon C, Marques A, Ulla M, Derost P, Debilly B, Durif F, de Chazeron I. Hallucinations in schizophrenia and Parkinson's disease: an analysis of sensory modalities involved and the repercussion on patients. Sci Rep 2016;6:38152.

[29] Tien AY. Distributions of hallucinations in the population. Soc Psychiatry Psychiatr Epidemiol 1991;26:287-92.

[30] Sommer IE, Daalman K, Rietkerk T, Diederen KM, Bakker S, Wijkstra J, Boks MP. Healthy individuals with auditory verbal hallucinations; who are they? Psychiatric assessments of a selected sample of 103 subjects. Schizophr Bull 2010;36:633-41.

[31] Heckers S. Studies of auditory verbal hallucinations. Psychophysiology 2016;53:305-7.

[32] White T, Gottesman I. Brain connectivity and gyrification as endophenotypes for schizophrenia: weight of the evidence. Curr Top Med Chem 2012;12:2393-403.

[33] Levitan C, Ward PB, Catts SV. Superior temporal gyral volumes and laterality correlates of auditory hallucinations in schizophrenia. Biol Psychiatry 1999;46:955-62.

[34] Nenadic I, Smesny S, Schlosser RG, Sauer H, Gaser C. Auditory hallucinations

and brain structure in schizophrenia: voxel-based morphometric study. Br J Psychiatry 2010;196:412-3.

[35] Chen X, Liang S, Pu W, Song Y, Mwansisya TE, Yang Q, Liu H, Liu Z, Shan B, Xue Z. Reduced cortical thickness in right Heschl's gyrus associated with auditory verbal hallucinations severity in first-episode schizophrenia. BMC Psychiatry 2015;15:152.

[36] Huang P, Xi Y, Lu ZL, Chen Y, Li X, Li W, Zhu X, Cui LB, Tan Q, Liu W, Li C, Miao D, Yin H. Decreased bilateral thalamic gray matter volume in first-episode schizophrenia with prominent hallucinatory symptoms: A volumetric MRI study. Sci Rep 2015;5:14505.

[37] Wigand M, Kubicki M, Clemm von Hohenberg C, Leicht G, Karch S, Eckbo R, Pelavin PE, Hawley K, Rujescu D, Bouix S, Shenton ME, Mulert C. Auditory verbal hallucinations and the interhemispheric auditory pathway in chronic schizophrenia. World J Biol Psychiatry 2015;16:31-14.

[38] Leroux E, Delcroix N, Dollfus S. Abnormalities of language pathways in schizophrenia patients with and without a lifetime history of auditory verbal hallucinations: A DTI-based tractography study. World J Biol Psychiatry 2017 Jan 25:1-11. doi: 10.1080/15622975.2016.1274053. [Epub ahead of print]

[39] Xi YB, Guo F, Li H, Chang X, Sun JB, Zhu YQ, Liu WM, Cui LB, Chen G, Wang HN, Yin H. The structural connectivity pathology of first-episode schizophrenia based on the cardinal symptom of auditory verbal hallucinations. Psychiatry Res 2016;257:25-30.

[40] 席一斌, 刘文明, 刘康, 汪田田, 折霞, 印弘, 宦怡, 杨小斌. 基于纤维骨架的空间统计的精神分裂幻听患者的全脑白质各向异性分数研究. 实用放射学杂志 2013;29:689-92.

[41] de Weijer AD, Mandl RC, Diederen KM, Neggers SF, Kahn RS, Hulshoff Pol HE, Sommer IE. Microstructural alterations of the arcuate fasciculus in schizophrenia patients with frequent auditory verbal hallucinations. Schizophr Res 2011;130:68-77.

[42] Catani M, Craig MC, Forkel SJ, Kanaan R, Picchioni M, Toulopoulou T, Shergill S, Williams S, Murphy DG, McGuire P. Altered integrity of perisylvian language pathways

in schizophrenia: relationship to auditory hallucinations. Biol Psychiatry 2011;70:1143-50.

[43] Benetti S, Pettersson-Yeo W, Allen P, Catani M, Williams S, Barsaglini A, Kambeitz-Ilankovic LM, McGuire P, Mechelli A. Auditory Verbal Hallucinations and Brain Dysconnectivity in the Perisylvian Language Network: A Multimodal Investigation. Schizophr Bull 2015;41:192-200.

[44] Rotarska-Jagiela A, Oertel-Knoechel V, DeMartino F, van de Ven V, Formisano E, Roebroeck A, Rami A, Schoenmeyer R, Haenschel C, Hendler T, Maurer K, Vogeley K, Linden DE. Anatomical brain connectivity and positive symptoms of schizophrenia: a diffusion tensor imaging study. Psychiatry Res 2009;174:9-16.

[45] Psomiades M, Fonteneau C, Mondino M, Luck D, Haesebaert F, Suaud-Chagny MF, Brunelin J. Integrity of the arcuate fasciculus in patients with schizophrenia with auditory verbal hallucinations: A DTI-tractography study. Neuroimage Clin 2016;12:970-75.

[46] McCarthy-Jones S, Oestreich LK, Whitford TJ. Reduced integrity of the left arcuate fasciculus is specifically associated with auditory verbal hallucinations in schizophrenia. Schizophr Res 2015;162:1-6.

[47] Shergill SS, Kanaan RA, Chitnis XA, O'Daly O, Jones DK, Frangou S, Williams SC, Howard RJ, Barker GJ, Murray RM, McGuire P. A diffusion tensor imaging study of fasciculi in schizophrenia. Am J Psychiatry 2007;164:467-73.

[48] Whitford TJ, Lee SW, Oh JS, de Luis-Garcia R, Savadjiev P, Alvarado JL, Westin CF, Niznikiewicz M, Nestor PG, McCarley RW, Kubicki M, Shenton ME. Localized abnormalities in the cingulum bundle in patients with schizophrenia: A Diffusion Tensor tractography study. Neuroimage Clin 2014;5:93-9.

[49] Oestreich LK, McCarthy-Jones S, Whitford TJ. Decreased integrity of the fronto-temporal fibers of the left inferior occipito-frontal fasciculus associated with auditory verbal hallucinations in schizophrenia. Brain Imaging Behav 2016;10:445-54.

[50] Wu CH, Hwang TJ, Chen PJ, Chou TL, Hsu YC, Liu CM, Wang HL, Chen CM, Hua MS, Hwu HG, Isaac Tseng WY. Reduced structural integrity and functional lateralization of the dorsal language pathway correlate with hallucinations in

schizophrenia: A combined diffusion spectrum imaging and functional magnetic resonance imaging study. Psychiatry Res 2014;224:303-10.

[51] Lawrie SM, Buechel C, Whalley HC, Frith CD, Friston KJ, Johnstone EC. Reduced frontotemporal functional connectivity in schizophrenia associated with auditory hallucinations. Biol Psychiatry 2002;51:1008-11.

[52] Han SD, Nestor PG, Hale-Spencer M, Cohen A, Niznikiewicz M, McCarley RW, Wible CG. Functional neuroimaging of word priming in males with chronic schizophrenia. Neuroimage 2007;35:273-82.

[53] Chang X, Xi YB, Cui LB, Wang HN, Sun JB, Zhu YQ, Huang P, Collin G, Liu K, Xi M, Qi S, Tan QR, Miao DM, Yin H. Distinct inter-hemispheric dysconnectivity in schizophrenia patients with and without auditory verbal hallucinations. Sci Rep 2015;5:11218.

[54] Zhu J, Wang C, Liu F, Qin W, Li J, Zhuo C. Alterations of Functional and Structural Networks in Schizophrenia Patients with Auditory Verbal Hallucinations. Front Hum Neurosci 2016;10:114.

[55] Homan P, Kindler J, Hauf M, Hubl D, Dierks T. Cerebral blood flow identifies responders to transcranial magnetic stimulation in auditory verbal hallucinations. Transl Psychiatry 2012;2:e189.

[56] Homan P, Kindler J, Hauf M, Walther S, Hubl D, Dierks T. Repeated measurements of cerebral blood flow in the left superior temporal gyrus reveal tonic hyperactivity in patients with auditory verbal hallucinations: a possible trait marker. Front Hum Neurosci 2013;7:304.

[57] Homan P, Kindler J, Federspiel A, Flury R, Hubl D, Hauf M, Dierks T. Muting the voice: a case of arterial spin labeling-monitored transcranial direct current stimulation treatment of auditory verbal hallucinations. Am J Psychiatry 2011;168:853-4.

[58] Zhuo C, Zhu J, Qin W, Qu H, Ma X, Yu C. Cerebral blood flow alterations specific to auditory verbal hallucinations in schizophrenia. Br J Psychiatry 2017;210:209-15.

[59] He Y, Chen ZJ, Evans AC. Small-world anatomical networks in the human brain

revealed by cortical thickness from MRI. Cereb Cortex 2007;17:2407-19.

[60] Knochel C, Oertel-Knochel V, Schonmeyer R, Rotarska-Jagiela A, van de Ven V, Prvulovic D, Haenschel C, Uhlhaas P, Pantel J, Hampel H, Linden DE. Interhemispheric hypoconnectivity in schizophrenia: fiber integrity and volume differences of the corpus callosum in patients and unaffected relatives. Neuroimage 2012;59:926-34.

[61] Lee K, Yoshida T, Kubicki M, Bouix S, Westin CF, Kindlmann G, Niznikiewicz M, Cohen A, McCarley RW, Shenton ME. Increased diffusivity in superior temporal gyrus in patients with schizophrenia: a Diffusion Tensor Imaging study. Schizophr Res 2009;108:33-40.

[62] Geoffroy PA, Houenou J, Duhamel A, Amad A, De Weijer AD, Curcic-Blake B, Linden DE, Thomas P, Jardri R. The arcuate fasciculus in auditory-verbal hallucinations: A meta-analysis of diffusion-tensor-imaging studies. Schizophr Res 2014;159:234-7.

[63] Chyzhyk D, Grana M, Ongur D, Shinn AK. Discrimination of schizophrenia auditory hallucinators by machine learning of resting-state functional MRI. Int J Neural Syst 2015;25:1550007.

[64] Kindler J, Homan P, Jann K, Federspiel A, Flury R, Hauf M, Strik W, Dierks T, Hubl D. Reduced neuronal activity in language-related regions after transcranial magnetic stimulation therapy for auditory verbal hallucinations. Biol Psychiatry 2013;73:518-24.

[65] Escarti MJ, de la Iglesia-Vaya M, Marti-Bonmati L, Robles M, Carbonell J, Lull JJ, Garcia-Marti G, Manjon JV, Aguilar EJ, Aleman A, Sanjuan J. Increased amygdala and parahippocampal gyrus activation in schizophrenic patients with auditory hallucinations: an fMRI study using independent component analysis. Schizophr Res 2010;117:31-41.

[66] Alonso-Solis A, Vives-Gilabert Y, Grasa E, Portella MJ, Rabella M, Sauras RB, Roldan A, Nunez-Marin F, Gomez-Anson B, Perez V, Alvarez E, Corripio I. Resting-state functional connectivity alterations in the default network of schizophrenia patients with persistent auditory verbal hallucinations. Schizophr Res 2015;161:261-8.

[67] Amad A, Cachia A, Gorwood P, Pins D, Delmaire C, Rolland B, Mondino M, Thomas P, Jardri R. The multimodal connectivity of the hippocampal complex in auditory and visual hallucinations. Mol Psychiatry 2014;19:184-91.

[68] Shinn AK, Baker JT, Cohen BM, Ongur D. Functional connectivity of left Heschl's gyrus in vulnerability to auditory hallucinations in schizophrenia. Schizophr Res 2013;143:260-8.

[69] Hoffman RE, Fernandez T, Pittman B, Hampson M. Elevated functional connectivity along a corticostriatal loop and the mechanism of auditory/verbal hallucinations in patients with schizophrenia. Biol Psychiatry 2011;69:407-14.

[70] Rolland B, Amad A, Poulet E, Bordet R, Vignaud A, Bation R, Delmaire C, Thomas P, Cottencin O, Jardri R. Resting-state functional connectivity of the nucleus accumbens in auditory and visual hallucinations in schizophrenia. Schizophr Bull 2015;41:291-9.

[71] Modinos G, Ormel J, Aleman A. Altered activation and functional connectivity of neural systems supporting cognitive control of emotion in psychosis proneness. Schizophr Res 2010;118:88-97.

[72] Liemburg EJ, Vercammen A, Ter Horst GJ, Curcic-Blake B, Knegtering H, Aleman A. Abnormal connectivity between attentional, language and auditory networks in schizophrenia. Schizophr Res 2012;135:15-22.

[73] Wolf ND, Sambataro F, Vasic N, Frasch K, Schmid M, Schonfeldt-Lecuona C, Thomann PA, Wolf RC. Dysconnectivity of multiple resting-state networks in patients with schizophrenia who have persistent auditory verbal hallucinations. J Psychiatry Neurosci 2011;36:366-74.

[74] Vercammen A, Knegtering H, Liemburg EJ, den Boer JA, Aleman A. Functional connectivity of the temporo-parietal region in schizophrenia: effects of rTMS treatment of auditory hallucinations. J Psychiatr Res 2010;44:725-31.

[75] Vercammen A, Knegtering H, den Boer JA, Liemburg EJ, Aleman A. Auditory hallucinations in schizophrenia are associated with reduced functional connectivity of the temporo-parietal area. Biol Psychiatry 2010;67:912-8.

[76] Alonso-Solis A, Vives-Gilabert Y, Portella MJ, Rabella M, Grasa EM, Roldan A, Keymer-Gausset A, Molins C, Nunez-Marin F, Gomez-Anson B, Alvarez E, Corripio I. Altered amplitude of low frequency fluctuations in schizophrenia patients with persistent

auditory verbal hallucinations. Schizophr Res 2017 Jan 28. pii: S0920-9964(17)30055-5. doi: 10.1016/j.schres.2017.01.042. [Epub ahead of print]

[77] Friston KJ. Functional and effective connectivity: a review. Brain Connect 2011;1:13-36.

[78] Curcic-Blake B, Liemburg E, Vercammen A, Swart M, Knegtering H, Bruggeman R, Aleman A. When Broca goes uninformed: reduced information flow to Broca's area in schizophrenia patients with auditory hallucinations. Schizophr Bull 2013;39:1087-95.

[79] Bastos-Leite AJ, Ridgway GR, Silveira C, Norton A, Reis S, Friston KJ. Dysconnectivity within the default mode in first-episode schizophrenia: a stochastic dynamic causal modeling study with functional magnetic resonance imaging. Schizophr Bull 2015;41:144-53.

[80] Onitsuka T, Shenton ME, Salisbury DF, Dickey CC, Kasai K, Toner SK, Frumin M, Kikinis R, Jolesz FA, McCarley RW. Middle and inferior temporal gyrus gray matter volume abnormalities in chronic schizophrenia: an MRI study. Am J Psychiatry 2004;161:1603-11.

[81] Palaniyappan L, Balain V, Radua J, Liddle PF. Structural correlates of auditory hallucinations in schizophrenia: a meta-analysis. Schizophr Res 2012;137:169-73.

[82] Modinos G, Costafreda SG, van Tol MJ, McGuire PK, Aleman A, Allen P. Neuroanatomy of auditory verbal hallucinations in schizophrenia: a quantitative meta-analysis of voxel-based morphometry studies. Cortex 2013;49:1046-55.

[83] Jardri R, Pouchet A, Pins D, Thomas P. Cortical activations during auditory verbal hallucinations in schizophrenia: a coordinate-based meta-analysis. Am J Psychiatry 2011;168:73-81.

[84] Kuhn S, Gallinat J. Quantitative meta-analysis on state and trait aspects of auditory verbal hallucinations in schizophrenia. Schizophr Bull 2012;38:779-86.

[85] Kompus K, Westerhausen R, Hugdahl K. The "paradoxical" engagement of the primary auditory cortex in patients with auditory verbal hallucinations: a meta-analysis of functional neuroimaging studies. Neuropsychologia 2011;49:3361-9.

[86] Zmigrod L, Garrison JR, Carr J, Simons JS. The neural mechanisms of hallucinations: A quantitative meta-analysis of neuroimaging studies. Neurosci Biobehav Rev 2016;69:113-23.

[87] Bohlken MM, Hugdahl K, Sommer IE. Auditory verbal hallucinations: neuroimaging and treatment. Psychol Med 2017;47:199-208.

[88] Steinmann S, Leicht G, Mulert C. Interhemispheric auditory connectivity: structure and function related to auditory verbal hallucinations. Front Hum Neurosci 2014;8:55.

[89] Aboitiz F, Scheibel AB, Fisher RS, Zaidel E. Fiber composition of the human corpus callosum. Brain Res 1992;598:143-53.

[90] Hubl D, Koenig T, Strik W, Federspiel A, Kreis R, Boesch C, Maier SE, Schroth G, Lovblad K, Dierks T. Pathways that make voices: white matter changes in auditory hallucinations. Arch Gen Psychiatry 2004;61:658-68.

[91] Mulert C, Kirsch V, Whitford TJ, Alvarado J, Pelavin P, McCarley RW, Kubicki M, Salisbury DF, Shenton ME. Hearing voices: a role of interhemispheric auditory connectivity? World J Biol Psychiatry 2012;13:153-8.

[92] Gavrilescu M, Rossell S, Stuart GW, Shea TL, Innes-Brown H, Henshall K, McKay C, Sergejew AA, Copolov D, Egan GF. Reduced connectivity of the auditory cortex in patients with auditory hallucinations: a resting state functional magnetic resonance imaging study. Psychol Med 2010;40:1149-58.

[93] Briend F, Leroux E, Delcroix N, Razafimandimby A, Etard O, Dollfus S. Impact of rTMS on functional connectivity within the language network in schizophrenia patients with auditory hallucinations. Schizophr Res 2017 Feb 8. pii: S0920-9964(17)30067-1. doi: 10.1016/j.schres.2017.01.049. [Epub ahead of print]

[94] Farde L, Suhara T, Nyberg S, Karlsson P, Nakashima Y, Hietala J, Halldin C. A PET-study of [11C]FLB 457 binding to extrastriatal D2-dopamine receptors in healthy subjects and antipsychotic drug-treated patients. Psychopharmacology (Berl) 1997;133:396-404.

[95] Chun S, Westmoreland JJ, Bayazitov IT, Eddins D, Pani AK, Smeyne RJ, Yu J,

Blundon JA, Zakharenko SS. Specific disruption of thalamic inputs to the auditory cortex in schizophrenia models. Science 2014;344:1178-82.

[96] Guo W, Liu F, Liu J, Yu L, Zhang J, Zhang Z, Xiao C, Zhai J, Zhao J. Abnormal causal connectivity by structural deficits in first-episode, drug-naive schizophrenia at rest. Schizophr Bull 2015;41:57-65.

[97] Genzel L, Dresler M, Cornu M, Jager E, Konrad B, Adamczyk M, Friess E, Steiger A, Czisch M, Goya-Maldonado R. Medial prefrontal-hippocampal connectivity and motor memory consolidation in depression and schizophrenia. Biol Psychiatry 2015;77:177-86.

[98] Pinault D. Dysfunctional thalamus-related networks in schizophrenia. Schizophr Bull 2011;37:238-43.

[99] Sellers K, Zyka V, Lumsden AG, Delogu A. Transcriptional control of GABAergic neuronal subtype identity in the thalamus. Neural Dev 2014;9:14.

[100] Guller Y, Ferrarelli F, Shackman AJ, Sarasso S, Peterson MJ, Langheim FJ, Meyerand ME, Tononi G, Postle BR. Probing thalamic integrity in schizophrenia using concurrent transcranial magnetic stimulation and functional magnetic resonance imaging. Arch Gen Psychiatry 2012;69:662-71.

[101] Behrendt RP. Dysregulation of thalamic sensory "transmission" in schizophrenia: neurochemical vulnerability to hallucinations. J Psychopharmacol 2006;20:356-72.

[102] Salviati M, Bersani FS, Valeriani G, Minichino A, Panico R, Romano GF, Mazzei F, Testugini V, Altissimi G, Cianfrone G. A brain centred view of psychiatric comorbidity in tinnitus: from otology to hodology. Neural Plast 2014;2014:817852.

[103] Treadway MT, Zald DH. Reconsidering anhedonia in depression: lessons from translational neuroscience. Neurosci Biobehav Rev 2011;35:537-55.

[104] van den Heuvel MP, Sporns O, Collin G, Scheewe T, Mandl RC, Cahn W, Goni J, Hulshoff Pol HE, Kahn RS. Abnormal rich club organization and functional brain dynamics in schizophrenia. JAMA Psychiatry 2013;70:783-92.

[105] van den Heuvel MP, Fornito A. Brain networks in schizophrenia. Neuropsychol

Rev 2014;24:32-48.

[106] Alderson-Day B, Diederen K, Fernyhough C, Ford JM, Horga G, Margulies DS, McCarthy-Jones S, Northoff G, Shine JM, Turner J, van de Ven V, van Lutterveld R, Waters F, Jardri R. Auditory Hallucinations and the Brain's Resting-State Networks: Findings and Methodological Observations. Schizophr Bull 2016;42:1110-23.

[107] Horga G, Fernandez-Egea E, Mane A, Font M, Schatz KC, Falcon C, Lomena F, Bernardo M, Parellada E. Brain metabolism during hallucination-like auditory stimulation in schizophrenia. PLoS One 2014;9:e84987.

[108] Adams RA, Stephan KE, Brown HR, Frith CD, Friston KJ. The computational anatomy of psychosis. Front Psychiatry 2013;4:47.

[109] Jardri R, Deneve S. Circular inferences in schizophrenia. Brain 2013;136:3227-41.

[110] Baldeweg T, Hirsch SR. Mismatch negativity indexes illness-specific impairments of cortical plasticity in schizophrenia: A comparison with bipolar disorder and Alzheimer's disease. Int J Psychophysiol 2015;95:145-55.

[111] Fogelson N, Litvak V, Peled A, Fernandez-del-Olmo M, Friston K. The functional anatomy of schizophrenia: A dynamic causal modeling study of predictive coding. Schizophr Res 2014;158:204-12.

[112] Siddi S, Petretto DR, Burrai C, Scanu R, Baita A, Trincas P, Trogu E, Campus L, Contu A, Preti A. The role of set-shifting in auditory verbal hallucinations. Compr Psychiatry 2017;74:162-72.

[113] Thoma RJ, Meier A, Houck J, Clark VP, Lewine JD, Turner J, Calhoun V, Stephen J. Diminished auditory sensory gating during active auditory verbal hallucinations. Schizophr Res 2017 Jan 18. pii: S0920-9964(17)30034-8. doi: 10.1016/j.schres.2017.01.023. [Epub ahead of print]

[114] Raichle ME. Behind the scenes of functional brain imaging: a historical and physiological perspective. Proc Natl Acad Sci U S A 1998;95:765-72.

[115] Hu WT, Wang Z, Lee VM, Trojanowski JQ, Detre JA, Grossman M. Distinct cerebral perfusion patterns in FTLD and AD. Neurology 2010;75:881-8.

[116] Du AT, Jahng GH, Hayasaka S, Kramer JH, Rosen HJ, Gorno-Tempini ML, Rankin KP, Miller BL, Weiner MW, Schuff N. Hypoperfusion in frontotemporal dementia and Alzheimer disease by arterial spin labeling MRI. Neurology 2006;67:1215-20.

[117] Zhu J, Zhuo C, Qin W, Xu Y, Xu L, Liu X, Yu C. Altered resting-state cerebral blood flow and its connectivity in schizophrenia. J Psychiatr Res 2015;63:28-35.

[118] Melie-Garcia L, Sanabria-Diaz G, Sanchez-Catasus C. Studying the topological organization of the cerebral blood flow fluctuations in resting state. Neuroimage 2013;64:173-84.

[119] Kindler J, Jann K, Homan P, Hauf M, Walther S, Strik W, Dierks T, Hubl D. Static and dynamic characteristics of cerebral blood flow during the resting state in schizophrenia. Schizophr Bull 2015;41:163-70.

[120] Kay SR, Fiszbein A, Opler LA. The positive and negative syndrome scale (PANSS) for schizophrenia. Schizophr Bull 1987;13:261-76.

[121] Hoffman RE, Hawkins KA, Gueorguieva R, Boutros NN, Rachid F, Carroll K, Krystal JH. Transcranial magnetic stimulation of left temporoparietal cortex and medication-resistant auditory hallucinations. Arch Gen Psychiatry 2003;60:49-56.

[122] Loewy RL, Bearden CE, Johnson JK, Raine A, Cannon TD. The prodromal questionnaire (PQ): preliminary validation of a self-report screening measure for prodromal and psychotic syndromes. Schizophr Res 2005;79:117-25.

[123] Wang Z, Aguirre GK, Rao H, Wang J, Fernandez-Seara MA, Childress AR, Detre JA. Empirical optimization of ASL data analysis using an ASL data processing toolbox: ASLtbx. Magn Reson Imaging 2008;26:261-9.

[124] Wang Z. Improving cerebral blood flow quantification for arterial spin labeled perfusion MRI by removing residual motion artifacts and global signal fluctuations. Magn Reson Imaging 2012;30:1409-15.

[125] Tzourio-Mazoyer N, Landeau B, Papathanassiou D, Crivello F, Etard O, Delcroix N, Mazoyer B, Joliot M. Automated anatomical labeling of activations in SPM using a macroscopic anatomical parcellation of the MNI MRI single-subject brain. Neuroimage 2002;15:273-89.

[126] Song XW, Dong ZY, Long XY, Li SF, Zuo XN, Zhu CZ, He Y, Yan CG, Zang YF. REST: a toolkit for resting-state functional magnetic resonance imaging data processing. PLoS One 2011;6:e25031.

[127] Moseley P, Fernyhough C, Ellison A. Auditory verbal hallucinations as atypical inner speech monitoring, and the potential of neurostimulation as a treatment option. Neurosci Biobehav Rev 2013;37:2794-805.

[128] Raij TT, Riekki TJ. Poor supplementary motor area activation differentiates auditory verbal hallucination from imagining the hallucination. Neuroimage Clin 2012;1:75-80.

[129] Tremblay S, Shiller DM, Ostry DJ. Somatosensory basis of speech production. Nature 2003;423:866-9.

[130] Scheef L, Manka C, Daamen M, Kuhn KU, Maier W, Schild HH, Jessen F. Resting-state perfusion in nonmedicated schizophrenic patients: a continuous arterial spin-labeling 3.0-T MR study. Radiology 2010;256:253-60.

[131] Pinkham A, Loughead J, Ruparel K, Wu WC, Overton E, Gur R. Resting quantitative cerebral blood flow in schizophrenia measured by pulsed arterial spin labeling perfusion MRI. Psychiatry Res 2011;194:64-72.

[132] Alsop DC, Detre JA, Golay X, Gunther M, Hendrikse J, Hernandez-Garcia L, Lu H, MacIntosh BJ, Parkes LM, Smits M, van Osch MJ, Wang DJ, Wong EC, Zaharchuk G. Recommended implementation of arterial spin-labeled perfusion MRI for clinical applications: A consensus of the ISMRM perfusion study group and the European consortium for ASL in dementia. Magn Reson Med 2015;73:102-16.

[133] Liu F, Zhuo C, Yu C. Altered cerebral blood flow covariance network in schizophrenia. Front Neurosci 2016;10:308.

[134] Nauta WJ. Neural associations of the frontal cortex. Acta Neurobiol Exp (Wars) 1972;32:125-40.

[135] Hofer S, Frahm J. Topography of the human corpus callosum revisited--comprehensive fiber tractography using diffusion tensor magnetic resonance imaging. Neuroimage 2006;32:989-94.

[136] Mondino M, Jardri R, Suaud-Chagny MF, Saoud M, Poulet E, Brunelin J. Effects of fronto-temporal transcranial direct current stimulation on auditory verbal hallucinations and resting-state functional connectivity of the left temporo-parietal junction in patients with schizophrenia. Schizophr Bull 2016;42:318-26.

[137] Sommer IE, Clos M, Meijering AL, Diederen KM, Eickhoff SB. Resting state functional connectivity in patients with chronic hallucinations. PLoS One 2012;7:e43516.

[138] Clos M, Diederen KM, Meijering AL, Sommer IE, Eickhoff SB. Aberrant connectivity of areas for decoding degraded speech in patients with auditory verbal hallucinations. Brain Struct Funct 2014;219:581-94.

[139] Kawaguchi S, Ukai S, Shinosaki K, Ishii R, Yamamoto M, Ogawa A, Mizuno-Matsumoto Y, Fujita N, Yoshimine T, Takeda M. Information processing flow and neural activations in the dorsolateral prefrontal cortex in the Stroop task in schizophrenic patients. A spatially filtered MEG analysis with high temporal and spatial resolution. Neuropsychobiology 2005;51:191-203.

[140] Brunelin J, Mondino M, Gassab L, Haesebaert F, Gaha L, Suaud-Chagny MF, Saoud M, Mechri A, Poulet E. Examining transcranial direct-current stimulation (tDCS) as a treatment for hallucinations in schizophrenia. Am J Psychiatry 2012;169:719-24.

[141] Andrade C. Transcranial direct current stimulation for refractory auditory hallucinations in schizophrenia. J Clin Psychiatry 2013;74:e1054-8.

[142] Mondino M, Haesebaert F, Poulet E, Suaud-Chagny MF, Brunelin J. Fronto-temporal transcranial Direct Current Stimulation (tDCS) reduces source-monitoring deficits and auditory hallucinations in patients with schizophrenia. Schizophr Res 2015;161:515-6.

[143] Brunoni AR, Shiozawa P, Truong D, Javitt DC, Elkis H, Fregni F, Bikson M. Understanding tDCS effects in schizophrenia: a systematic review of clinical data and an integrated computation modeling analysis. Expert Rev Med Devices 2014;11:383-94.

[144] Gromann PM, Tracy DK, Giampietro V, Brammer MJ, Krabbendam L, Shergill SS. Examining frontotemporal connectivity and rTMS in healthy controls: implications for auditory hallucinations in schizophrenia. Neuropsychology 2012;26:127-32.

[145] Lennox BR, Park SB, Medley I, Morris PG, Jones PB. The functional anatomy of auditory hallucinations in schizophrenia. Psychiatry Res 2000;100:13-20.

[146] Allen P, Modinos G, Hubl D, Shields G, Cachia A, Jardri R, Thomas P, Woodward T, Shotbolt P, Plaze M, Hoffman R. Neuroimaging auditory hallucinations in schizophrenia: from neuroanatomy to neurochemistry and beyond. Schizophr Bull 2012;38:695-703.

[147] Garcia-Marti G, Aguilar EJ, Lull JJ, Marti-Bonmati L, Escarti MJ, Manjon JV, Moratal D, Robles M, Sanjuan J. Schizophrenia with auditory hallucinations: a voxel-based morphometry study. Prog Neuropsychopharmacol Biol Psychiatry 2008;32:72-80.

[148] Stephane M, Barton S, Boutros NN. Auditory verbal hallucinations and dysfunction of the neural substrates of speech. Schizophr Res 2001;50:61-78.

[149] Rubinov M, Sporns O. Complex network measures of brain connectivity: uses and interpretations. Neuroimage 2010;52:1059-69.

[150] Estrada E, Hatano N. Communicability in complex networks. Phys Rev E Stat Nonlin Soft Matter Phys 2008;77:036111.

[151] Zeng LL, Shen H, Liu L, Hu D. Unsupervised classification of major depression using functional connectivity MRI. Hum Brain Mapp 2014;35:1630-41.

[152] Sporns O, Tononi G, Kotter R. The human connectome: A structural description of the human brain. PLoS Comput Biol 2005;1:e42.

[153] Sporns O. The human connectome: a complex network. Ann N Y Acad Sci 2011;1224:109-25.

[154] van den Heuvel MP, Bullmore ET, Sporns O. Comparative Connectomics. Trends Cogn Sci 2016;20:345-61.

[155] van den Heuvel MP, Kahn RS. Abnormal brain wiring as a pathogenetic mechanism in schizophrenia. Biol Psychiatry 2011;70:1107-8.

[156] van den Heuvel MP, Yeo BT. A Spotlight on Bridging Microscale and Macroscale Human Brain Architecture. Neuron 2017;93:1248-51.

[157] Sporns O, Honey CJ, Kotter R. Identification and classification of hubs in brain

networks. PLoS One 2007;2:e1049.

[158] van den Heuvel MP, Sporns O. Network hubs in the human brain. Trends Cogn Sci 2013;17:683-96.

[159] van den Heuvel MP, Sporns O. Rich-club organization of the human connectome. J Neurosci 2011;31:15775-86.

[160] van den Heuvel MP, Kahn RS, Goni J, Sporns O. High-cost, high-capacity backbone for global brain communication. Proc Natl Acad Sci U S A 2012;109:11372-7.

[161] Davis KL, Stewart DG, Friedman JI, Buchsbaum M, Harvey PD, Hof PR, Buxbaum J, Haroutunian V. White matter changes in schizophrenia: evidence for myelin-related dysfunction. Arch Gen Psychiatry 2003;60:443-56.

[162] Fitzsimmons J, Kubicki M, Shenton ME. Review of functional and anatomical brain connectivity findings in schizophrenia. Curr Opin Psychiatry 2013;26:172-87.

[163] Keshavan MS, Nasrallah HA, Tandon R. Schizophrenia, "Just the Facts" 6. Moving ahead with the schizophrenia concept: from the elephant to the mouse. Schizophr Res 2011;127:3-13.

[164] Scheel M, Prokscha T, Bayerl M, Gallinat J, Montag C. Myelination deficits in schizophrenia: evidence from diffusion tensor imaging. Brain Struct Funct 2013;218:151-6.

[165] Seal ML, Yucel M, Fornito A, Wood SJ, Harrison BJ, Walterfang M, Pell GS, Pantelis C. Abnormal white matter microstructure in schizophrenia: a voxelwise analysis of axial and radial diffusivity. Schizophr Res 2008;101:106-10.

[166] Cammoun L, Gigandet X, Meskaldji D, Thiran JP, Sporns O, Do KQ, Maeder P, Meuli R, Hagmann P. Mapping the human connectome at multiple scales with diffusion spectrum MRI. J Neurosci Methods 2012;203:386-97.

[167] Karbasforoushan H, Woodward ND. Resting-state networks in schizophrenia. Curr Top Med Chem 2012;12:2404-14.

[168] Meda SA, Ruano G, Windemuth A, O'Neil K, Berwise C, Dunn SM, Boccaccio LE, Narayanan B, Kocherla M, Sprooten E, Keshavan MS, Tamminga CA, Sweeney JA, Clementz BA, Calhoun VD, Pearlson GD. Multivariate analysis reveals genetic

associations of the resting default mode network in psychotic bipolar disorder and schizophrenia. Proc Natl Acad Sci U S A 2014;111:E2066-75.

[169] Guo W, Yao D, Jiang J, Su Q, Zhang Z, Zhang J, Yu L, Xiao C. Abnormal default-mode network homogeneity in first-episode, drug-naive schizophrenia at rest. Prog Neuropsychopharmacol Biol Psychiatry 2014;49:16-20.

[170] Littow H, Huossa V, Karjalainen S, Jaaskelainen E, Haapea M, Miettunen J, Tervonen O, Isohanni M, Nikkinen J, Veijola J, Murray G, Kiviniemi VJ. Aberrant Functional Connectivity in the Default Mode and Central Executive Networks in Subjects with Schizophrenia - A Whole-Brain Resting-State ICA Study. Front Psychiatry 2015;6:26.

[171] Wang H, Zeng LL, Chen Y, Yin H, Tan Q, Hu D. Evidence of a dissociation pattern in default mode subnetwork functional connectivity in schizophrenia. Sci Rep 2015;5:14655.

[172] Meda SA, Gill A, Stevens MC, Lorenzoni RP, Glahn DC, Calhoun VD, Sweeney JA, Tamminga CA, Keshavan MS, Thaker G, Pearlson GD. Differences in resting-state functional magnetic resonance imaging functional network connectivity between schizophrenia and psychotic bipolar probands and their unaffected first-degree relatives. Biol Psychiatry 2012;71:881-9.

[173] Khadka S, Meda SA, Stevens MC, Glahn DC, Calhoun VD, Sweeney JA, Tamminga CA, Keshavan MS, O'Neil K, Schretlen D, Pearlson GD. Is aberrant functional connectivity a psychosis endophenotype? A resting state functional magnetic resonance imaging study. Biol Psychiatry 2013;74:458-66.

[174] Beckmann CF, DeLuca M, Devlin JT, Smith SM. Investigations into resting-state connectivity using independent component analysis. Philos Trans R Soc Lond B Biol Sci 2005;360:1001-13.

[175] Smith SM, Fox PT, Miller KL, Glahn DC, Fox PM, Mackay CE, Filippini N, Watkins KE, Toro R, Laird AR, Beckmann CF. Correspondence of the brain's functional architecture during activation and rest. Proc Natl Acad Sci U S A 2009;106:13040-5.

[176] Rosazza C, Minati L. Resting-state brain networks: literature review and clinical applications. Neurol Sci 2011;32:773-85.

[177] Damaraju E, Allen EA, Belger A, Ford JM, McEwen S, Mathalon DH, Mueller BA, Pearlson GD, Potkin SG, Preda A, Turner JA, Vaidya JG, van Erp TG, Calhoun VD. Dynamic functional connectivity analysis reveals transient states of dysconnectivity in schizophrenia. Neuroimage Clin 2014;5:298-308.

[178] Manoliu A, Riedl V, Zherdin A, Muhlau M, Schwerthoffer D, Scherr M, Peters H, Zimmer C, Forstl H, Bauml J, Wohlschlager AM, Sorg C. Aberrant dependence of default mode/central executive network interactions on anterior insular salience network activity in schizophrenia. Schizophr Bull 2014;40:428-37.

[179] Kaufmann T, Skatun KC, Alnaes D, Doan NT, Duff EP, Tonnesen S, Roussos E, Ueland T, Aminoff SR, Lagerberg TV, Agartz I, Melle IS, Smith SM, Andreassen OA, Westlye LT. Disintegration of Sensorimotor Brain Networks in Schizophrenia. Schizophr Bull 2015;41:1326-35.

[180] Logothetis NK, Pauls J, Augath M, Trinath T, Oeltermann A. Neurophysiological investigation of the basis of the fMRI signal. Nature 2001;412:150-7.

[181] Cordes D, Haughton VM, Arfanakis K, Carew JD, Turski PA, Moritz CH, Quigley MA, Meyerand ME. Frequencies contributing to functional connectivity in the cerebral cortex in "resting-state" data. AJNR Am J Neuroradiol 2001;22:1326-33.

[182] Mohamed MA, Yousem DM, Tekes A, Browner N, Calhoun VD. Correlation between the amplitude of cortical activation and reaction time: a functional MRI study. AJR Am J Roentgenol 2004;183:759-65.

[183] Filippini N, MacIntosh BJ, Hough MG, Goodwin GM, Frisoni GB, Smith SM, Matthews PM, Beckmann CF, Mackay CE. Distinct patterns of brain activity in young carriers of the APOE-epsilon4 allele. Proc Natl Acad Sci U S A 2009;106:7209-14.

[184] Amadi U, Ilie A, Johansen-Berg H, Stagg CJ. Polarity-specific effects of motor transcranial direct current stimulation on fMRI resting state networks. Neuroimage 2013;88C:155-61.

[185] Nichols TE, Holmes AP. Nonparametric permutation tests for functional neuroimaging: a primer with examples. Hum Brain Mapp 2002;15:1-25.

[186] Zou QH, Zhu CZ, Yang Y, Zuo XN, Long XY, Cao QJ, Wang YF, Zang YF. An

improved approach to detection of amplitude of low-frequency fluctuation (ALFF) for resting-state fMRI: fractional ALFF. J Neurosci Methods 2008;172:137-41.

[187] Keeser D, Meindl T, Bor J, Palm U, Pogarell O, Mulert C, Brunelin J, Moller HJ, Reiser M, Padberg F. Prefrontal transcranial direct current stimulation changes connectivity of resting-state networks during fMRI. J Neurosci 2011;31:15284-93.

[188] Price CJ. A review and synthesis of the first 20 years of PET and fMRI studies of heard speech, spoken language and reading. Neuroimage 2012;62:816-47.

[189] Price CJ. The anatomy of language: a review of 100 fMRI studies published in 2009. Ann N Y Acad Sci 2010;1191:62-88.

[190] Obeso JA, Rodriguez-Oroz MC, Stamelou M, Bhatia KP, Burn DJ. The expanding universe of disorders of the basal ganglia. Lancet 2014;384:523-31.

[191] van Tol MJ, van der Meer L, Bruggeman R, Modinos G, Knegtering H, Aleman A. Voxel-based gray and white matter morphometry correlates of hallucinations in schizophrenia: The superior temporal gyrus does not stand alone. Neuroimage Clin 2014;4:249-57.

[192] Buckner RL, Andrews-Hanna JR, Schacter DL. The brain's default network: anatomy, function, and relevance to disease. Ann N Y Acad Sci 2008;1124:1-38.

[193] Rotarska-Jagiela A, van de Ven V, Oertel-Knochel V, Uhlhaas PJ, Vogeley K, Linden DE. Resting-state functional network correlates of psychotic symptoms in schizophrenia. Schizophr Res 2010;117:21-30.

[194] Alitto HJ, Usrey WM. Corticothalamic feedback and sensory processing. Curr Opin Neurobiol 2003;13:440-5.

[195] Ford JM, Dierks T, Fisher DJ, Herrmann CS, Hubl D, Kindler J, Koenig T, Mathalon DH, Spencer KM, Strik W, van Lutterveld R. Neurophysiological studies of auditory verbal hallucinations. Schizophr Bull 2012;38:715-23.

[196] Cho R, Wu W. Mechanisms of auditory verbal hallucination in schizophrenia. Front Psychiatry 2013;4:155.

[197] Hugdahl K. Auditory hallucinations: A review of the ERC "VOICE" project. World J Psychiatry 2015;5:193-209.

[198] Zang Y, Jiang T, Lu Y, He Y, Tian L. Regional homogeneity approach to fMRI data analysis. Neuroimage 2004;22:394-400.

[199] Lui S, Yao L, Xiao Y, Keedy SK, Reilly JL, Keefe RS, Tamminga CA, Keshavan MS, Pearlson GD, Gong Q, Sweeney JA. Resting-state brain function in schizophrenia and psychotic bipolar probands and their first-degree relatives. Psychol Med 2015;45:97-108.

[200] Ford JM, Palzes VA, Roach BJ, Potkin SG, van Erp TG, Turner JA, Mueller BA, Calhoun VD, Voyvodic J, Belger A, Bustillo J, Vaidya JG, Preda A, McEwen SC, Mathalon DH. Visual Hallucinations Are Associated With Hyperconnectivity Between the Amygdala and Visual Cortex in People With a Diagnosis of Schizophrenia. Schizophr Bull 2015;41:223-32.

[201] Lavigne KM, Rapin LA, Metzak PD, Whitman JC, Jung K, Dohen M, Loevenbruck H, Woodward TS. Left-dominant temporal-frontal hypercoupling in schizophrenia patients with hallucinations during speech perception. Schizophr Bull 2015;41:259-67.

[202] Yan CG, Zang YF. DPARSF: A MATLAB Toolbox for "Pipeline" Data Analysis of Resting-State fMRI. Front Syst Neurosci 2010;4:13.

[203] Xia M, Wang J, He Y. BrainNet Viewer: a network visualization tool for human brain connectomics. PLoS One 2013;8:e68910.

[204] Friston KJ, Frith CD. Schizophrenia: a disconnection syndrome? Clin Neurosci 1995;3:89-97.

[205] Friston KJ. The disconnection hypothesis. Schizophr Res 1998;30:115-25.

[206] Stephan KE, Friston KJ, Frith CD. Dysconnection in schizophrenia: from abnormal synaptic plasticity to failures of self-monitoring. Schizophr Bull 2009;35:509-27.

[207] Whitford TJ, Kubicki M, Schneiderman JS, O'Donnell LJ, King R, Alvarado JL, Khan U, Markant D, Nestor PG, Niznikiewicz M, McCarley RW, Westin CF, Shenton ME. Corpus callosum abnormalities and their association with psychotic symptoms in patients with schizophrenia. Biol Psychiatry 2010;68:70-7.

[208] Kubota M, Miyata J, Sasamoto A, Sugihara G, Yoshida H, Kawada R, Fujimoto S, Tanaka Y, Sawamoto N, Fukuyama H, Takahashi H, Murai T. Thalamocortical disconnection in the orbitofrontal region associated with cortical thinning in schizophrenia. JAMA Psychiatry 2013;70:12-21.

[209] Liu B, Zhang X, Hou B, Li J, Qiu C, Qin W, Yu C, Jiang T. The impact of MIR137 on dorsolateral prefrontal-hippocampal functional connectivity in healthy subjects. Neuropsychopharmacology 2014;39:2153-60.

[210] Tu PC, Hsieh JC, Li CT, Bai YM, Su TP. Cortico-striatal disconnection within the cingulo-opercular network in schizophrenia revealed by intrinsic functional connectivity analysis: a resting fMRI study. Neuroimage 2012;59:238-47.

[211] Kandel ER, Schwartz JH, Jessell TM, Siegelbaum SA, Hudspeth AJ. Principles of Neural Science, 5th Edition. New York City:The McGraw-Hill Education 2013:982-98.

[212] Woodward ND, Karbasforoushan H, Heckers S. Thalamocortical dysconnectivity in schizophrenia. Am J Psychiatry 2012;169:1092-9.

[213] Jardri R, Thomas P, Delmaire C, Delion P, Pins D. The neurodynamic organization of modality-dependent hallucinations. Cereb Cortex 2013;23:1108-17.

[214] Seok JH, Park HJ, Chun JW, Lee SK, Cho HS, Kwon JS, Kim JJ. White matter abnormalities associated with auditory hallucinations in schizophrenia: a combined study of voxel-based analyses of diffusion tensor imaging and structural magnetic resonance imaging. Psychiatry Res 2007;156:93-104.

[215] Curcic-Blake B, Nanetti L, van der Meer L, Cerliani L, Renken R, Pijnenborg GH, Aleman A. Not on speaking terms: hallucinations and structural network disconnectivity in schizophrenia. Brain Struct Funct 2015;220:407-18.

[216] de Weijer AD, Neggers SF, Diederen KM, Mandl RC, Kahn RS, Hulshoff Pol HE, Sommer IE. Aberrations in the arcuate fasciculus are associated with auditory verbal hallucinations in psychotic and in non-psychotic individuals. Hum Brain Mapp 2013;34:626-34.

[217] Knochel C, O'Dwyer L, Alves G, Reinke B, Magerkurth J, Rotarska-Jagiela A, Prvulovic D, Hampel H, Linden DE, Oertel-Knochel V. Association between white matter

fiber integrity and subclinical psychotic symptoms in schizophrenia patients and unaffected relatives. Schizophr Res 2012;140:129-35.

[218] Frith C, Rees G, Friston K. Psychosis and the experience of self. Brain systems underlying self-monitoring. Ann N Y Acad Sci 1998;843:170-8.

[219] Allen P, Aleman A, McGuire PK. Inner speech models of auditory verbal hallucinations: evidence from behavioural and neuroimaging studies. Int Rev Psychiatry 2007;19:407-15.

[220] Friston KJ, Harrison L, Penny W. Dynamic causal modelling. Neuroimage 2003;19:1273-302.

[221] Li B, Wang X, Yao S, Hu D, Friston K. Task-Dependent Modulation of Effective Connectivity within the Default Mode Network. Front Psychol 2012;3:206.

[222] Li B, Daunizeau J, Stephan KE, Penny W, Hu D, Friston K. Generalised filtering and stochastic DCM for fMRI. Neuroimage 2011;58:442-57.

[223] Cui LB, Liu J, Wang LX, Li C, Xi YB, Guo F, Wang HN, Zhang LC, Liu WM, He H, Tian P, Lu H, Yin H. Anterior cingulate cortex-related connectivity in first-episode schizophrenia: a spectral dynamic causal modeling study with functional magnetic resonance imaging. Front Hum Neurosci 2015;9:589.

[224] Li B, Friston KJ, Liu J, Liu Y, Zhang G, Cao F, Su L, Yao S, Lu H, Hu D. Impaired frontal-basal ganglia connectivity in adolescents with internet addiction. Sci Rep 2014;4:5027.

[225] Ma L, Steinberg JL, Hasan KM, Narayana PA, Kramer LA, Moeller FG. Stochastic dynamic causal modeling of working memory connections in cocaine dependence. Hum Brain Mapp 2014;35:760-78.

[226] Keller SS, Crow T, Foundas A, Amunts K, Roberts N. Broca's area: nomenclature, anatomy, typology and asymmetry. Brain Lang 2009;109:29-48.

[227] Friston KJ, Stephan K, Li BJ, Daunizeau J. Generalised Filtering. Math Probl Eng 2010;2010:Article ID 621670.

[228] Fletcher PC, Frith CD. Perceiving is believing: a Bayesian approach to explaining the positive symptoms of schizophrenia. Nat Rev Neurosci 2009;10:48-58.

[229] Andreasen NC, Paradiso S, O'Leary DS. "Cognitive dysmetria" as an integrative theory of schizophrenia: a dysfunction in cortical-subcortical-cerebellar circuitry? Schizophr Bull 1998;24:203-18.

[230] Fox CJ, Iaria G, Barton JJ. Disconnection in prosopagnosia and face processing. Cortex 2008;44:996-1009.

[231] Dauvermann MR, Whalley HC, Romaniuk L, Valton V, Owens DG, Johnstone EC, Lawrie SM, Moorhead TW. The application of nonlinear Dynamic Causal Modelling for fMRI in subjects at high genetic risk of schizophrenia. Neuroimage 2013;73:16-29.

[232] Cui LB, Chen G, Xu ZL, Liu L, Wang HN, Guo L, Liu WM, Liu TT, Qi S, Liu K, Qin W, Sun JB, Xi YB, Yin H. Cerebral blood flow and its connectivity features of auditory verbal hallucinations in schizophrenia: A perfusion study. Psychiatry Res 2016;260:53-61.

[233] Cui LB, Liu L, Guo F, Chen YC, Chen G, Xi M, Qin W, Sun JB, Li C, Xi YB, Wang HN, Yin H. Disturbed Brain Activity in Resting-State Networks of Patients with First-Episode Schizophrenia with Auditory Verbal Hallucinations: A Cross-sectional Functional MR Imaging Study. Radiology 2017;283:810-9.

[234] Cui LB, Liu K, Li C, Wang LX, Guo F, Tian P, Wu YJ, Guo L, Liu WM, Xi YB, Wang HN, Yin H. Putamen-related regional and network functional deficits in first-episode schizophrenia with auditory verbal hallucinations. Schizophr Res 2016;173:13-22.

[235] Li B, Cui LB, Xi YB, Friston KJ, Guo F, Wang HN, Zhang LC, Bai YH, Tan QR, Yin H, Lu H. Abnormal Effective Connectivity in the Brain is Involved in Auditory Verbal Hallucinations in Schizophrenia. Neurosci Bull 2017;33:281-91.

附　　录

另外，博士期间参与的脑功能磁共振成像相关的其他研究包括首发精神分裂症及其一级亲属、肝性脊髓病的脑结构与功能研究，具体如下：

Appendix 1: A spectral dynamic causal modeling study in first-episode schizophrenia

Long-Biao Cui, Jian Liu, Liu-Xian Wang, Chen Li, Yi-Bin Xi, Fan Guo, Hua-Ning Wang, Lin-Chuan Zhang, Wen-Ming Liu, Hong He, Ping Tian, Hongbing Lu, Hong Yin

Front Hum Neurosci, 2015; 9:589.

Understanding the neural basis of SZ is important for shedding light on the neurobiological mechanisms underlying this mental disorder. Structural and functional alterations in the anterior cingulate cortex (ACC), dorsolateral prefrontal cortex (DLPFC), hippocampus, and medial prefrontal cortex (MPFC) have been implicated in the neurobiology of SZ. However, the effective connectivity among them in SZ remains unclear. The current study investigated how neuronal pathways involving these regions were affected in first-episode SZ using functional magnetic resonance imaging (fMRI).

1.1 Subjects

The study sample consisted of 49 first-episode SZ patients from early intervention services within the outpatient clinic and inpatient department at Xijing Hospital, and 50 healthy controls (HCs) recruited by advertisement from the local community (**Table A1-1**). Please see 1.1.1 of the main text. All participants gave written informed consent approved by the local Research Ethics Committee (Xijing Hospital, Fourth Military Medical

University) after a complete description of this study.

1.2 Methods

1.2.1 Image acquisition

The fMRI images were acquired on a 3.0-T Siemens Magnetom Trio Tim scanner. Please see 1.2.1 and 2.2.1 of the main text.

1.2.2 Data preprocessing

Please see 5.2.2 of the main text.

1.2.3 General linear model

Please see 5.2.3 of the main text.

1.2.4 Regions of interest

For each participant, symmetric eight regions of interest (ROIs) including bilateral ACC, DLPFC, hippocampi, and MPFC were selected (**Fig. A1-1**). Please see 5.2.4 of the main text.

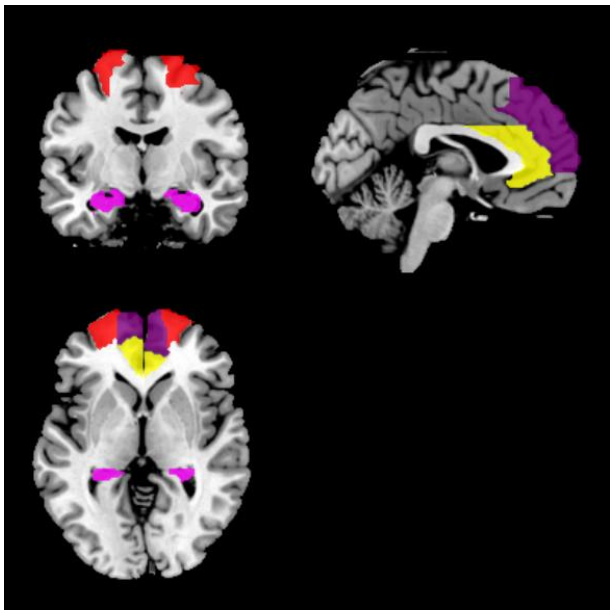

Fig. A1-1 Locations of the masks

Red indicates DLPFC; yellow indicates ACC; dark purple indicates MPFC; violet indicates the hippocampus.

1.2.5 Spectral dynamic causal modeling

Effective connectivity among the bilateral ACC, DLPFC, hippocampi, and MPFC was investigated using spectral DCM as described elsewhere. In the absence of a particular hypothesis or model space we used the fully connected model for an exploratory analysis of all possible reduced models, without one or more connections: after the full DCM for each participant was inverted, we employed a network discovery procedure using Bayesian model reduction (BMR) to find the best model that explains the data. This procedure tests every possible model nested within the fully connected model. The model with the highest posterior probability is chosen as the winning model during this procedure. This BMR procedure is an efficient way to score a large model space without having to invert every reduced model. A fully connected model was constructed for each subject. This model was then inverted using generalized filtering. The model selection procedure was used to identify the model best explaining how the data are generated. Thus, we used a network discovery scheme in order to identify the optimal model pooling over all subjects. Model evidence of a fully connected model was used to approximate the model evidence of all the possible models and search for the model with the largest evidence. This network discovery-based model selection method can find the best model in the whole model space only by estimating parameters of a fully connected model.

On the basis of spectral DCM analysis, the connection strength described the strength of a coupling according to the rate at which neuronal responses were induced in the target region (in other words connection strengths are effectively rate constants in 1/s, Hz). The resulting (maximum a posteriori) estimates of connectivity were then treated as summary statistics for classical random effects inference at the second (between subject) level using appropriate t-tests. We reported (Bonferroni corrected) *P* values for all other connections to demonstrate the specificity of the differences. Then, we characterized the differences using Bayesian parameter averaging (BPA) for each group separately after network discovery procedure. See the flowchart of our each step (**Fig. A1-2**).

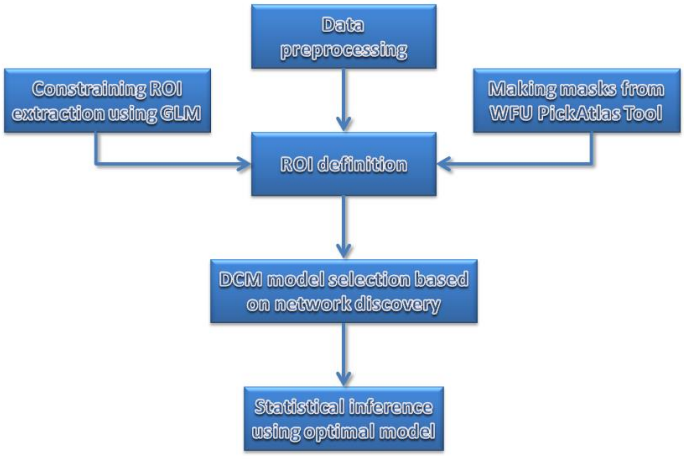

Fig. A1-2 Steps for data analysis

The resulting constant images were used for constraining the ROI extraction step in the spDCM.

1.3 Results

1.3.1 Clinical data

The demographic and clinical data are shown in **Table A1-1**. No significant difference was present between SZ patients and HCs on any demographic variables.

Table A1-1 Demographic and clinical characteristics of first-episode SZ patients (n = 49) and HCs (n = 50)

Characteristics	SZ Patients	HCs	Statistics	*P*
Age (years)	26 ± 6	27 ± 4	$t = 1.57$	0.12
Sex (male/female)	29/20	31/19	$\chi^2 = 0.08$	0.77
Ethnicity	Han (Chinese)	Han (Chinese)		
Handedness (right/left)	49/0	50/0		
Duration of illness (months)	10 ± 14	—		
PANSS Total Score	162 ± 27	—		

PANSS Positive Score	24 ±8	—
PANSS Negative Score	24 ±7	—
PANSS General Psychopathology	49 ±9	—

PANSS, Positive and Negative Syndrome Scale.

1.3.2 Network discovery-based model selection findings

Having inverted a fully connected model with full extrinsic connectivity, the log model evidence for all reduced models (models with one or more missing connections) was then assessed. **Fig. A1-3** shows the network discovery procedure compared the evidence of all reduced models for each group and the results of post-hoc optimization. The left panel is for SZ patients and right panel refers to HCs. The fully connected model was the full model with the highest evidence. The procedure selected the fully connected model as the best model with a posterior probability of almost 1. The fully connected model had 49 parameters describing the extrinsic connections between nodes and the intrinsic (self-connections) within nodes. This suggested that the fully connected model was the best explanation for these data, indicating eligible and rational ROI selection.

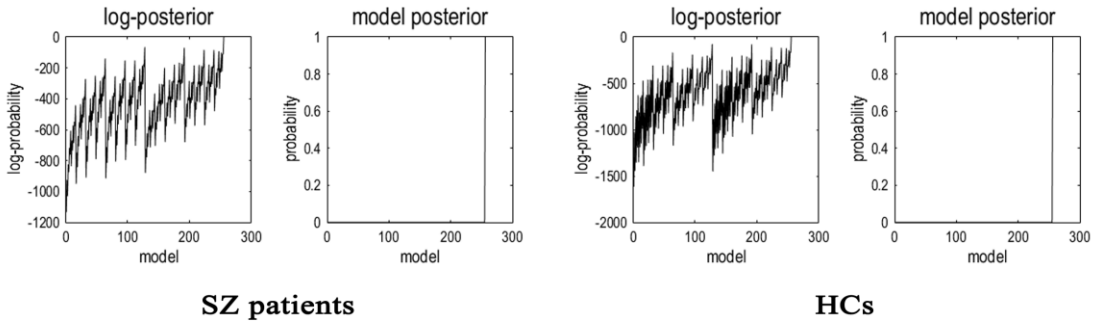

Fig. A1-3 Results of the post-hoc optimization or network findings

The corresponding conditional parameter estimates were shown over the 49 (intrinsic and extrinsic) connections. The profiles of model evidences are shown with the posterior probability for each model. In both groups, the full model had a probability of almost 1 and a log-probability of almost 0. As shown in the figure, the model with the highest evidence was the fully connected model based on the results of post-hoc optimization or

network findings.

1.3.3 Effective connectivity

The BPA results of the effective connectivity are shown in **Fig. A1-4**. We set the threshold to 0.9 Hz. SZ patients exerted decreased connections from the left hippocampus to left DLPFC and from the left DLPFC to right MPFC.

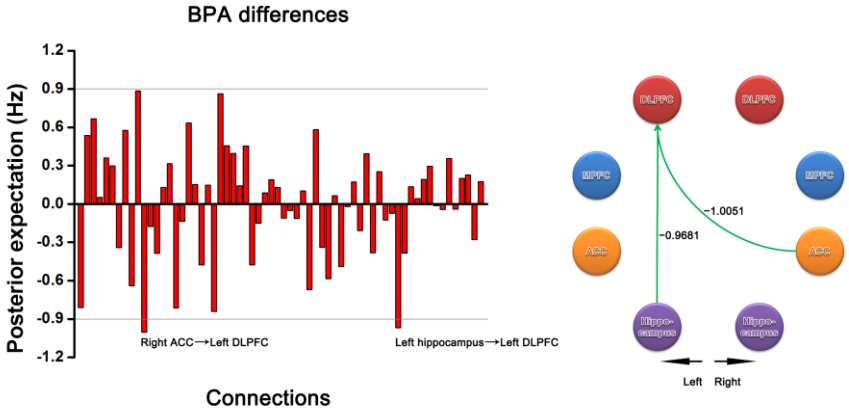

Fig. A1-4 Significant effective connectivity (between the group level) among ROIs in the SZ patients and HCs

The left panel shows the BPA of the differences for spectral DCM. The right panel shows only those edges on the graph that survive the threshold of 0.9 Hz in the left panel, i.e., the decreased (green) connections in SZ patients relative to HCs.

1.4 Conclusion

The present study characterized the abnormal effective connectivity *in vivo* in first-episode SZ by means of spDCM, revealing anterior cingulate cortico/hippocampal-prefrontal hypoconnectivity. spDCM revealed abnormal effective connectivity involving PFC and hippocampus in patients with first-episode SZ. This suggests the SZ subjects fail to recruit these neural pathways. This study further provides a link between SZ and dysconnection hypothesis, creating an ideal situation to associate mechanisms behind SZ with aberrant connectivity among these cognition and memory-related regions.

Appendix 2: A stochastic dynamic causal modeling study in unaffected first-degree relatives of first-episode schizophrenia

Yi-Bin Xi, Chen Li, **Long-Biao Cui**, Jian Liu, Fan Guo, Liang Li, Ting-Ting Liu, Kang Liu, Gang Chen, Min Xi, Hua-Ning Wang, Hong Yin (co-first author)

Front Hum Neurosci, 2016; 10:383.

Familial risk plays a significant role in the etiology of SZ. Many studies using neuroimaging have demonstrated structural and functional alterations in relatives of SZ patients, with significant results found in diverse brain regions involving the ACC, caudate, DLPFC, and hippocampus. This study investigated whether unaffected relatives of first episode SZ differ from HCs in effective connectivity measures among these regions.

2.1 Subjects

We assessed 50 HCs and 46 unaffected first-degree relatives of patients with first episode SZ (age- and gender-matched to HCs) (**Table A2-1**). The DSM-IV-TR consensus diagnoses were established by two trained senior clinical psychiatrists with all clinical data and Structured Clinical Interviews for DSM Diagnoses interviews: inter-rater reliability was higher than 90% among raters. Relatives of probands were free of Axis I psychopathology and not taking psychoactive medications. Participants were recruited via word of mouth and advertisements at the Fourth Military Medical University; all provided written informed consent approved by the institutional review board of Xijing Hospital.

2.2 Methods

2.2.1 Data acquisition

The resting state fMRI images were collected on the 3.0-T Siemens Magnetom Trio Tim scanner. Please see 1.2.1 and 2.2.1 of the main text.

2.2.2 Data preprocessing

Please see 5.2.2 of the main text.

2.2.3 General linear model

Please see 5.2.3 of the main text.

2.2.4 Regions of interest

For each subject, we studied the effective connectivity among seven ROIs including the left DLPFC (consists of Frontal_Sup_L and Frontal_Sup_Medial_L), and the bilateral ACC (Cingulum_Ant_L and Cingulum_Ant_R), caudate nuclei (Caudate_L and Caudate_R), and hippocampi (Hippocampus_L and Hippocampus_R) (**Fig. A2-1**). Please see 5.2.4 of the main text.

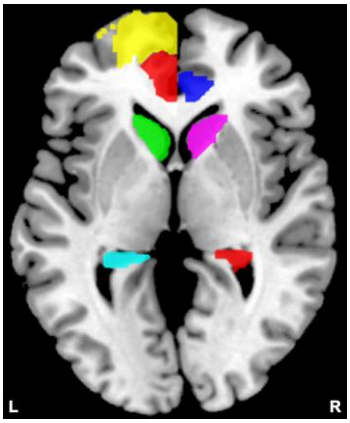

Fig. A2-1 Locations of the masks

Yellow indicates the left DLPFC; semitransparent red indicates the left ACC, and blue indicates the right ACC; green indicates the left caudate, and violet indicates the right caudate; cyan indicates the left hippocampus, and red indicates the right hippocampus.

2.2.5 Model specification and parameter estimation

In the current study, we aimed to search over all possible models generated from the connections among the seven ROIs. In this case, we did not limit our analysis to simply compareing a few competing hypothesis (models). In contrast, we used a data-driven approach to search over all possible models. Specifically, a fully connected model (full

model) with bidirectional connections between any pair of regions was constructed for each subject (**Fig. A2-2**). Parameter estimates and model evidence of the full model was obtained using generalized filtering which is a recently developed scheme for sDCM model inversion and parameter estimation (Friston et al., 2010). After the full model was inverted, we employed a network discovery procedure (Friston et al., 2011) to search for the best reduced model which has the highest model evidence. A reduced model has the same group of ROIs as the full model, but only a subgroup of the connections in the full model (i.e., some of the connections are absent in the reduced model). The network discovery scheme provides approximation of the model evidences of all the possible reduced models without inverting every reduced model. The reduced models and the full model are then scored according to their model evidence. Model which has the highest model evidence was chosen as the winning model. Parameter estimates of the winning model were also obtained using the network discovery scheme and used for group analysis and making inferences on effective connectivity between brain regions.

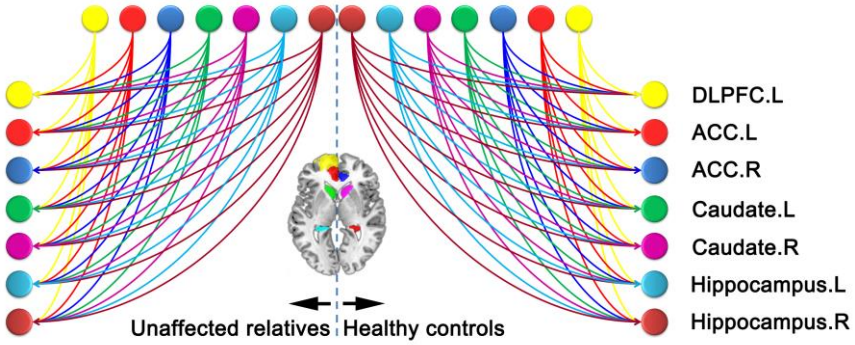

Fig. A2-2 Fully connected model constructed

The lines with arrowheads between distinct ROIs refer to the connections in the left panel for relatives of SZ patients and right panel for HCs. The color of each node is in line with that of **Fig. A2-1**. ACC, anterior cingulate cortex; DLPFC, dorsolateral prefrontal cortex.

2.2.6 Group Analysis

On the basis of sDCM analysis, the strength of connection described the coupling strength according to the rate at which neuronal responses were triggered in the target area

(connection strengths are effectively rate constants in 1/s, Hz). To see whether these differences could be estimated and detected reliably, we characterized the differences using BPA. We used BPA for each group separately after network discovery procedure. We can then go on to discuss the results based on largest two or three connection differences, thereby being as a guiding principle to set the threshold (strength of connections measured in Hz).

2.3 Results

2.3.1 Demographical characteristics

No significant differences were present between SZ patients' first-degree relatives and HCs on any demographic variables (**Table A2-1**).

Table A2-1 Demographical data of the participants

Variables	First-degree relatives of SZ patients	HCs	Statistics	*P* value
Age (y)	28 ±5	27 ±4	$t = -0.35$	0.73
Gender (M/F)	22/24	31/19	$\chi^2 = 1.95$	0.22
Ethnicity	Han (Chinese)	Han (Chinese)	—	—
Handedness (R/L)	46/0	50/0	—	—
Education (y)	15 ±1	15 ±2	$t = 0.23$	0.82
Smoking status (S/N)	11/35	18/32	$\chi^2 = 1.66$	0.27

M, male; F, female; R, right; L, left; S, smoker; N, nonsmoker.

2.3.2 Network discovery-based model selection results

The evidence of all reduced models was compared by the network discovery procedure for each group (**Fig. A2-3**). The left panel is for first-degree relatives of SZ patients and right panel refers to HCs. The procedure selected the fully connected model as the best model with a posterior probability of almost 1. The fully connected model had 49 parameters describing the extrinsic connections between nodes and the intrinsic (self-connections) within nodes. In **Fig. A2-3**, the profiles of model evidences are shown

with the posterior probability for each model. In both groups, the full model had a log-probability of almost 0 and probability of 1. Therefore, they shared the identical winning model.

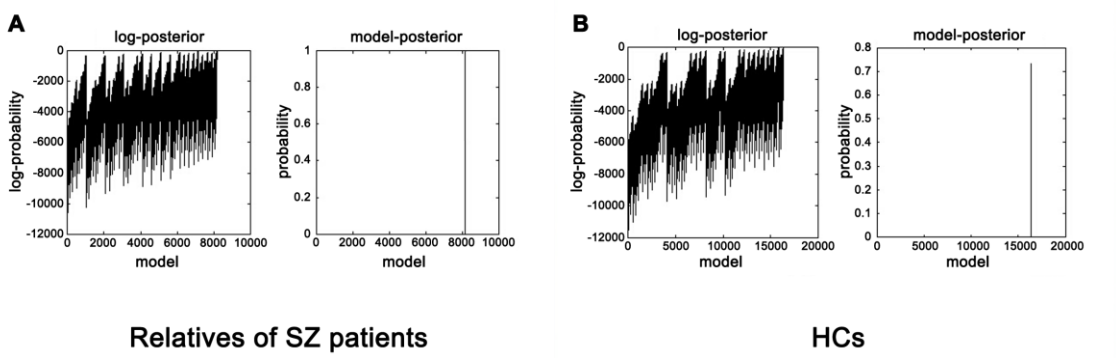

Fig. A2-3 Results of the post-hoc optimization

The corresponding conditional parameter estimates were shown over the 49 (extrinsic and intrinsic) connections in relatives of SZ patients (A) and HCs (B). This figure suggested that the fully connected model was the best explanation for the data.

2.3.3 Effectivity connectivity

BPA results of the effective connectivity can be seen in **Fig. A2-4**. When using BPA, in the context of uncovering the group differences, as a guiding principle it would be best to choose top two or three connections and then we set the threshold to 0.06 Hz. SZ patients' relatives exerted increased connection from the left ACC to right hippocampus, but decreased connection from the right ACC to right hippocampus as compared to HCs.

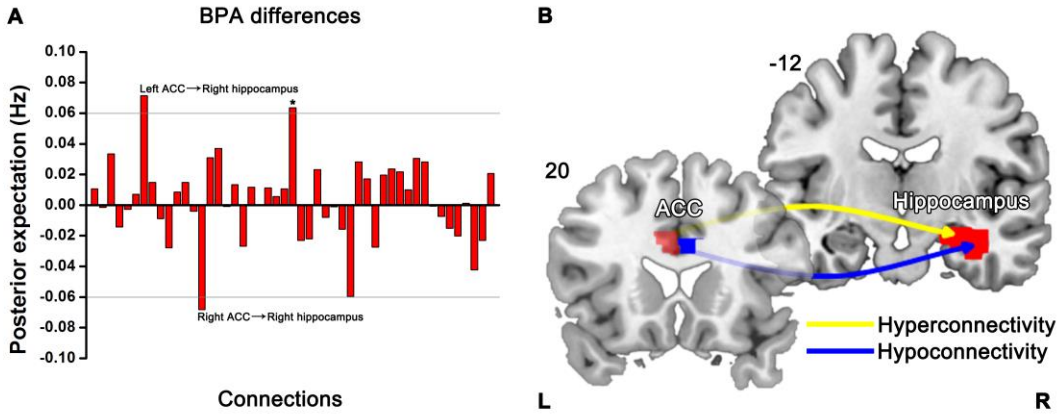

Fig. A2-4 Significant effective connectivity (between the group level) among ROIs in

the first-degree relatives of SZ patients and HCs

A: BPA of the differences for sDCM shows only those edges on the graph that survive the threshold of 0.06 Hz, i.e., the increased (Left ACC-right hippocampus) and decreased (right ACC-right hippocampus) connections in relatives compared to HCs. B: Schematic illustration showing connectivity patterns in first-degree relatives of SZ patients. "*" indicates self-connection of the left caudate. The slice location (coordinate) is marked in the upper-left.

2.4 Conlusion

Our findings show the pattern of effective connectivity among DLPFC, ACC, hippocampus, and caudate in the familial high risk population of SZ patients, which may be tied to a familial risk of SZ. Specifically, we found that increased effective connectivity from the left ACC to right hippocampus and decreased effective connectivity from the right ACC to right hippocampus in unaffected first-degree relatives of first episode SZ patients. The anterior cingulate cortico-hippocampal dysconnectivity may therefore serve as a potential sign of a general vulnerability to develop SZ.

Appendix 3: Perfusion and its connectivity of first-episode schizophrenia patients and their unaffected first-degree relatives

Long-Biao Cui, Liu-Xian Wang, Ping Tian, Hua-Ning Wang, Min Cai, Fan Guo, Chen Li, Yu-Jing Wu, Peng-Gang Qiao, Zi-Liang Xu, Lin Liu, Hong He, Wen-Jun Wu, Yi-Bin Xi, Hong Yin

Submitted to *Sci Rep*

Neural substrates behind SZ and its heritability mediated by cerebral function are largely unknown. Cerebral blood flow (CBF), as a biomarker of activation in the brain, reflects the neuronal metabolism, and is promisingly used to detect brain alteration thereby shedding light on the underpinnings of SZ and features of their relatives at high genetic risk. SZ patients have exhibited increased or decreased CBF in different brain regions, with hypoperfusion in the frontal lobes, anterior and medial cingulated gyri and the parietal lobe, while increased perfusion in the cerebellum, brainstem and thalamus. However, the results, especially the activated brain regions, are not all inclusive or consistent. The aim of the current study was to detect the CBF alteration patterns in SZ and their first-degree relatives.

3.1 Subjects

This study was approved by the local ethical committee, and all participants provided written informed consent after complete description of the study. A total of demographically matched 51 SZ patients, 33 unaffected first-degree relatives of these SZ patients, and 53 HCs were included in the experiment (**Table A3-1**).

3.2 Methods

3.3.1 Image acquisition

MRI data were collected on a 3.0 T Siemens Magnetom Trio Tim scanner using an eight-channel phased array head coil (Siemens, Germany) between July 2013 and October 2015. Please see 1.1.1 of the main text.

3.3.2 CBF calculation

Please see 1.2.2 of the main text.

3.3.3 CBF connectivity analysis

Please see 1.2.3 of the main text.

3.3.4 Statistical analysis

Please see 1.2.4 of the main text.

3.3 Results

3.3.1 Demographic and clinical data

The demographic and clinical data are shown in **Table A3-1**. There were significant differences in education years between SZ patients and unaffected relatives, SZ patients and HCs. No other obvious differences were found.

Table A3-1 Demographical and clinical characteristics of three groups

Characteristics	SZ patients	Unaffective relatives	HCs
Age (years)	26 ± 6	28 ± 5	27 ± 4
Sex (male/female)	25/20	23/9	32/19
Ethnicity	Han (Chinese)	Han (Chinese)	Han (Chinese)
Education (years)	13 ± 2*,#	14 ± 2	15 ± 2
Handedness (right/left)	45/0	32/0	51/0
Smoking status (smoker/nonsmoker)	11/34	8/24	18/33
PANSS Total Score	24 ± 8	—	—
PANSS Positive Score	23 ± 7	—	—

PANSS Negative Score	49 ±8	—	—
PANSS General Psychopathology	161 ±28	—	—

*P < 0.05 versus unaffected relatives; #P < 0.05 versus HCs.

3.3.2 Brain regions with significant differences in CBF

Whole brain CBF values of each subject were calculated before analysis. Differences between SZ patients and HCs, SZ patients and unaffected relatives are displayed in **Fig. A3-1** and **Table A3-2**. ANOVA showed significant difference of CBF in the bilateral middle/superior temporal gyri, precuneus, cuneus, superior occipital gyri and cingulate gyri, and left medial superior frontal gyrus (P < 0.005, AlphaSim correction, cluster > 27). Compared with HCs, SZ patients had higher CBF values in the left medial superior frontal gyrus and right precuneus (P < 0.005, AlphaSim correction, cluster > 27). Analysis between SZ patients and unaffected relatives demonstrated that SZ patients had obvious decreased CBF values in the left middle temporal gyrus (P < 0.005, AlphaSim correction, cluster > 27). In addition to the former analysis, we also compared CBF values between unaffected relatives and HCs. Unaffected relatives demonstrated increased CBF values in the bilateral middle temporal gyri and precuneus, left superior temporal gyrus and superior occipital gyrus, and right cuneus (P < 0.005, AlphaSim correction, cluster > 27).

Table A3-2 Brain regions with significant differences in CBF

Regions	**Cluster size**	**Peak F/T value**	**Peak MNI coordinate**		
			X	Y	Z
ANOVA					
Left MTG	104	9.8593	−52	−54	2
Left MTG/STG	175	14.3602	−60	−40	6
Right MTG/STG	233	10.4084	62	−34	4
Left cuneus/precuneus/SOG	71	7.2865	−18	−64	24
Right cuneus	29	6.3264	14	−86	18

Right precuneus/SOG	72	8.7688	24	−64	28
Right precuneus	64	7.9461	12	−66	50
Bilateral MCG	95	6.7861	2	−24	30
Left medial SFG	88	10.0719	−6	50	34
SZ > HCs					
Left medial SFG	49	3.9741	−6	52	34
Right precuneus	37	3.7397	12	−66	52
SZ < Unaffected relatives					
Left MTG	51	−4.2625	−64	−42	4
Unaffected relatives > HCs					
Right STG	163	4.5259	66	−32	6
Right MTG	34	3.6221	54	−58	6
Left MTG	239	5.3947	−60	−42	6
Right precuneus	31	3.9009	8	−46	62
Left precuneus	37	3.8766	2	−66	26
Right cuneus	59	3.9966	22	−64	28
Left SOG	44	4.0131	−20	−64	24

MCG, middle cingulate gyrus; MTG, middle temporal gyrus; SFG, superior frontal gyrus; SOG, superior occipital gyrus; STG, superior temporal gyrus.

3.3.3 Correlation analysis

Correlation analysis between image measures and PANSS total score showed that CBF values in the left middle temporal gyrus manifested a significantly negative correlation with PANSS total score ($r = -0.371$, $P = 0.012$).

3.3.4 CBF connectivity

By calculating Pearson's correlation between regional CBF across subjects, we

obtained three 90 × 90 CBF connectivity matrices, exhibiting correlation coefficient value for each group, as shown in **Fig. A3-2.** In each matrix, the green color stand for non-correlation, and red and blue colors represent positive and negative trend of correlation, respectively. All 90 components' CBF connectivity of whole brain can be observed from the matrix of each group. Similar pattern of CBF connectivity was detected in SZ patients and their unaffected relatives.

In order to directly perceive the CBF correlation of each group, we used BrainNet View to present the connectivity patterns with correlation coefficient value larger than 0.6 or less than −0.6, including the connectivity of all ninety modules of the whole brain (**Fig. A3-3**). Then, *z* values of connections with significant difference between SZ patients and their unaffected relatives are listed in **Table A3-3**.

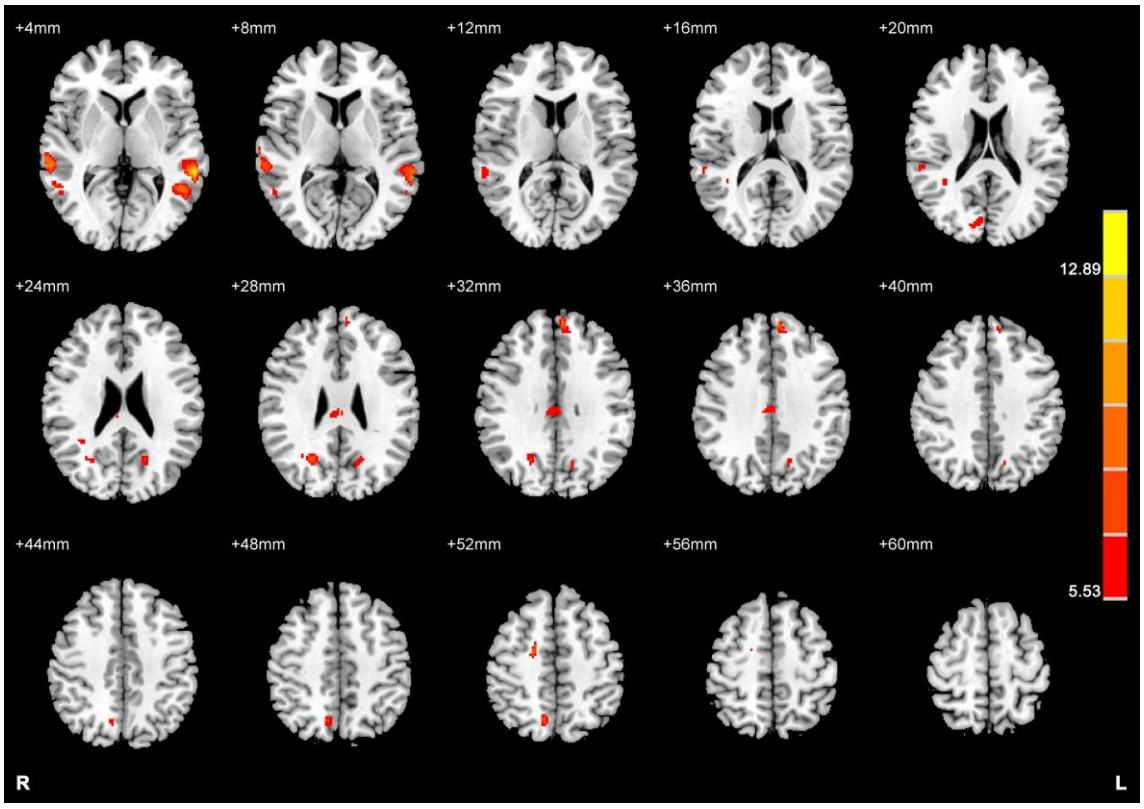

Fig. A3-1 Comparisons of CBF among three groups using ANOVA

The coordinate of each slice is marked in the upper-left. The color bar on the right indicates the F values.

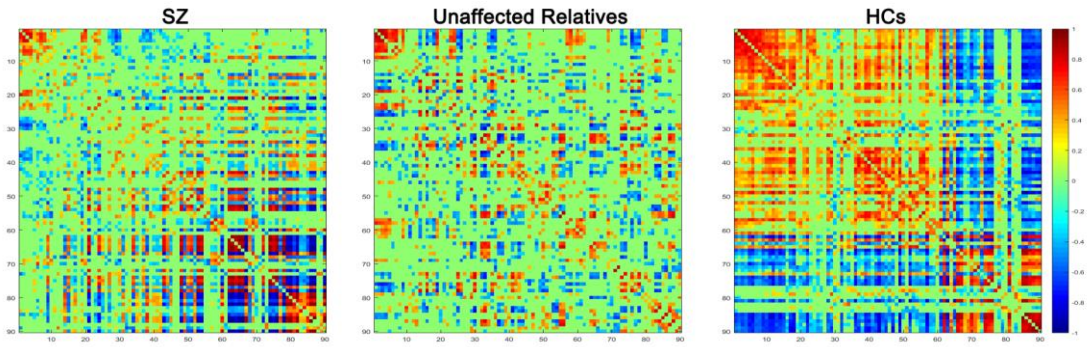

Fig. A3-2 The CBF connectivity matrix obtained by calculating Pearson's correlation

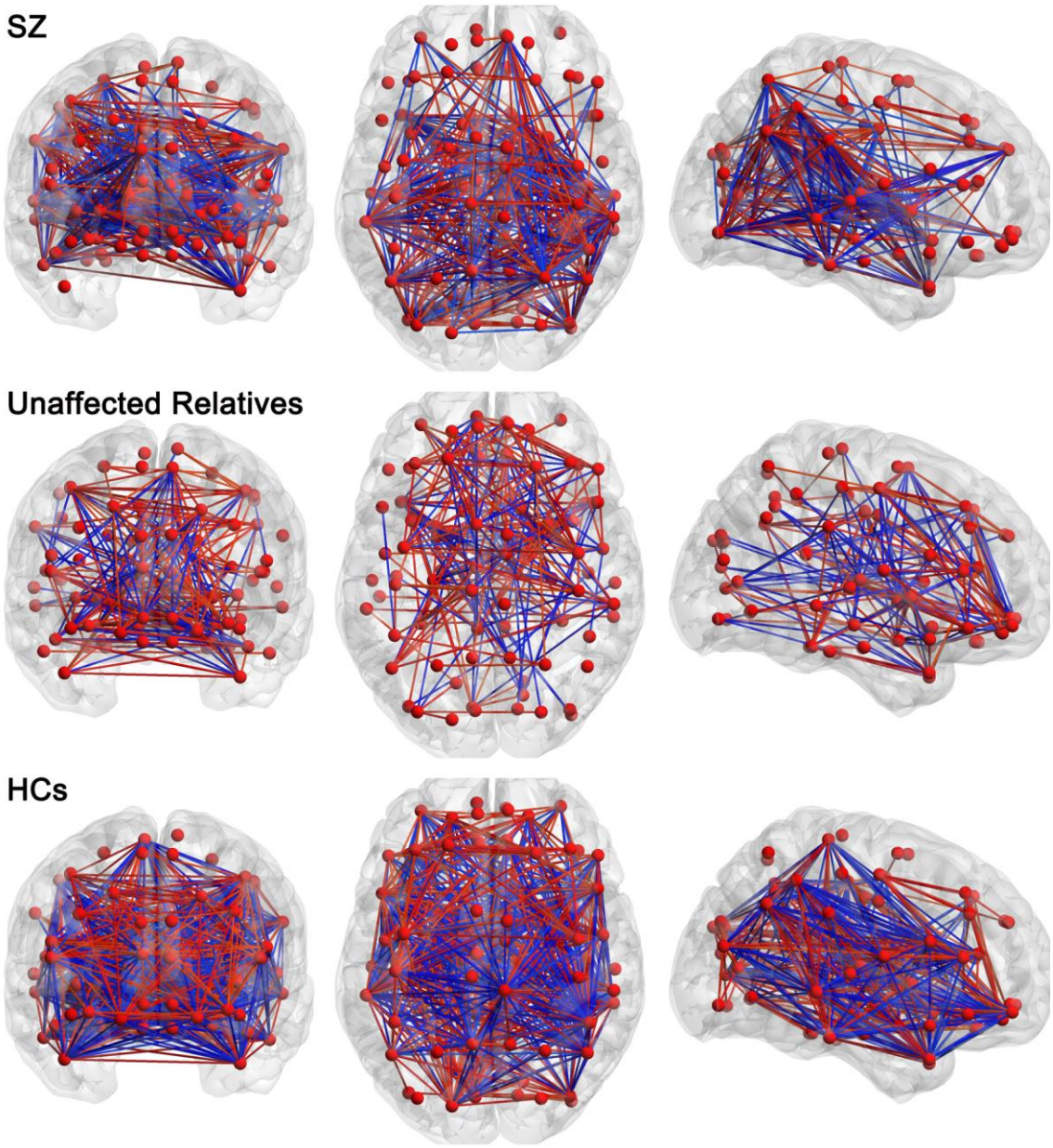

Fig. A3-3 The CBF networks showing connections with correlation coefficient value

larger than 0.6 or less than −0.6

Line color indicates the positive (red) or negative (blue) coefficient.

Table A3-3 *z* values of significantly different connectivity with regions of different CBF between SZ patients and their unaffected relatives

Connectivity	***z* values**	***P* values**
SZ > REL		
Left MTG-right hippocampus	3.2682	0.0038
Left MTG-left auditory cortex	3.2902	0.0036
Left MTG-right auditory cortex	3.7759	0.0006
Left MTG-left STG	2.8149	0.0152
Left MTG-right STG	3.5689	0.0014
Left MTG-left MTG (temporal pole)	3.3776	0.0027
Left MTG-right ITG	3.6094	0.0012
SZ < REL		
Left MTG-left lingual gyrus	−3.1136	0.0063
Left MTG-left IOG	−3.2017	0.0047
Left MTG-right IOG	−2.9308	0.0109
Left MTG-right inferior parietal lobule	−3.6329	0.0011
Left MTG-right SMG	−2.9428	0.0105
Left MTG-left angular gyrus	−5.3643	0.0000
Left MTG-right angular gyrus	−2.9255	0.0111
Left MTG-right putamen	−2.9335	0.0108
Left MTG-right pallidum	−4.6493	0.0000
Left MTG-right thalamus	−2.9342	0.0108

IOG, inferior occipital gyrus; ITG, inferior temporal gyrus; MTG, middle temporal gyrus; SMG, supramarginal gyrus; STG, superior temporal gyrus.

Notably, SZ patients and their unaffected relatives revealed disrupted pattern of characteristic path length, and they also exhibited relatively small clustering index, and low local efficiency and global efficiency in contrast to HCs (**Fig. A3-4**). Moreover, unaffected relatives were with intermediate level between HCs and SZ patients for local efficiency and global efficiency. Generally, both SZ patient group and their unaffected relatives showed deficit communication within the network compared with HCs.

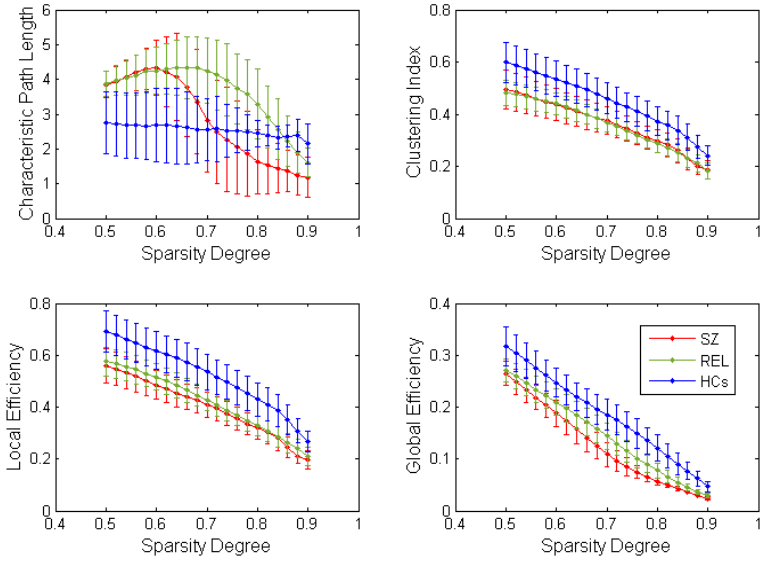

Fig. A3-4 Global network properties as function of sparsity degree.

The characteristic path length, clustering index, local efficiency, and global efficiency decrease as the sparsity degree increases. SZ, schizophrenia; REL, relatives; HCs, healthy controls.

3.4 Conclusion

In summary, the present study reveals CBF change in first-episode, drug-naïve SZ patients and their first-degree relatives, demonstrated CBF alterations pronounced in brain regions within DMN and deficit CBF connectivity patterns, and further elucidated association between CBF values with clinical symptoms. Our results may help exploring pathogenesis underlying SZ itself and the heritability in liability of SZ.

Appendix 4: Disease definition for schizophrenia by functional connectivity using radiomics strategy

Long-Biao Cui, Lin Liu, Hua-Ning Wang, Liu-Xian Wang, Fan Guo, Yi-Bin Xi, Ting-Ting Liu, Chen Li, Ping Tian, Kang Liu, Wen-Jun Wu, Yi-Huan Chen, Wei Qin, Hong Yin

Submitted to *Schizophr Bull*

SZ is considered as a severe psychiatric disorder with high clinical heterogeneity. Specific biomarker reflecting its neurobiological substrates is required for diagnosis and treatment selection of SZ. Fortunately, evidence from neuroimaging has implicated disrupted functional connectivity in the pathophysiology. We aimed to develop and validate a method of disease definition for SZ by resting-state functional connectivity using radiomics strategy. In this study, on the basis of the dysconnectivity theory of SZ and by means of radiomics approaches, we aimed to develop and validate a method of disease definition for SZ by resting-state functional connectivity using radiomics strategy in first-episode untreated patients, improving objective SZ individualized diagnosis using quantitative and specific biomarker in clinical practice.

4.1 Subjects

This study was approved by the local Research Ethics Committee. All participants gave written informed consent after a full description of the aims and design of the study. Two samples of first-episode SZ patients were recruited in the Department of Psychiatry, Xijing Hospital; one from May 2011 and Sep 2013 and another from April 2015 to December 2016. The DSM-IV-TR and DSM-V were used for these two groups,

respectively, and consensus diagnoses of SZ were made using all the available information. In addition, two groups of HCs were recruited from the local community by advertisement at the same period when SZ patients were recruited. A total of 108 SZ patients and 121 HCs participated in this study (**Table A4-1**).

Table A4-1 Demographical and Clinical Data of Participants

	Data set 1		Data set 2	
Characteristic	**Patients (n = 52)**	**HCs (n = 66)**	**Patients (n = 56)**	**HCs (n = 55)**
Age (y)	26 ±6	29 ±7	23 ±6	32 ±11
Gender (M/F)	31/21	33/33	30/26	26/29
Education level (y)	13 ±2	15 ±2	11 ±3	15 ±4
Scanner (T)	3.0	3.0	3.0	3.0
Duration of illness (mon)	11 ±14	—	14 ±20	—
PANSS score				
Total score	97 ±17	—	85 ±14	—
Positive score	24 ±8	—	22 ±5	—
Negative score	24 ±7	—	20 ±6	—
General score	49 ±9	—	43 ±9	—

4.2 Methods

4.2.1 Image acquisition

High-resolution T1-weighted anatomical imaging and resting-state BOLD-fMRI were obtained for both data sets. Two data sets were aquired on a Siemens 3.0 T Magnetom Trio Tim MR scanner and GE Discovery MR750 3.0 T scanner in the Department of Radiology, Xijing Hospital, respectively. Specific scanning parameters varied by MRI scanner (**Table A4-2**).

4.2.2 Dara preprocessing

Functional image preprocessing was carried out using CONN software (http://web.mit.edu/swg/software.htm). Briefly, after excluding the first 10 images to

ensure the signal to reach equilibrium, functional images were corrected for head motion and temporal differences. The subject was excluded if any translation or rotation parameters in this subject's data set were exceeded ± 1 mm and/or ± 1°. The corrected functional images were firstly co-registered to each subject's T1 images without reslicing. Then, T1 images were normalized to the Montreal Neurological Institute (MNI) space, which generated a transformed matrix from native space to MNI space. Functional images were than transformed to the MNI space using this matrix and resampled at $2 \times 2 \times 2$ mm^3. Outlier detection was performed on the normalized images. Finally, all images were smoothed with a 6 mm FWHM Gaussian kernel.21 Then, we randomly selected 80% of total subjects as training data set (total 183 subjects) and 20% as the validating data set (total 46 subjects).

Table A4-2 Detailed Scanning Parameters

	Siemens scanner		**GE scanner**	
	Structural data	**Functional data**	**Structural data**	**Functional data**
Repetition time (ms)	2530	2000	8.2	2000
Echo time (ms)	3.5	30	3.2	30
Flip angle (°)	7	90	9	90
Field of view (mm^2)	256 × 256	220 × 220	256 × 256	240 × 240
Matrix	256 × 256	64 × 64	256 × 256	64 × 64
Slice thickness (mm)	1	4	1	3.5
Section gap (mm)	0	0.6	0	0
Number of slices	192	33	196	45

4.2.3 Network constructed

AAL cortical and subcortical atlas was used to parcellate the whole brain into 90 non-cerebellar anatomical ROIs. For each subject, each ROI time series was extracted as the average time series across all voxels within that region. To remove spurious sources of variance, all of ROI time series were performed by the following steps: 1) linear

detrending; 2) regressing out the six head motion parameters and their first-level derivative, the averaged cerebrospinal fluid and white matter signals, and the scrubbing signal from the time series; 3) 0.01-0.1Hz band-pass filtering. All of these were done by using CONN software. Finally, Pearson correlation coefficients were calculated between each pair of preprocessed ROI time series, and a temporal correlation matrix (N × N, where N = 90 is the number of ROI in AAL atlas) was obtained for each subject.

4.2.4 Feature selection

Original features were selected as those edges which the connectivity coefficient were significantly differences using two sample *t*-tests ($P < 0.05$, uncorrected for multiple comparisons). Considering the individual variation, leave-one out method was used to insure the stability of selected edges. Briefly, 183 times two sample t-tests were performed. Each time, one subject in order was excluded. Only those edges which had stably significantly at each time were selected. In this step, 117 original features were included.

Least Absolute Shrinkage and Selection Operator (LASSO) method with 10-fold crossing validation using mean of square error (MSE) as cost function was performed to eliminate the multi-collinearity among 117 original features and shrink these features into few more important features according to MSE + 1SE (standard error) Criteria. In this step, 32 features (LASSO features) were remained.

Support vector machine (SVM) method was used to estimate the status (SZ or not) of each subject based on the features. The SVM procedures included t-test filtering to include only reliably different features, linear kernel separation and soft margin separation. In our research, 10-fold cross-validation which is widely used in machine learning approaches and provides a good estimate of accuracy, was further used to estimate group classification and prediction accuracies, and repeated for 1000 times. Accuracy, sensitivity, specificity were computed to quantify the classification performance. The ROC curve is reported using R version 3.2.3 (R Foundation for Statistical Computing). The area under the ROC curve (AUC) represents the classification power of a classifier, and a larger AUC indicates a better classification power.

The permutation test was applied to determine whether the accuracy obtained above

were significantly higher than values expected by chance. Specifically, we permuted the class labels (1: SZ patients, 0: HCs) across the entire sample 1000 times without replacement, and the entire classification procedure was reapplied each time. The *P* value for the accuracy was calculated by dividing the number of permutations that showed a higher value than the actual value for the real sample by the total number of permutations.

4.2.5 Evaluation metrics

The Pearson correlation coefficients between real values and predicted values and normalized MSE (NMSE) for prediction precision, and coefficient of determination (R^2) and Bayesian Information Criterion (BIC) for model fitting were used as evaluating indicators. Correlation coefficients measures the linear dependence between predicted value and real value and is less affected by the distribution of the input, which had been used in many study to evaluate the performance of the prediction model. NMSE measures the difference between predicted value and real value. R^2 and BIC measure the extent of model fitting and the extent of model simplification, respectively.

4.2.6 Validating the performance

Finally, the validating data set MR images were implemented to evaluate the classifier performance. We repeated the above processing and computed the accuracy, sensitivity, and specificity.

4.3 Results

4.3.1 Functional connectivity features building

Fig. A4-1 highlights all the 117 functional connectivity features with group differences used from SZ patients and HCs for classification analysis ($P < 0.05$, uncorrected for multiple comparisons). Here, for clear presentation, **Fig. A4-1B** and **C** show connectivity differences between cortical and limbic areas, and cortical and subcortical areas, respectively.

4.3.2 Feature selection

Of functional connectivity features, 117 features were reduced to 32 potential predictors on the basis of 183 subjects in the training data set, and were those with

nonzero coefficients in the LASSO logistic regression model (**Fig. A4-2**).

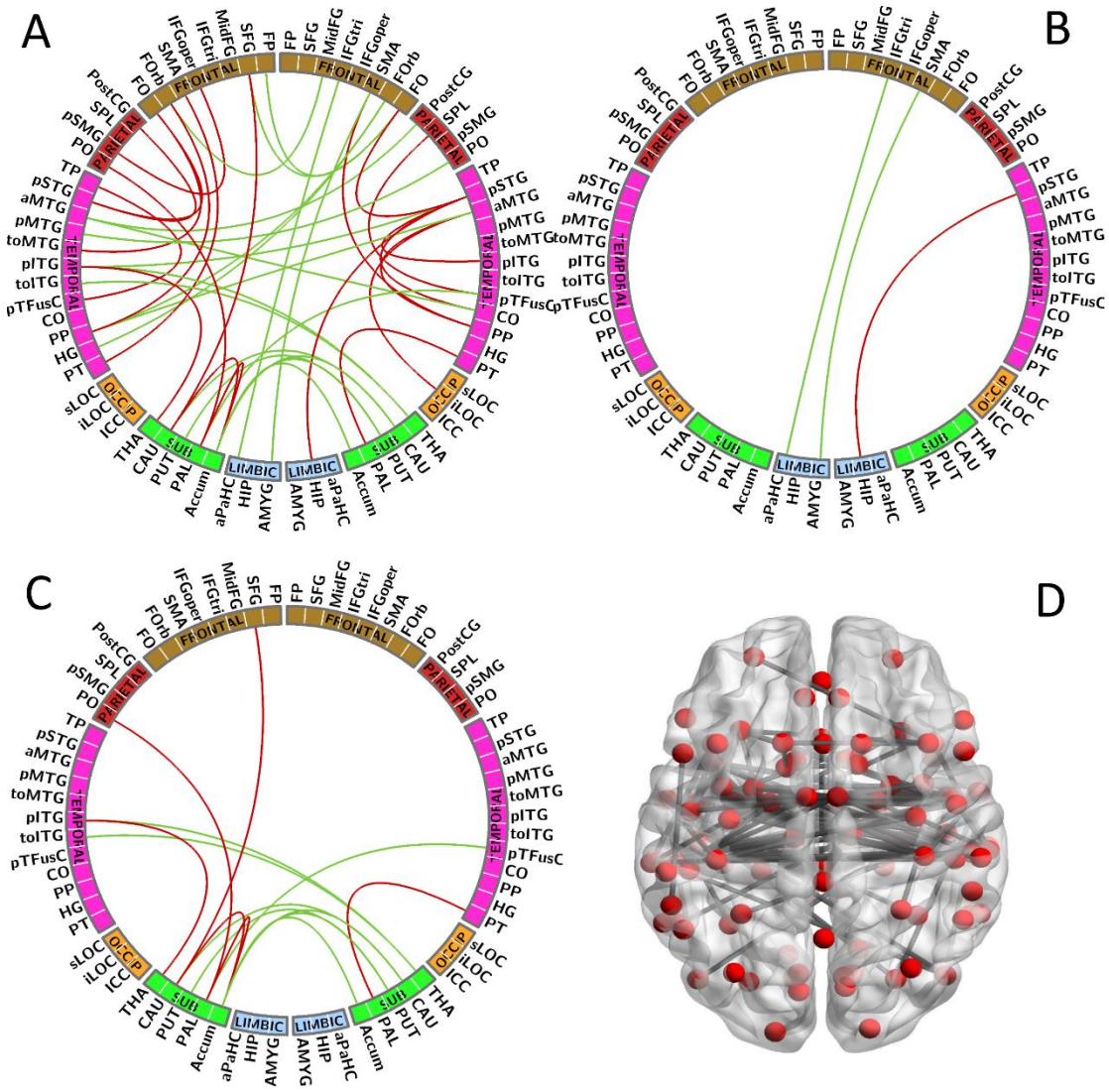

Fig. A4-1 Functional connectivity features building

(A) All (117 connections) of the functional connectivity features between SZ patients and HCs using two-sample *t*-test ($P < 0.05$, uncorrected for multiple comparisons). (B) Connections between cortical and limbic system areas. (C) Connections between cortical and subcortical areas. (D) 3D structural displayed the nodes and connections of 117 features. Red line: connections between the same hemisphere, green line: connections between the different hemisphere.

4.3.3 SVM analysis and classification

In the training data set, the SVM classifier accurately discriminated SZ patients from

HCs on the basis of the ROC curve, with an accuracy of 87.09% (**Fig. A4-3**). The specificity and sensitivity was 86.79% and 87.22%, respectively. The permutation tests showed $P < 0.001$ for accuracy (**Fig. A4-3**). Thus, the prediction accuracy for SZ patients had a significantly higher level than that of chance.

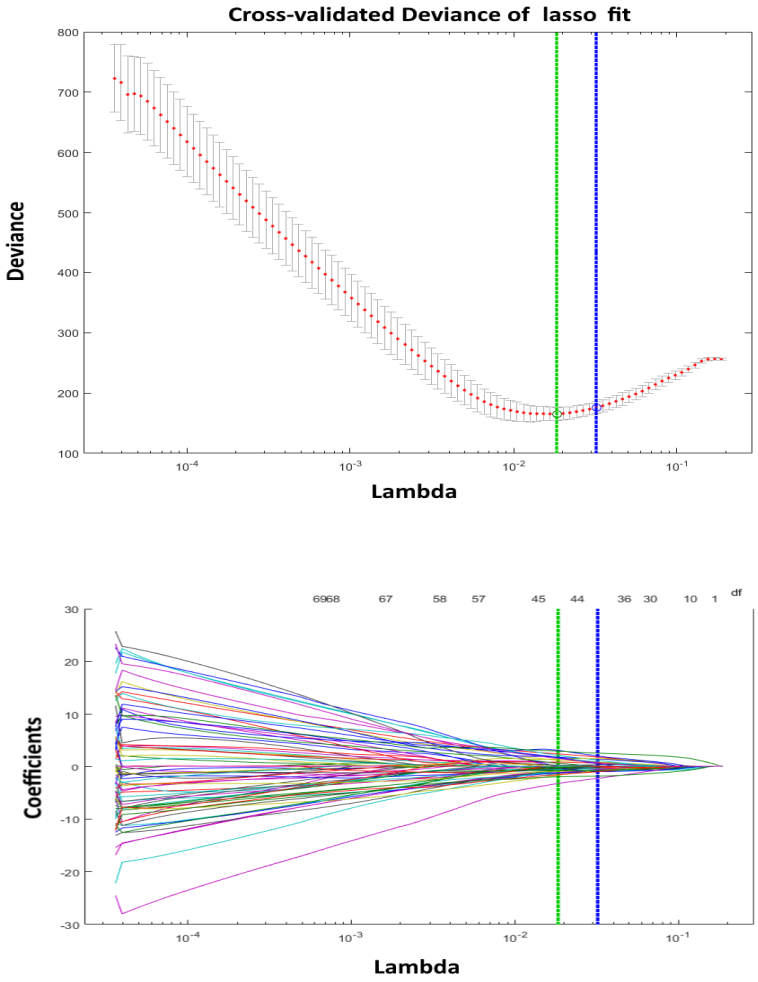

Fig. A4-2 Feature selection using the least absolute shrinkage and selection operator (LASSO) binary logistic regression model

In the upper panel, tuning parameter (lambda, λ) selection in the LASSO model used 10-fold cross-validation via minimum criteria. Dotted vertical lines were drawn at the optimal values by using the minimum criteria and the 1 standard error (SE) of the minimum criteria (the 1SE criteria). In the lower panel, LASSO coefficient profiles of the 117 features. Vertical line was drawn at the value selected using 10-fold cross-validation,

where optimal lambda resulted in 32 nonzero coefficients.

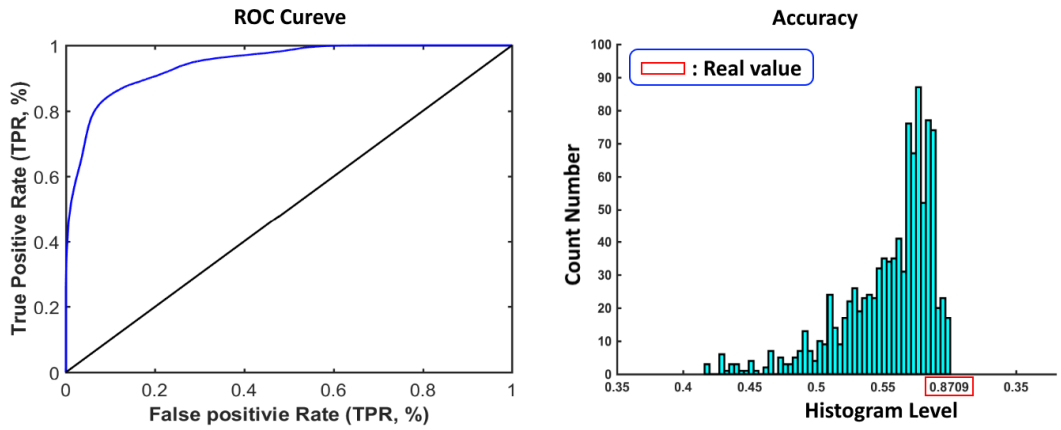

Fig. A4-3 Classification results

In the left panel, ROC curve for the identification of SZ patients by functional connectivity features. The x-axis is the false positive rate (FPR); the y-axis is the true positive rate (TPR). In the right panel, the histogram is the permutation distribution of the accuracy of functional connectivity features. The values obtained using the real labels are indicated by the red box.

4.3.4 Diagnostic validation of functional connectivity features

The functional connectivity features was further confirmed in the validating data set. In this cohort, the accuracy, specificity and sensitivity were 82.61%, 88.00% and 76.19%, respectively.

4.4 Conclusion

In the current study, we explored whether functional connectivity biomarker define SZ using radiomics strategy. Specifically, the accuracy was 87.09% for the purpose of diagnosing SZ patients by applying functional connectivity features, with a validation in the independent replication data set (accuracy = 82.61%). Evidence from the current study points to the disease definition for SZ by functional connectivity features using radiomics

strategy. Our findings are helpful to facilitate objective SZ individualized diagnosis using quantitative and specific biomarker reflecting its neurobiological substrates in different sites.

Appendix 5: Dysconnectivity with anatomical basis in the brain are associated with post-TIPS hepatic myelopathy patients with cirrhosis

Long-Biao Cui, Shuyao Ren, Yi-Bin Xi, Ling-Li Zeng, Gang Chen, Kang Liu, Tianlei Yu, Chuangye He, Wengang Guo, Zhanxin Yin, Zhengyu Wang, Jing Niu, Bohan Luo, Dewen Hu, Guohong Han, Hong Yin

Sumitted to *J Hepatology*

As a rare and likely overlooked complication in chronic liver disease patients with portosystemic shunts, hepatic myelopathy (HM) is characterized by severe and mostly irreversible neurologic symptoms and may be secondary to surgical procedures such as transjugular intrahepatic portosystemic shunt (TIPS). HM patients, pronouncedly presenting with a progressive symmetric spastic paraparesis of the lower limbs, are usually resistant to medial therapy and ultimately wheelchair-bound with dramatically decreased quality of life. However, routine examinations could not be useful for diagnosing HM, because their results are usually normal or non-specific abnormal in patients with HM. The diagnosis of HM, established on clinical grounds after excluding other possible causes of spastic paraparesis, is a difficult clinical problem due to largely unknown neuropathological underpinnings behind HM and a lack of specific biomarkers for this devastating disorder. Cerebral functional magnetic resonance imaging (fMRI) that detects slight alteration of the regional and network-level brain activity might be helpful in the early diagnosis of HM, which promisingly helps to guide the treatments and improve the outcome of patients with HM. We aimed to investigate: (1) whether motor system in the brain of HM shows altered patterns of functional connectivity, (2) what the anatomical

basis behind it is, and (3) the potential clinical significance of these alterations.

4.1 Subjects

After undergoing careful medical history taking, physical examination, and imaging and laboratory examinations, 23 patients with HM and 23 matched patients without HM after TIPS due to bleeding esophageal varices with a history of liver cirrhosis induced by hepatitis B or C virus infection, as described in our previous studies, from the Xijing Hospital of Digestive Diseases between November 2005 and March 2014 were enrolled in the current study (**Table A5-1**). Diagnostic criteria of HM were as follows: (1) history of decompensated hepatic cirrhosis and clinical manifestations, (2) formation of a portosystemic stent after TIPS, (3) typical clinical features of myelopathy, especially progressive spastic paraplegia of the lower limbs without obvious atrophy and shallow sensory and sphincter dysfunction, (4) recurrent or transient HE, (5) liver dysfunction, and (6) without spinal cord space-occupying mass, multiple sclerosis, amyotrophic lateral sclerosis, human immunodeficiency virus (HIV) infection, syphilis, or hepatolenticular degeneration. Twenty-four healthy controls, free from liver disease, were enrolled in the current study. Each subject underwent a review of medical history, physical examination, gastroendoscopy, abdominal computed tomography, and liver ultrasonography. The following exclusion criteria applied to all groups: (1) history of psychiatric, neurologic or systematic illness, (2) diagnosis of substance abuse in the prior 30 days or substance dependence in the prior 6 months, (3) pregnancy and being during lactation, (4) MRI contraindications, and (5) head motion > 3 mm and/or 2 ° during fMRI scan. The local ethics committee approved this study, and all the participants provided written informed consent.

Table A5-1 Demographic and clinical characteristics of participants

Items	HM (n = 23)	Non-HM (n =23)	HCs (n = 24)	*P* value
Age, years	51 ±9	45 ±8	50 ±11	0.08

Sex, male/female	21/2	21/2	20/4	0.61
Education, years	9 ±4	8 ±4	10 ±3	0.18
Handness, left/right	0/23	0/23	0/24	—
Liver function				
Child-Pugh classification, A/B/C	4/16/3	10/10/3	—	0.14
Liver function scores	8 ±2	7 ±2	—	0.08
Hepatic encephalopathy stage, 0/1/2/3/4	5/6/8/2/2	0/9/12/2/0	—	0.06
Paraparesis (+/–)	23/0	0/23	0/24	—
Neurological examination				
Limb muscle strength grading	3 ±1	5 ±0	5 ±0	—
Increased tone (+/–)	15/8	0/23	0/24	—
Hyperreflexia (+/–)	17/6	0/23	0/24	—
Babinski sign (+/−)	18/5	0/23	0/24	—
Ataxia (+/−)	2/21	0/23	0/24	—
Tremor	4/19	0/23	0/24	—
Paresthesias	2/21	0/23	0/24	—

4.2 Methods

4.3.1 Image acquisition

MRI data were collected on a 3.0 T Siemens Magnetom Trio Tim scanner using an eight-channel phased array head coil (Siemens, Germany) between July 2013 and October 2015. Please see 1.2.1 and 2.2.1 of the main text.

4.3.2 Data preprocessing and functional connectivity analysis

The five initial images were discarded. fMRI data were processed using the procedures as described in detail previously with Statistical Parametric Mapping package (SPM8, Wellcome Department of Cognitive Neurology, London, UK; http://www.fil.ion.uncl.ac.uk/spm) by the following steps: (1) slice timing correction; (2) rigid body correction for head motion; (3) atlas registration with an EPI template in the Montreal Neurological Institute (MNI) atlas space, resampling to 3-mm isotropic voxels

and spatially smoothing using a Gaussian kernel of 6 mm full-width-at-half-maximum; (4) normalization for global mean signal intensity across runs; (5) linear detrend and low-pass temporal filtering of less than 0.08 Hz; and (6) regression of nuisance variables including the six parameters obtained by rigid-body head-motion correction, global signal, ventricular and white matter signals, and the first temporal derivatives of all of the above.

We included cortical and subcortical motor areas involving motor and motor control as seed regions (Pool et al, Neuroimage). Coordinates of these regions from activation likelihood estimation meta-analyses (M1: Hardwick et al., 2012; PMd: Witt et al., 2008; SMA: Rehme et al., 2012; pre-SMA: Keuken et al., 2014; putamen: Hardwick et al., 2012) were used for the resting-state analysis (**Table A5-2**). The time series of the respective ROIs in each subject was subsequently represented by the averaged BOLD signals within a sphere with a radius of 8-mm centered at the seed voxel MNI coordinate. For each subject, Pearson's correlation coefficients were then calculated between the time courses of the seed reference and all other voxels in the brain. Finally, the Fisher r-to-z transformation was used to convert correlation coefficients of the functional connectivity maps to z-maps in order to produce approximately normally distributed data.

Table A5-2 MNI coordinates of seed regions

Seed regions	Left			Right		
	X	Y	Z	X	Y	Z
M1	−38	−24	62	34	−22	62
PMd	−16	−20	48	34	−8	52
SMA	−8	0	54	8	0	54
Pre-SMA	−8	18	46	8	12	58
Putamen	−26	4	4	26	0	2

4.3.3 Gray matter and white matter volume analysis

The anatomical images were preprocessed using SPM8. First, the New Segment procedure was performed to segment the T1-weighted MRI images into six partitions, i.e.,

gray matter, white matter, cerebrospinal fluid and three other background partitions based on a modified mixed model cluster analysis technique. Second, a template was generated from the entire image dataset using the DARTEL procedure, and the resulting images were spatially normalized into the MNI space using an affine spatial normalization. Third, the gray matter images were spatially normalized to the relative template (1.5-mm isotropic voxels) and smoothed with an 8 mm full-width-at-half-maximum isotropic Gaussian kernel.

4.3.4 Statistical analysis

For the z-maps of each ROI, one-sample t-tests were performed for each subject group ($P < 0.001$, uncorrected; cluster size ≥ 10 voxels). An inhouse script was run to create a mask from the one-sample t-test results of the three groups for each ROI. Two-sample t-tests were performed on the z-maps between groups applying the masks (voxel-wise $P < 0.001$ in conjunction with cluster-wise $P < 0.05$ to correct for multiple comparisons based on Gaussian random field theory; cluster size ≥ 10 voxels). In the gray matter volume analysis, a threshold of *P* value less than 0.001 (uncorrected) with a cluster threshold of 50 was used in SPM8.

Pearson correlation coefficients were separately computed in abnormal connectivity with clinical data for each patient group. A Receiver Operating Characteristic (ROC) analysis was performed to distinguish HM from Non-HM patients on the basis of the strength of connectivity. SPSS 16.0 (IBM SPSS Statistics) was used for additional statistical analysis. *P* value less than 0.05 was considered statistically significant.

4.3 Results

4.3.1 Functional connectivity

When comparing HM and Non-HM, we found weaker right SMA-seeded functional connectivity with bilateral insula and thalamus, left cerebellum and middle temporal gyrus, and right middle cingulate gyrus and midbrain in HM patients (**Fig. A5-1** and **Table A5-3**). There was also decreased functional connectivity between the right putamen and right midbrain in HM patients as compared to Non-HM patients. Besides, both patients with

and without HM showed extensive reduced functional connectivity in contrast to HCs (**Table A5-3**).

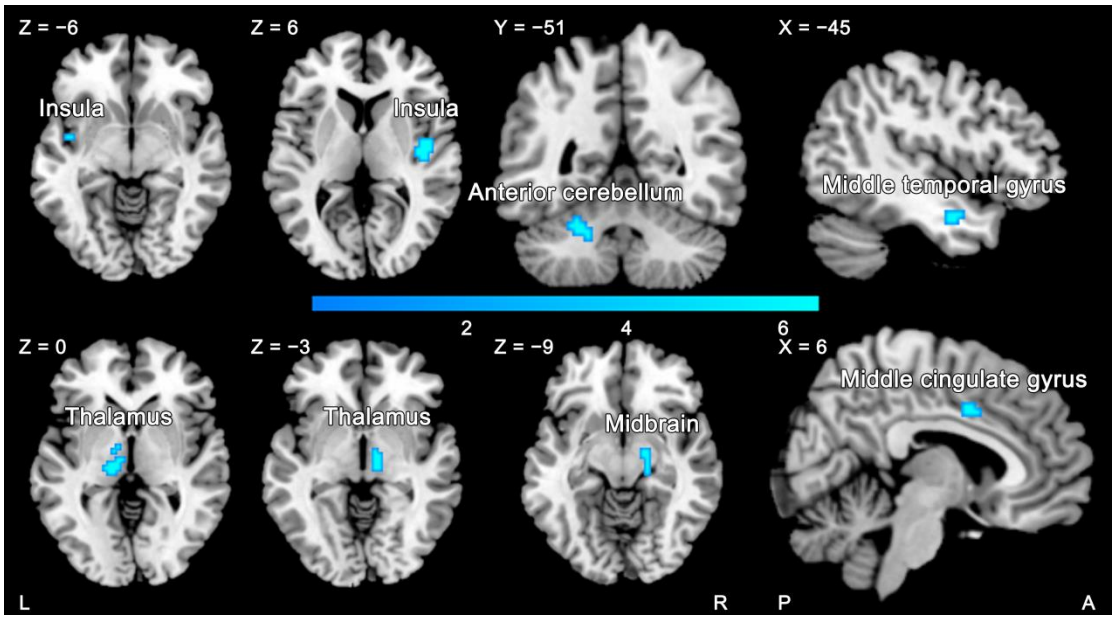

Fig. A5-1 The right SMA-seeded functional connectivity with differences between HM and Non-HM patients ($P < 0.001$, cluster size ≥ 10)

Color bar represents T values. The slice location is marked in the upper-left.

Table A5-3 The Right SMA- and putamen-seeded functional connectivity with differences

ROIs	Voxel	Peak MNI coordinate			Regions	T value
		X	Y	Z		
Right SMA						
HM vs Non-HM	15	−18	−51	−33	Left anterior cerebellum	−3.8939
	10	−45	−3	−24	Left MTG	−4.1215
	15	−42	−3	−6	Left insula	−4.2732
	10	18	−21	−9	Right midbrain	−4.1973
	58	−15	−24	0	Left thalamus	−4.6777
	25	9	−15	−3	Right thalamus	−4.3490
	39	42	−12	6	Right insula	−6.4477

	11	6	6	36	Right DCG	−4.1215
HM vs HCs	13	−27	−54	−27	Left cerebellum	−3.9415
	94	−42	3	15	Left Rolandic operculum	−4.8110
	13	57	9	9	Right IFG, opercular part	−4.2700
	137	−57	−21	18	Lef t supramarginal gyrus	−4.9269
	18	−30	45	21	Left MFG	−3.8836
	13	48	−12	27	Right supramarginal gyrus	−4.1734
	11	45	−6	39	Right precentral gyrus	−3.7676
	87	9	3	45	Right SMA	−4.3666
	15	18	−9	69	Right SFG	−3.9802
Non-HM vs HCs	20	−45	−21	−9	Left STG/MTG	5.1860
	72	−60	−18	24	Left postcentral gyrus	−5.0284
	11	51	−12	27	Right postcentral gyrus	−3.8452
	20	42	3	54	Right MFG	−4.0030
Right putamen						
HM vs Non-HM	18	12	−12	−6	Right midbrain	−4.3512
HM vs HCs	12	−9	−60	−33	Left cerebellum	−4.0733
	11	−24	−57	−36	Left cerebellum	−3.6807
	92	27	3	3	Right putamen	−4.5885
	42	12	−9	−6	Right midbrain	−6.2571
	18	−15	−12	−6	Left thalamus	−4.4904
	70	−21	9	−3	Left putamen	−4.4413
	22	12	9	42	Right DCG	−4.1959
	15	6	18	60	Left SMA	−3.8033
Non-HM vs HCs	20	33	−57	−42	Right cerebellum	−3.9308
	25	12	6	−9	Right putamen/caudate	−4.8129
	106	3	24	21	Right ACG	−4.4294

	15	27	42	27	Right MFG	−3.8541
	29	45	6	45	Right precentral gyrus	−4.8896
	45	3	18	63	Right SMA	−3.9500

ACG, anterior cingulate gyrus; MCG, middle cingulate gyrus; IFG, inferior frontal gyrus; MFG, middle frontal gyrus; MTG, middle temporal gyrus; SFG, superior frontal gyrus; STG, superior/middle temporal gyrus

4.3.2 Gray matter and white matter volume

To search for the anatomical basis of altered functional connectivity, we compared the gray matter and white matter volume between HM and Non-HM patients (**Table A5-4**). Among these brain areas with decreased volume in HM patients relative to Non-HM patients (P < 0.001, uncorrected), the right insula and left cerebellum just revealed hypoconnectivity with the right SMA (**Fig. A5-2**). Moreover, the white matter volume reduced in the right corona radiata beneath the seed region, right SMA (**Fig. A5-3**).

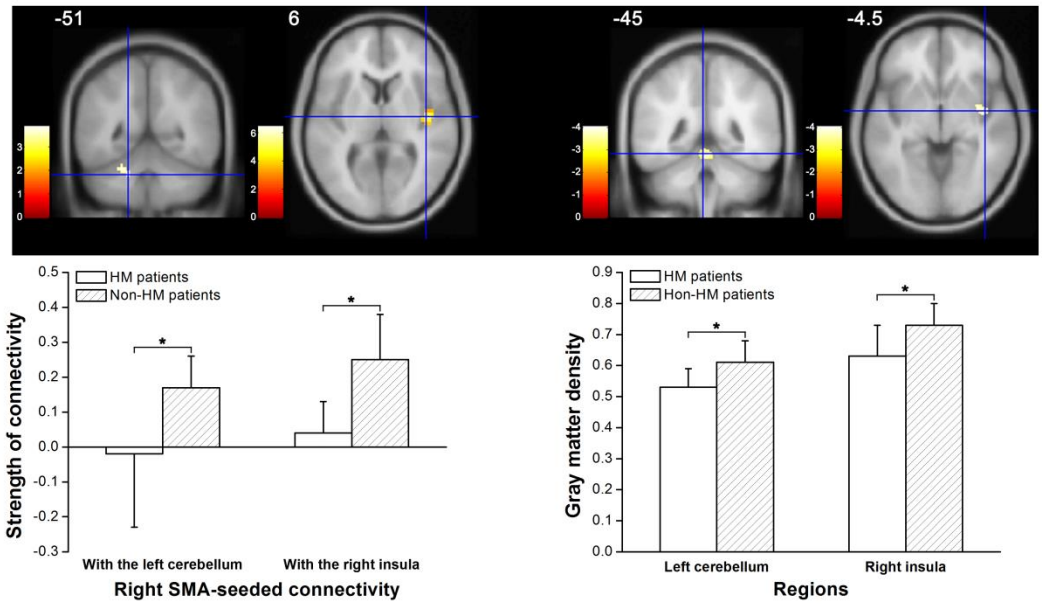

Fig. A5-2 Altered functional connectivity with anatomical basis

HM patients showed significantly reduced right SMA-seeded connectivity with the left cerebellum and right insula (left panel) and gray matter volume in the left cerebellum and right insula (right panel) as compared to Non-HM patients. $^{*}P$ < 0.001 (uncorrected) between HM and Non-HM patients.

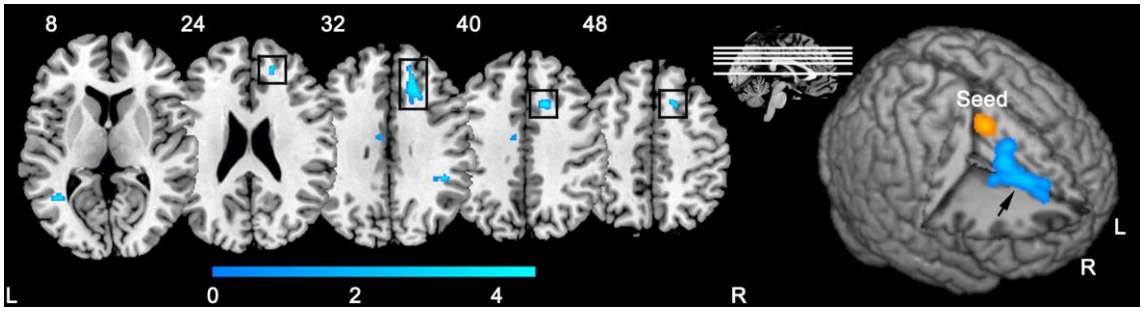

Fig. A5-3 Altered white matter volume

HM patients showed significantly reduced volume of the white matter (arrow in the right panel, as marked with a black frame in the left panel) under the right SMA (seed) as compared to Non-HM patients. $^{*}P < 0.001$ (uncorrected) between HM and Non-HM patients.

Table A5-4 Regions of gray matter and white matter volume with differences between HM and Non-HM

Comparison	Voxel	Peak MNI coordinate			Regions	T value
		X	Y	Z		
Gray matter						
HM > Non-HM	76	−18	1.5	−39	Left fusiform gyrus	4.4900
	98	24	−18	−34.5	Right hippocampus	4.5443
	61	31.5	−40.5	−3	Right hippocampus	4.6167
	131	−19.5	−63	15	Left calcarine/precuneus	4.5805
HM < Non-HM	50	−9	−102	−13.5	Left lingual gyrus	−3.6531
	175	24	−96	−9	Right IOG	−4.4440
	217	−3	−45	−13.5	Left anterior cerebellum	−4.3687
	55	27	−85.5	−13.5	Right IOG	−4.8018
	173	42	−6	−4.5	Right insula	−4.0485
	57	40.5	−79.5	22.5	Right MOG	−4.4440

	59	30	−84	24	Right MOG	−4.0862
White matter						
HM < Non-HM						
	463	13.5	18	37.5	Right ACR	−4.6588
	58	45	−42	30	Right SMG	−3.7636
	82	−43.5	−57	7.5	Left PTR	−3.9098
	73	−10.5	−10.5	36	Left cingulum	−3.8915

ACR, anterior corona radiata; IOG, inferior occipital gyrus; MOG, middle occipital gyrus; PTR, posterior thalamic radiation; SMG, supramarginal gyrus.

4.3.3 Correlation and ROC analyses

The strength of right SMA-seeded functional connectivity was positively correlated with folic acid level in HM patients (r = 0.59, P = 0.04) (**Fig. A5-4**). We also detected clinical correlation trends with the strength of other connectivity (**Table A5-5**). In addition to clinical correlation, the strength of right SMA-seeded functional connectivity also showed the best diagnostic value of distinguishing HM patients from Non-HM patients (area under curve: 0.90; 95%CI: 0.81, 1.00) (**Fig. A5-4**). The diagnostic performance of other connectivity is listed in **Table A5-6**.

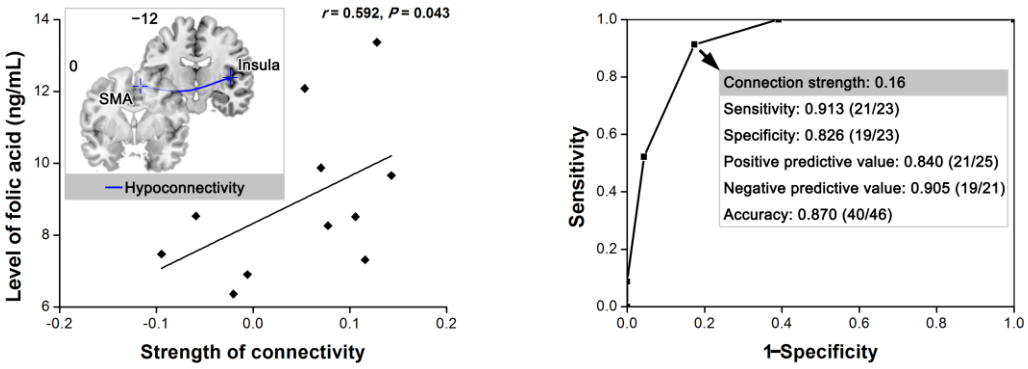

Fig. A5-4 The right SMA-seeded functional connectivity with the right insula showing clinical significance

There was a positive correlation between the decreased strength of this connectivity the

folic acid level in HM patients (left panel). Sensitivity, specificity and accuracy for distinguishing HM from Non-HM patients were 0.913 (21/23), 0.826 (19/23) and 0.870 (40/46) when the cut-off value of strength of connectivity was set at 0.16 (right panel).

Table A5-5 Correlation of clinical data and strength of functional connectivity

Seed regions	Regions connected	Clinical data	*r*	*P* value
Right SMA	Right insula	Folic acid	0.59	0.04
	Left anterior cerebellum	Muscle strength	−0.51	0.08
Right putamen	Right midbrain	Vitamin B12	0.54	0.07

Table A5-6 ROC analysis of connectivity for distinguishing HM from Non-HM

Seed regions	Regions connected	AUC	95%CI	*P* value
Right SMA	Right insula	0.902	0.807, 0.997	0.000
	Left insula	0.851	0.735, 0.967	0.000
	Right thalamus	0.828	0.711, 0.945	0.000
	Left thalamus	0.879	0.783, 0.975	0.000
	Left anterior cerebellum	0.819	0.685, 0.952	0.000
	Left middle temporal gyrus	0.824	0.706, 0.943	0.000
	Right middle cingulate gyrus	0.809	0.687, 0.931	0.000
	Right midbrain	0.837	0.725, 0.950	0.000
Right putamen	Right midbrain	0.847	0.733, 0.960	0.001

AUC, area under curve; 95%CI, 95% confidential interval.

4.4 Conclusion

In conclusion, this study shows motor regions-seeded functional connectivity differences and gray matter volume alterations supporting the abnormal connectivity among HM and Non-HM patients after TIPS and HCs. Furthermore, our study also reveals

the aberrant connectivity's correlation with clinical and laboratory findings, as well as its diagnostic value to discriminate HM from Non-HM patients. Its dysconnectivity with other motor regions including the insula, thalamus, midbrain and anterior cerebellum could be therefore considered to be implicated in dysfunctional movement monitoring, as a descending and/or ascending neural pathway (**Fig. A5-5**).

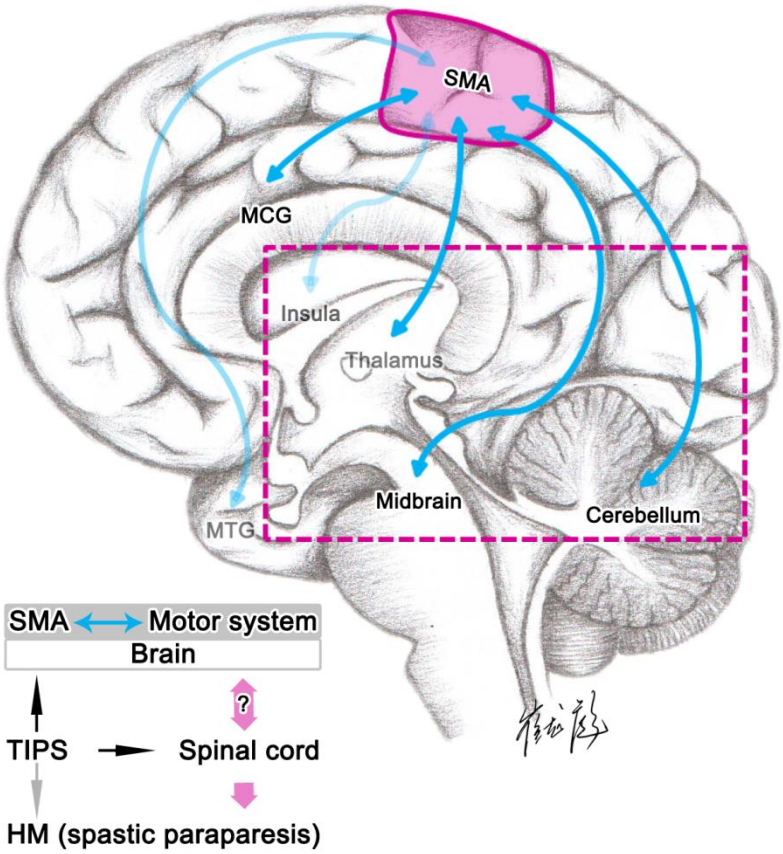

Fig. A5-5 Summary of findings involving SMA in patients with HM after TIPS

The SMA of HM patients showed decreased connectivity with the insula, thalamus, midbrain, cerebellum, middle temporal gyrus, and middle cingulate gyrus. Our study might shed light on the neural underpinnings behind HM after TIPS. The crosstalk between the brain and spinal cord and the linkage between this neural regulation and the onset of HM will deserve further investigation in the future to predict and prevent HM at an early stage after TIPS, as well as improve the outcome of HM.

On the one hand, this might cause disability to modulate the performance in the case

of motor errors, resulting in HM patients' progressive myelopathy ranging from walking difficulty to paraparesis in the end. On the other, the neurological status of HM patients is likely to disrupt their brain activity, exhibiting imbalance among motor regions in relation to movement monitoring. The crosstalk between the brain and spinal cord and the linkage between this neural regulation and the onset of HM will deserve further investigation in the future, particularly focusing on the brain and the cerebrospinal interaction, to predict and prevent HM at an early stage after TIPS, as well as improve the outcome of HM.

个人简历和研究成果

1. 个人简历

崔龙彪，男，汉族，1989 年 2 月出生，黑龙江齐齐哈尔人，2007 年 12 月加入中国共产党。现为第四军医大学西京医院放射科博士研究生，导师：印弘教授，目前主要从事神经精神疾病的脑功能磁共振成像研究，期间曾赴荷兰乌特列支大学留学。

1994.09-1996.06，黑龙江省齐齐哈尔市昂昂溪区榆树屯后五家子小学

1996.09-1998.06，黑龙江省齐齐哈尔市昂昂溪区昂昂溪乡红星小学

1998.09-1999.06，黑龙江省齐齐哈尔市昂昂溪区第三小学

1999.09-2003.06，黑龙江省齐齐哈尔市第二十三中学

2003.09-2006.06，黑龙江省齐齐哈尔市实验中学

2006.09-2011.06，第四军医大学，临床医学，本科

2011.09-2014.06，第四军医大学，航空航天医学系，硕士研究生，导师：余志斌教授

2014.09-2017.06，第四军医大学，西京医院放射科，博士研究生，导师：印弘教授

2015.08-2015.10，西安电子科技大学，生命科学与技术学院，访问学生

2016.05-2016.07，国防科学技术大学，机电工程与自动化学院，访问学生

2017.01-2017.07，荷兰乌特列支大学医学中心，联合培养博士研究生，国外导师：René S. Kahn 教授

2. 技能证书

临床执业医师考试：471.25 分（2016）

全国英语等级考试五级（PETS-5）：笔试 61 分，听力 25 分，口语 3 分（2014）

3. 研究成果

发表论文

现已发表学术论文 32 篇（第一/共一作者 19 篇），其中以第一/共一作者在

Radiology 等 SCI 收录期刊发表论文 13 篇（累计影响因子 44.284，大于 5 者 3 篇，单篇最高 6.798），主要涉及神经精神疾病功能影像、肿瘤影像等领域：

[1] **Cui LB**, Liu L, Guo F, Chen YC, Chen G, Xi M, Qin W, Sun JB, Li C, Xi YB, Wang HN, Yin H. Disturbed brain activity in resting state networks of first-episode schizophrenia patients with auditory verbal hallucinations: a cross-sectional functional MR imaging study. **Radiology**, 2017; 283(3):810-819. (IF = 6.798, Times Cited: 1)

[2] **Cui LB**, Liu K, Li C, Wang LX, Guo F, Tian P, Wu YJ, Guo L, Liu WM, Xi YB, Wang HN, Yin H. Putamen-related regional and network functional deficits in first-episode schizophrenia with auditory verbal hallucinations. **Schizophr Res**, 2016; 173(1-2):13-22. (IF = 4.453, Times Cited: 9)

[3] **Cui LB**, Liu J, Wang LX, Li C, Xi YB, Guo F, Wang HN, Zhang LC, Liu WM, He H, Tian P, Lu HB, Yin H. Anterior cingulate cortex-related connectivity in first-episode schizophrenia: a spectral dynamic causal modeling study with functional magnetic resonance imaging. **Front Hum Neurosci**, 2015; 9:589. (IF = 3.634, Times Cited: 11)

[4] **Cui LB**, Chen G, Xu ZL, Liu L, Wang HN, Guo L, Liu WM, Liu TT, Qi S, Liu K, Qin W, Sun JB, Xi YB, Yin H. Cerebral blood flow and its connectivity features of auditory verbal hallucinations in schizophrenia: a perfusion study. **Psychiatry Res Neuroimaging**, 2017; 260:53-61. (IF = 2.477)

[5] Li BJ, **Cui LB**, Xi YB, Friston KJ, Guo F, Wang HN, Zhang LC, Bai YH, Tan QR, Yin H, Lu HB. Abnormal effective connectivity in the brain is involved in auditory verbal hallucinations in schizophrenia. **Neuroscience Bull**, 2017; 33(3):281-291. (**Co-first author**, IF = 2.322)

[6] Chang X, Xi YB, **Cui LB**, Wang HN, Sun JB, Zhu YQ, Huang P, Collin G, Liu K, Xi M, Qi S, Tan QR, Miao DM, Yin H. Distinct inter-hemispheric dysconnectivity in schizophrenia patients with and without auditory verbal hallucinations. **Sci Rep**, 2015; 5:11218. (**Co-first author**, IF = 5.228, Times cited: 12)

[7] Xi YB, Li C, **Cui LB**, Liu J, Guo F, Li L, Liu TT, Liu K, Chen G, Xi M, Wang HN, Yin H. Anterior cingulate cortico-hippocampal dysconnectivity in unaffected relatives of schizophrenia patients: a stochastic dynamic causal modeling study. **Front Hum Neurosci**,

2016; 10:383. (**Co-first author**, IF = 3.634, Times Cited: 1)

[8] Zhang J, **Cui LB**, Tang X, Ren XL, Shi JR, Yang HN, Zhang Y, Li ZK, Wu CG, Jian W, Zhao F, Ti XY, Yin H. DW MRI at 3.0-T versus FDG PET/CT for detection of malignant pulmonary tumors. **Int J Cancer**, 2014; 134(3):606-611. (**Co-first author**, IF = 5.085, Times cited: 13)

[9] Liu LP, **Cui LB**, Zhang XX, Cao J, Chang N, Tang X, Qi S, Zhang XL, Yin H, Zhang J. Diagnostic performance of diffusion-weighted magnetic resonance imaging in bone malignancy: a systematic review and meta-analysis. **Medicine**, 2015; 45(94):e1998. (**Co-first author**, IF = 1.206, Times cited: 3)

[10] Liu LP, Zhang XX, **Cui LB**, Yang JL, Yang HN, Zhang Y, Zhou Y, Tang X, Qi S, Fang Y, Zhang J, Yin H. Preliminary comparison of diffusion-weighted MRI and PET/CT in predicting histologic type and malignancy of lung cancer. **Clin Respir J**, 2017; 11(2):151-158. (**Co-first author**, IF = 2.147, Times cited: 7)

[11] Qi S, Mu YF, **Cui LB**, Zhang J, Guo F, Tan QR, Shi M, Liu K, Xi YB, Zhang NY, Zhang XL, He Y, Yang J, Yin H. Anomalous gray matter structural networks in recent onset post-traumatic stress disorder. **Brain Imaging Behav**, 2017 Mar 14. doi: 10.1007/s11682-017-9693-z. (**Co-first author**, In press, IF = 3.667)

[12] Qi S, Mu YF, **Cui LB**, Li R, Shi M, Liu Y, Xu JQ, Zhang J, Yang J, Yin H. Association of optic radiations integrity with cortical thickness in children with anisometropic amblyopia. **Neurosci Bull**, 2016; 32(1):51-60. (**Co-first author**, IF = 2.322, Times cited: 4)

[13] **Cui LB**, Li BW, Jin XH, Zhao L, Shi J. Progressive changes of orexin system in a rat model of 6-hydroxydopamine-induced Parkinson's Disease. **Neurosci Bull**, 2010; 26(5):381-387. (IF = 1.311, Times cited: 18)

[14] Chang X, Collin G, Xi YB, **Cui LB**, Scholtens LH, Sommer IE, Wang HN, Yin H, Kahn RS, van den Heuvel MP. Resting-state functional connectivity in medication-naïve schizophrenia patients with and without auditory verbal hallucinations: a preliminary study. Schizophr Res, 2017 Jan 24. pii: S0920-9964(17)30037-3. doi: 10.1016/j.schres.2017.01.024. [Epub ahead of print] (IF = 4.453)

[15] Huang P, Xi YB, Lu ZL, Chen YC, Li XR, Li WG, Zhu X, **Cui LB**, Tan QR, Liu WM, Li C, Miao DM, Yin H. Decreased bilateral thalamic gray matter volume in first-episode schizophrenia with prominent hallucinatory symptoms: A volumetric MRI study. **Sci Rep**, 2015; 5:14505. (IF = 5.228, Times cited: 7)

[16] Xi YB, Guo F, Li H, Chang X, Sun JB, Zhu YQ, Liu WM, **Cui LB**, Chen G, Wang HN, Yin H. The structural connectivity pathology of first-episode schizophrenia based on the cardinal symptom of auditory verbal hallucinations. **Psychiatry Res Neuroimaging**, 2016; 257:25-30. (IF = 2.477)

[17] Li L, Li BJ, Bai YH, Wang HN, Liu WL, Tian P, Zhang LC, Guo F, **Cui LB**, Yin H, Lu HB, Tan QR. Abnormal resting state effective connectivity within the default mode network in major depressive disorder: a spectral dynamic causal modeling study. **Brain Behav**, 2017. (Accepted, IF = 2.128)

[18] **Cui LB**, Li BW, Cui YY, Shi J, Dong YL, Du MX. Volumetric measurement of enlarged cavum septi pellucidi and cavum vergae: a pilot study of a stereological method applied in neuroimaging. **神经解剖学杂志**, 2014; 30(2):173-177.

[19] **崔龙彪**, 圣娟娟, 王云英, 余志斌. 腹主动脉缩窄 20 周大鼠心肌细胞的自噬通量. **生理学报**, 2013; 65(3):301-308.

[20] **崔龙彪**, 金晓航, 史娟. 中枢神经系统内的 TRPC6 离子通道. **神经解剖学杂志**, 2011; 27(5):565-570.

[21] **Cui LB**. To medical or surgical treatment? First choice for management of acute simple appendicitis. **医学争鸣**, 2014; 5(2):35-37.

[22] **Cui LB**, Zhang HJ. Leopard skin-like fundus oculi induced by LASIK? **医学争鸣**, 2013; 4(6):7.

[23] **崔龙彪**. 应保护民族医药的研发. **医学争鸣**, 2013; 4(2):26.

[24] 张海军, **崔龙彪**, 岳原, 杜成, 常耀明, 史娟, 谢满江. STZ 诱导的 2 型糖尿病大鼠心肌组织 TRPC7 的表达上调. **心脏杂志**, 2014; 26(4):403-407.

[25] 赵琳, **崔龙彪**, 史娟, 李云庆. 不同刺激方式对大鼠穹窿周区 orexin-A 表达的形态学研究. **神经解剖学杂志**, 2010; 26(4):401-405.

[26] 刘蓉蓉, **崔龙彪**, 李博为, 金晓航, 李会莉, 史娟, 李云庆. 不同高渗刺激对下

丘脑视上核和室旁核神经元功能状态的影响. **神经解剖学杂志**, 2008; 24(5):458-462.

[27] 王艺璇, 高云涛, **崔龙彪**, 茹凝玉, 张海军, 焦博, 余志斌. 他莫昔芬对糖尿病大鼠心肌 CD147 糖基化与 MMPs 的影响. **中国应用生理学杂志**, 2015; 31(1):1-5.

[28] 李洁, 张艰, **崔龙彪**. 螺旋 CT 与弥散加权磁共振成像对肺部良恶性病变诊断价值研究. **陕西医学杂志**, 2016, 45(7):877-878.

[29] 田萍, 席一斌, 李陈, **崔龙彪**, 印弘. 精神分裂症患者透明隔间腔的 MRI 形态学研究. **放射学实践**, 2016; 31(8): 721-724.

[30] 吴雨静, 刘康, 任书瑶, **崔龙彪**, 席一斌, 陈纲, 韩国宏, 印弘. 肝性脊髓病患者自发脑活动局部一致性的变化. **实用放射学杂志**, 2017; 33(3):357-360.

[31] 李陈, 席一斌, 陈纲, 田萍, **崔龙彪**, 刘康, 吴雨静, 印弘. 首发精神分裂症幻听患者的全脑白质变化研究. **实用放射学杂志**, 2016; 32(1):1-4.

[32] 田萍, 李陈, 席一斌, 刘康, **崔龙彪**, 吴雨静, 印弘. 脉络丛肿瘤的影像学征象与病理对照分析. **放射学实践**, 2016; 31(4):346-349.

参编专著

余志斌, **崔龙彪**. 心肌细胞骨架. In: 余志斌主编, 心肌细胞的分子解剖. 第四军医大学出版社, 2013.（“十二五”国家重点出版规划图书，2013 年国家出版基金资助项目）

申请专利

张磊，费舟，王成果，**崔龙彪**，董飞．一种组织片漂洗盒：中国，20179815.8. 2010-11-24.

基金项目

[1] 第四军医大学博士学位论文课题资助“基于多模态磁共振成像的首发精神分裂症幻听症状相关的脑结构与功能研究”（批准号：2014D07）；负责人：**崔龙彪**，导师：印弘，辅导教师：席一斌；起止年月：2015-01 至 2015-12

[2] 第四军医大学学员课外科学研究课题立项项目“TRPC6 与帕金森病发病关系的行为学研究”（批准号：08865-12）；负责人：**崔龙彪**，李博为，指导教师：史娟；起止年月：2008-10 至 2009-10

[3] 国家自然科学基金面上项目“难治性精神分裂症幻听机制的神经影像学研究”（批准号：81571651）；负责人：印弘，参与人：**崔龙彪**，席一斌，郭钒，李宝娟，郭力，刘康，李陈，田萍，武文珺；起止年月：2016-01 至 2019-12

[4] 国家自然科学基金面上项目“TRPC7 调控疼痛状态下加压素合成和释放的机制研究”（批准号：31571188）；负责人：史娟，参与人：寇珍珍，张勇，鲁亚成，**崔龙彪**，王舰，尹俊斌，吴振宇，王立新，冯斑；起止年月：2016-01 至 2019-12

[5] 国家自然科学基金青年项目“精神分裂症额叶髓鞘发育异常的磁共振研究”（批准号：81601474）；负责人：席一斌，参与人：郭钒，**崔龙彪**，李宝娟，郭力，武文珺，李陈，王柳仙；起止年月：2017-01 至 2019-12

[6] 国家自然科学基金青年项目“木僵患者“失连接假说”的多模态脑网络机制的磁共振研究”（批准号：81601456）；负责人：齐顺，参与人：刘莹，李宝娟，刘洋，**崔龙彪**，席敏，慕允凤，王虹，田萍；起止年月：2017-01 至 2019-12

[7] 国家自然科学基金青年项目“GSK-3β/PINK1-Parkin 通路调控脑缺血中线粒体自噬的作用及机制研究”（批准号：81400952）；负责人：郭钒，参与人：王枫，席一斌，齐顺，马磊，史立凯，**崔龙彪**，刘康；起止年月：2015-01 至 2017-12

[8] 国家自然科学基金青年项目“AMPK 可能经减轻心肌细胞内质网应激而发挥抗凋亡作用”（批准号：31300979）；负责人：张琳，参与人：茹凝玉，焦博，圣娟娟，**崔龙彪**，张海军，窦建平，白云刚；起止年月：2014-01 至 2016-12

[9] 国家自然科学基金青年项目“Calpain-2 核转位调节腹主动脉缩窄大鼠肥大心肌细胞凋亡易感性的机制”（批准号：31200862）；负责人：常惠，参与人：圣娟娟，岳志杰，王云英，徐彭涛，**崔龙彪**，焦博，张文成，茹凝玉；起止年月：2013-01 至 2015-12

学术会议

[1] **Cui LB**, Xi YB, Zeng LL, Han GH, Yin H. Resting functional connectivity and anatomical basis in patients with hepatic myelopathy after transjugular intrahepatic portosystemic shunt. International Society for Magnetic Resonance in Medicine (ISMRM) 25th Annual Meeting & Exhibition. 4 月 22 日-27 日, 2017. Honolulu, America. (壁报展示)

[2] **Cui LB**, Yin H, Zhang J. Diagnosis, assessment and prediction of early response to

chemotherapy by using diffusion-weighted MRI in lung cancer. 17th World Conference on Lung Cancer. 12 月 4 日-7 日, 2016. Vienna, Austria. (壁报展示)

[3] **崔龙彪**. 疑难病例读片. 2016 西京影像高峰论坛. 11 月 17 日-18 日, 2016. 陕西西安.（大会发言）

[4] **崔龙彪**. 科研设计与写作——讲个完整的故事. 2016 年中国医师协会全国基层医院放射医师培训计划. 11 月 2 日, 2016. 陕西西安. (专题讲座)

[5] **Cui LB**, Guo F, Xi YB, Yin H. Disturbed brain activity in resting state networks of first-episode schizophrenia patients with auditory verbal hallucinations: a cross-sectional functional MR imaging study. 中华放射学学术大会 2016. 10 月 12 日-15 日, 2016. 江苏苏州. (分组报告)

[6] **Cui LB**, Yin H, Zhang J. Diagnostic performance and assessment of diffusion-weighted magnetic resonance imaging in lung cancer. 中华医学会呼吸病学年会-2016（第十七次全国呼吸病学学术会议）. 9 月 22 日-25 日, 2016. 陕西西安. (分组报告)

[7] **Cui LB**, Li BJ, Xi YB, Yin H. Thalamic-auditory cortical-hippocampal dysconnectivity in first-episode schizophrenia patients with auditory verbal hallucinations. International Society for Magnetic Resonance in Medicine (ISMRM) 24th Annual Meeting & Exhibition. 5 月 7 日-13 日, 2016. Singapore. (分组报告)

[8] **Cui LB**, Yin H. Whole-body diffusion-weighted magnetic resonance imaging-based study for diagnosing and assessing lung cancer. Advanced Diffusion Workshop held by Siemens MR R&D collaboration. 7 月 26 日, 2015. 广东广州. (专题讲座)

[9] **崔龙彪**, 印弘. 精神分裂症幻听的结构及功能磁共振研究. 中华医学会放射学分会第十五届全国磁共振学术大会. 6 月 25 日-28 日, 2015. 湖北武汉. (专题讲座)

[10] **Cui LB**, Liu LP, Zhang XX, Zhang J, Yin H. Diagnostic performance of diffusion-weighted magnetic resonance imaging and positron emission tomography/computed tomography in cancer: A systematic review and meta-analysis. 第十一届中青年呼吸学者论坛. 10 月 17 日-19 日, 2014. 天津. (英文发言)

[11] Zhang J, **Cui LB**, Tang X, Zhang Y, Yang HN, Chen LZ, Ren XL, Shi JR, Yin H. Diffusion-weighted magnetic resonance imaging at 3.0-T versus fluorine 18

fluorodeoxyglucose positron emission tomography/computed tomography for detection of pulmonary malignant tumors. 15th World Conference on Lung Cancer. 10 月 27 日-10 月 30 日, 2013. Sydney, Australia. (分组报告)

[12] Zhang J, **Cui LB**, Tang X, Ren XL, Shi JR, Yang HN, Zhang Y, Li ZK, Wu CG, Jian W, Zhao F, Ti XY, Yin H. DW MRI at 3.0-T versus FDG PET/CT for detection of malignant pulmonary tumors. The European Cancer Congress 2013. 9 月 27 日-10 月 1 日, 2013. Amsterdam, Netherlands. (壁报展示)

[13] **Cui LB**, Ru NY, Yu ZB. CD147 mediates extracellular matrix remodeling of myocardium induced by angiotensin II in renovascular hypertension. 2013 年中国生理学会心血管生理学术会议. 9 月 23 日-26 日, 2013. 辽宁沈阳. (会议摘要)

[14] 史娟, 金晓航, **崔龙彪**, 李博为, 赵琳, 李云庆. TRPC6 和 TRPC7 在下丘脑视上核和室旁核的形态学. 中国解剖学会 2012 年学术年会. 10 月 19 日-22 日, 2012. 重庆. (会议摘要)

4. 荣获奖励

2006-2007 学年第四军医大学校长奖学金一等奖

2007-2008 学年第四军医大学校长奖学金一等奖

2008-2009 学年第四军医大学校长奖学金一等奖

2009-2010 学年第四军医大学校长奖学金一等奖

2009 年西京医院《物理诊断学》知识竞赛二等奖

2010 年西京医院《外科学》知识竞赛二等奖

2010 年西京医院外科临床技能竞赛三等奖

2011 年度第四军医大学硕士二等奖学金

2012 年度第四军医大学硕士二等奖学金

2013 年度第四军医大学硕士一等奖学金

2014 年第十一届中青年呼吸学者论坛优秀英文论文

2016 年国家留学基金管理委员会国家建设高水平大学公派研究生项目

致　　谢

寂寞寒窗廿三载，
今朝苦尽甘欲来。
拜谢师恩亲友爱，
繁花硕果径自开。

感谢国家自然科学基金（81571651）、国家留学基金管理委员会 2016 年建设国家高水平大学公派研究生项目（201603170143）、第四军医大学博士学位论文课题资助（2014D07）与原国家重点基础研究发展计划（2011CB707805）对本课题的资助。

知子莫若父，知徒莫若师。衷心感谢导师印弘教授及其夫人张艰教授长期的悉心指导与无私帮助。我与导师夫妇的最初相识是在 2009 年本科阶段的临床课上，因为各自独特的魅力，从那个时候起我便记住了二位老师；进入 2010 年临床实习阶段，先后在呼吸内科及放射科实习轮转，或许是相对不同的表现，二位老师便记住了我。从此，我的成长就从未与他们分开过，注定今生你我为师徒。此后的几年中，无论学业还是生活，我们一直联系密切，我也早已把老师夫妇认定为我的导师。直到 2014 年，学校政策调整，我才真正有幸报考成功，何其幸福。这些年，我跟老师的关系也十分有趣，多少次在老师的家庭聚会上“蹭吃蹭喝”，在老师面前还可以像个孩子一样想哭就哭、想笑就笑，因为“不良嗜好”会被他们以不同的形式“管教”。诚然，我又很怕老师，每每被问及课题进展或者工作出错时都会内心忐忑、惶惶不安。有一次我们的文章投到 *Lancet*，初审被拒后申诉成功，这也足见老师的研究水准已被最顶级的医学期刊认可。在对审稿意见回复及修改后，未经老师同意而擅自提交，当被问起时内心几乎是颤抖的，此时此刻方知自己的草率与鲁莽。好在沟通后编辑将系统重新开放，经与老师逐条改过后重新提交。那是我们与 *Lancet* 距离最近的一次，虽然是梦想，仍然希望有一天能够成真。

由于研究性质特殊，我的博士课题需要寻求多方合作，其中主要包括西京医院心身科、西安电子科技大学及国防科学技术大学。每次都是老师将相应单位的主要

负责人邀请到科里详谈，而去国防科学技术大学更是老师亲自带上我前往长沙，我才得以到各个单位纳入被试或处理数据。老师对我说过“月月有结果，月月有文章”，2014 年 8 月至今，课题组 *Radiology*、*Clin Cancer Res* 等高质量研究论文均在此期间完成并发表。由于老师的行政工作与临床工作繁忙，我们的课题讨论经常安排在晚上。记得有天深夜，几近 23:30 的时候我们还在临床教室讨论课题，老师自己也说思路确实跟不上了，这才结束讨论。就是这样数不清的日夜，我们才把研究工作积累到今天的状态。对于各类学习机会，只要上级批准，老师都让我去参加，而各种上台发言、申请奖项或资助的机会，也都会让我上，三年来也真是去过了很多地方，所谓“见多识广”大概就是这样的。博士期间，虽然尚未做到“读万卷书”，但起码做到了“行万里路”。另外，我的个人问题也一直都是老师关注的焦点，前前后后帮我创造了很多机会，只是自己不争气，一次次错失良机，心里还默念“不急，不急”。

在老师眼中我永远都是“优秀的小崔”，我知道这是对我的鼓励与厚望。七年来，一路同行、一路陪伴，我深深地感到自己已被父母般的老师“宠坏”，也在老师的呵护与浇灌下逐步成长。当年懵懂无知的追风少年，俨然就快成了男子汉。在这即将而立之时，我再次迎来了一个崭新阶段的转折与大考，老师就像一把大伞，为我遮风蔽雨，指导我的人生规划。曾给老师写下这样一段文字，现在正式献给我的老师。

有妳有你

躺在妳温暖柔软的臂弯里，
伏在你宽厚结实的肩膀上，
远离黑暗、冰冷，
以及无尽的恐惧。

呼吸爱的气息，
从跌倒处爬起，
越过汪洋和大地，
找到曾经的自己。

言传身教倾其技艺，
重塑坚强与刚毅，
明白孰轻孰重孰高孰低，
学会何时争取何时放弃。

当有天盘挽发髻，
有人陪妳吃饭、聊天、喝茶、看戏。
当有天发际后移，
有人陪你细细寻觅共度的美好回忆。

在放射科学习的几年中，我要感谢团队的每一个人，让我畅快地在黑白世界中体会多彩的绚丽。感谢席一斌师兄在科研和临床上一直不离不弃的辅导，科研上的协调与沟通能力都是他一步一步带出来的，特别是临床上，他对我说：“诊断就是先提炼获得信息，然后找特点信息，再然后试着推翻自己的结论，最后再诊断”。在他的帮助下，开创性地完成了2016年科室举办的西京影像高峰论坛上的疑难病例读片，久久不能忘怀他那充满力量的鼓励：“有信心就好，不怕，我帮你选病例”。师兄把各类提升机会均让我“一人独享”，也确实如他所说，“路都走过后才成长了”。感谢郭钒讲师、同学乔鹏岗博士生与刘康博士生以及师弟、师妹团田萍硕士、李陈硕士、吴雨静硕士生、王柳仙硕士生、刘婷婷硕士生、王兴瑞硕士生给予我这个后入行的新手的帮助，感谢唐兴博士生、齐顺博士生、李晓燕秘书、李心睿秘书、文娣娣秘书的帮助。为老师的那句话续上一句，希望我们的团队“人人有结果，人人有文章”。同时，感谢宦怡教授、孙立军教授、张劲松副教授、郑敏文副教授、魏光权副教授、任静副教授、徐俊卿副教授以及各位医师、技师、护士在学习与生活上的帮助。

受科室工作环境所限，入学之前导师就帮我联系到计算机应用教研室开展实验。十分感谢卢虹冰教授为我提供了优越的实验环境和宽松的学习氛围；同时，感谢李宝娟讲师在动态因果建模实验中给予的无私帮助，特别是她在美国期间虽工作繁忙，仍多次在线答疑解惑。感谢计算机应用教研室全体人员在实验与生活中给予的关照。

实验中采用的精神分裂症及肝性脊髓病患者分别由西京医院心身科谭庆荣教授与王化宁副教授团队及消化内科韩国宏教授团队协助纳入，在此表示衷心感谢。感

谢心身科及消化七科各位医师的努力，感谢每位患者及其家属对我们的信任及配合。

博士二年级期间，我曾前往西安电子科技大学生命科学与技术学院和国防科学技术大学机电工程与自动化学院学习，分别获得了秦伟教授团队（孙金铂讲师、柳琳博士生、徐子良博士生、朱元强博士生）、胡德文教授团队（曾令李副教授、魏慧琳博士生、张鹏硕士生）的全力支持，在此也一并表示感谢。

在国家留学基金委的资助下，我于博士三年级期间赴荷兰乌特列支大学医学中心（Universitair Medisch Centrum Utrecht，UMC Utrecht）精神病科公派留学。能够在异国他乡顺利地开展研究并舒适地生活特别需要感谢国家的资助和 UMC 提供的便利，以及国外导师 René S. Kahn 教授、共同国外导师 Martijn P. van den Heuvel 助理教授、常晓博士生、魏永斌博士生、Jeanette Sopacua 女士、Siemon C. de Lange 博士生、Lianne H. Scholtens 博士生、Hannelore K. van der Brugh 博士生以及实验室全体人员的鼎力相助，以及在 UMC 期间结识的各国友人。若用一句话总结我的留学经历，则为：半年间，书千行代码，成数篇拙章；行多远，经万般沉淀，取一瓣心香。

能够顺利完成学业，我要感谢医学心理学院苗丹民教授给予的大力支持，以及黄鹏讲师、廖扬博士对 DPARSF、REST 软件应用技术的帮助。

另外，感谢我的同学李博为硕士生、张海军硕士、韩佩君博士生、李椋博士生、刘甜博士生、徐肖攀博士生、杨菲博士生、徐杰博士生、苏鹏博士生给予的支持。

除此之外，还要感谢我的家人。他们长期的支持与鼓励、安慰与激励，使我在面对各种困难时变得勇敢和坚强。2012 年初，我的父母从齐齐哈尔赶来西安，并一直陪伴我至硕士毕业，也幸好有航空航天生理学教研室张琳师姐的无私相助，才使住处得以解决，又在 2016 年初再次来到西安。我们生活朴素，但乐在其中。就为了能与他们的儿子在一起，他们不辞劳苦，给多年独自在外生活的我带来家的温暖。

尚未感叹完本科五年的青葱岁月时，硕士三年早已转瞬即逝，而今，博士三年就快要达到终点线了。四医大、十一年、学医路，回想往日时光，许多你我不能忘，许多忘却不可提。这片令我曾经向往、而今依恋、未来怀念的热土，我深爱着她。

二十三年求学路，不求完美，但求完整。怀揣着那份情怀，继续上路……

2017 年 5 月 4 日于西安